TWO-PHASE (GAS-LIQUID) FLOW DISTRIBUTION IN THE OUTLET BRANCHES OF A HORIZONTAL MULTI-BRANCH HEADER

By

Zoskales Teclemariam

A thesis

presented to the University of Manitoba

in partial fulfillment of the

requirements for the degree of

Master of Science

in

Mechanical Engineering

Winnipeg, Manitoba, Canada 2000

THE UNIVERSITY OF MANITOBA

FACULTY OF GRADUATE STUDIES

*****

COPYRIGHT PERMISSION PAGE

Two-Phase (Gas-Liquid) Flow Distribution in the Outlet Branches of a Horizontal Multi-Branch Header

BY

Zoskales Teclemariam

A Thesis/Practicum submitted to the Faculty of Graduate Studies of The University of Manitoba in partial fulfillment of the requirements of the degree of

Master of Science

ABSTRACT

The study of two-phase flow in multiple branches discharging from headers or manifolds has become increasingly important since it has many industrial applications. Examples of these applications include shell-and-tube heat exchangers, boilers and evaporators, the primary heat-transport system of nuclear reactors, and wet-steam distribution systems for enhanced oil recovery.

The safety analysis of CANDU (CANada Deuterium Uranium) reactors includes postulated accident scenarios in which a steam-water mixture is to be present in the headers and the feeders (components of the CANDU heat-transport system). Knowledge of phase and liquid distribution in the headers and feeders is essential to predict behaviour of the reactor under LOCA conditions.

Very little published information is available on two-phase flow behaviour in the header-feeder system. Kowalski and Krishnan (1987) investigated vapour-pull-through and liquid-entrainment phenomena in the header. Experimental studies of liquid and vapour distribution in a replica of a CANDU header-feeder system were conducted by Kowalski and Hanna (1989). The authors measured water levels in the header as well as flows and void fraction in some feeders.

In the present study, an experimental flow loop was designed and constructed to investigate the two-phase flow distribution in a simulated CANDU header-feeder system.

The header in this experiment, made of a transparent material, was a scaled-down version of the one used in Kowalski and Krishnan (1987) using a scaling ratio of approximately 8.5:1. Experiments were conducted using air-water mixtures at room temperature and a nominal header pressure of 170.3 kPa (abs). The test matrix included one- and two-turret injection, two inlet water flow rates (15 and 30 kg/min) and four different air flow rates for each water flow rate, giving inlet qualities of 3%, 1.5%, 0.75% and 0.375%. The outlet flow rates of air and water were measured in all the feeders under the condition of equal pressure drop across the feeders.

The data, presented in tabulated and graphical forms, show that there is significant variation in air and water flow rates among the feeders, both in the axial and circumferential directions. The flow distribution among the feeders was found to be strongly dependent on the inlet flow conditions (mass flow rates of air and water) and the type of injection (one or two turrets). The flow conditions in the header were observed and these were able to be used in some circumstances to explain the outlet flow rate distribution in the feeders. Finally, correlating equations were developed for three-quarters of the experimental data using a Lockhart-Martinelli-type parameter and the feeder quality. These equations agreed with the experimental data with approximately 89% of the correlated experimental data falling within ±30% of the predicted values.

ACKNOWLEDGEMENTS

I would like to thank my advisors Dr. H.M. Soliman and Dr. G.E. Sims, for their valued guidance and encouragement towards the successful completion of this thesis. I would like to thank Mr. John Finken for his numerous hours of technical assistance in the laboratory and Mr. Irwin Penner for his skilful machining of the test section.

I very much appreciate the help of Dr. J.E. Kowalski of Atomic Energy of Canada Limited by way of his advice, participation in many discussions and liaison with AECL. I acknowledge the stimulating discussion with Professor B.J. Azzopardi and all-round help of my fellow students Mr. C. Van Gorp, Mr. E. Siow and Dr. M. Sujumnong. I thank the Department of Mechanical and Industrial Engineering for providing me with a Teaching Assistantship position. The financial assistance of AECL, Whitshell Laboratories, is also appreciated.

Last but not least, I would like to thank my family and close friends for their endless patience and support through out my graduate studies.

TABLE OF CONTENTS

PAGE

LIST OF FIGURES

LIST OF TABLES

NOMENCLATURE

a	correlation constant in Equation (4.3)
b	correlation constant in Equation (4.3)
C	uncertainty due to the calibration process
D	uncertainty due to discrimination in the instrument
d	branch diameter, *mm*
dev	deviation between the original and repeatability data, %
F	uncertainty due to fluctuations
h	vertical distance between the centreline of the branch and the flat interface, *m*
h_d	critical height at OGE or OLE, *m*
I	error in fitting of mathematical functions to the calibration data
l	separation distance between branches centre to centre, *m*
$\dot{m}$	mass flow rate, *kg/min*
N	the number of measurements made in the individual feeders
OGE	onset of gas entrainment
OLE	onset of liquid entrainment
P	pressure, *kPa*
R	gas constant, *kJ/(kg·K)*
R_l	hydraulic resistance, $(kg \cdot m)^{-0.5}$
$SLPM$	standard litres per minute
T	temperature, $^\circ C$ or K
V	voltage, *volts*

$\dot{V}$ volumetric flow rate, *SLPM* or cm^3/min

Greek

ρ density, kg/m^3

ΔP pressure difference, *kPa* or *cm of water*

$(\Phi_g)^2$ Lockhart-Martinelli-type parameter defined by Equation (4.1)

ω uncertainty

Subscripts

bar barometric

g gauge

$\dot{m}$ related to mass flow rate

$\dot{m}_1$ related to inlet gas mass flow rate

$\dot{m}_2$ related to fluctuation in the air-water interface in the separation (measuring) tank

o test section

P related to pressure

P_{bar} related to barometric pressure

P_g related to gauge pressure

R related to gas constant

sp single phase

T related to temperature

tp two phase

$\dot{V}$ related to volumetric flow rate

CHAPTER 1

INTRODUCTION

Many industrial applications involve two-phase flow in multiple branches (feeders) connected to headers or manifolds. Examples of these applications include boilers and evaporators, the primary heat-transport system of nuclear reactors, shell-and-tube heat exchangers, and wet-steam distribution systems for enhanced oil recovery.

An important application is the two-phase-flow situation that may arise during some postulated loss-of-coolant accidents (LOCAs) in CANDU (CANada Deuterium Uranium) nuclear reactors. The primary heat-transport system of a CANDU reactor consists of a large number of horizontal fuel channels connected by feeder pipes to the inlet and outlet horizontal headers located above the reactor core. The headers are large-diameter pipes (~0.4m) with multiple connections to other components in the reactor such as steam generators and pumps. The feeders on the headers are arranged in equally spaced banks along the length of the header. Each bank has five feeders attached to the header at different angles. Vertical turrets are connected to the top of each header. These turrets supply the cooling fluid to the inlet header and remove the cooling fluid from the outlet header. During a LOCA, two-phase liquid-vapour flow may occur in the headers and feeders. The distribution of the two-phase flow in the headers and feeders is a determining factor for the adequate removal of heat from the core.

Previous studies have made attempts to understand the two-phase flow phenomena in manifolds. Unfortunately, most of the literature has been limited to simple geometries and a maximum of three outlet branches, the results of which cannot easily be extended to apply to complex geometries such as a CANDU header-feeder configuration. Kowalski and Krishnan (1987) investigated vapour-pull-through and liquid-entrainment phenomena in the header. Experimental studies of liquid and vapour distribution in a replica of a CANDU header-feeder system were conducted by Kowalski and Hanna (1989). Two-phase mixtures of varying quality were injected into the inlet header during these tests. The flow rates and void fractions were measured in some of the feeders and water levels were measured in the header. That study did not include any visual observation of the flow patterns in the header due to the high pressures and temperatures involved.

The first objective of the present study is to perform two-phase flow experiments on a scaled-down version of the header that was used by Kowalski and Krishnan (1987) and Kowalski and Hanna (1989) such that the flow rate and quality in all the feeders can be measured independently. The second objective is to make visual observations of the flow patterns in the header at various inlet conditions. This information can be useful for validation of thermalhydraulic codes used in reactor safety analysis.

With the above objectives in mind, an experimental rig was constructed with the following specifications: The test section consists of a transparent header (38.1 mm in diameter and 484.8 mm long) equipped with two inlet turrets (36.2-mm I.D.) and 30 feeders (six banks of five feeders) of 6.4-mm I.D. These dimensions correspond to the

header used by Kowalski and Krishnan (1987) and Kowalski and Hanna (1989) with a scaled-down ratio of approximately 8.5:1. A photograph of the test section used in the present study is shown in Figure 1.1. The experiments were conducted with air-water (gas-liquid) mixtures at room temperature and a nominal absolute pressure in the header of 170.3 kPa (24.7 psi abs). The independent parameters in this experiment were identified as the type of injection (one turret or two turrets), inlet gas and inlet liquid flow rates. The dependent variables were the gas and liquid mass flow rate in the feeders, and the pressure drop across the feeders. A total of 16 tests were conducted using one- and two-turret injection and various inlet flow rates of gas and liquid. In each test, the individual outlet mass flow rates of gas and liquid from the feeders were measured under the condition of equal pressure drop across all 30 feeders. The feeder quality was calculated from the mass flow rates of the gas and liquid. Also, the flow conditions in the header were visually observed for the different inlet conditions and those observations were used, in some circumstances, to explain the outlet flow rate distribution in the feeders. Finally the data were correlated in terms of appropriate parameters. The terms 'air' and 'gas' are used interchangeably in this thesis as are the terms 'water' and 'liquid'. The terms 'branch' and 'feeder' are also used synonymously.

The importance of this study to the understanding of the flow behaviour in a CANDU header during LOCA situations is obvious. However, the applicability is not limited to CANDU reactors. The concepts derived from this study can be extended to other areas where a similar type of geometry and two-phase flow are encountered.

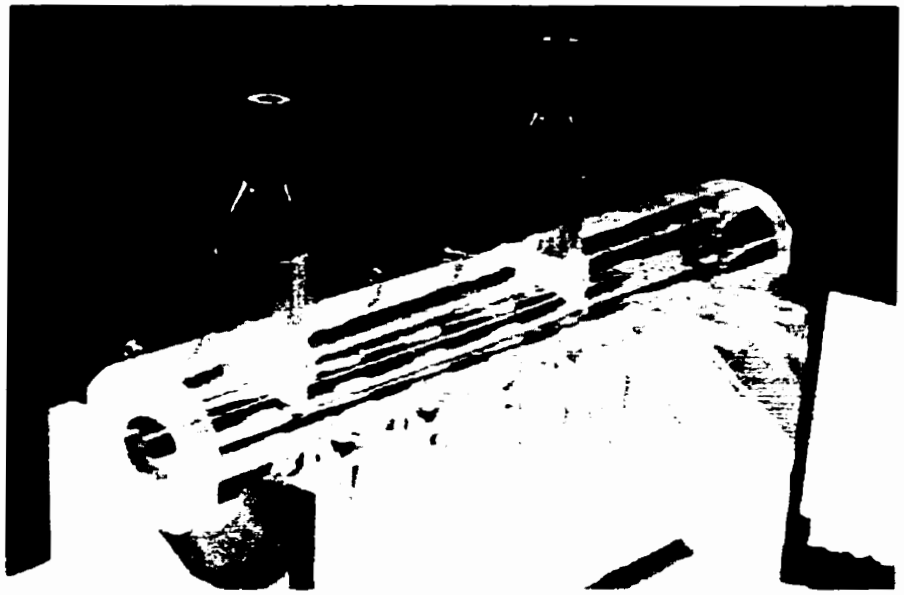

Figure 1.1 Photograph of the Test Section Used in the Current Study

CHAPTER 2

LITERATURE REVIEW

2.1 Introduction

This chapter gives a review of the literature that is relevant to the present study. For a stratified (gas-liquid) flow in a large vessel with small discharge branches, one of the following flow conditions could be present in a given branch; gas only, liquid only or a mixture (two-phase). The onset of gas entrainment (OGE) is defined as the point where gas starts to flow through a given branch that has only liquid flow. Similarly, the onset of liquid entrainment (OLE) is defined as the point where liquid starts to flow through a given branch that has only gas flow. Studies prior to the mid-1980s typically concentrated on the onsets of gas and liquid entrainment. A majority of the studies in the area of two-phase flow in a branch (relevant to the present study) came about after the mid-1980s and these will be reviewed in this chapter. Studies on two-phase flow in a single-discharge branch are reviewed first followed by two-phase flow in multiple-discharge branches.

2.2 Single-Discharge Investigations

Smoglie and Reinmann (1986) performed experiments with air-water flows in a horizontal pipe with a branch at the top, side, or bottom of the pipe. The apparatus consisted of a horizontal main pipe (206-mm I.D., 6-m total length) with a circular branch (inner diameter d = 6, 8, 12, or 20 mm). The experiments were performed with stratified cocurrent air-water flow in the horizontal pipe at ambient temperature and a

system pressure of 0.5 MPa. The flow through the branch was regulated by a valve. The authors developed correlations to predict the quality in the branch for each of the three orientations. The correlations were functions of the density ratio of the two phases and the dimensionless interface level h/h_d in the main pipe, where h is the vertical distance between the centreline of the branch and the flat interface in the main pipe and h_d is the critical height where OGE or OLE occurred. As such, the authors claimed that the correlations were valid for any arbitrary fluid properties and arbitrary flow geometries downstream of the branch entrance. Correlations for the OGE and OLE were also developed.

Schrock et al. (1986) conducted two-phase flow experiments in a horizontal pipe with top, side or bottom branches. The two-fluid combinations used were steam-water and air-water. The main pipe was 102 mm in diameter and the branches were 4, 6, or 10 mm in diameter. The absolute system pressure used was as high as 1.07 MPa. Correlations, that are functions of the dimensionless interface level h/h_d, were developed for the branch quality.

Yonomoto and Tasaka (1988) investigated experimentally and theoretically the phenomenon of two-phase flow discharged from a stratified two-phase region through a small break orifice (branch). A horizontal square duct with an inner side length of 190 mm and orifice sizes of 10 or 20 mm were used in the experiments. The experiments were conducted at a maximum system pressure of 0.7 MPa and room temperature in a steady-state condition. The experimental parameters were the following: orifice

orientation (top, side or bottom), orifice diameter, pressure, water level in the duct, differential pressure across the orifice, and inlet and outlet flow rates of air and water. The experimental results agreed to a large extent with their correlations for the quality and mass flux in the break orifice. Yonomoto and Tasaka (1990) made some empirical modifications to the models in Yonomoto and Tasaka (1988) and conducted more experiments to investigate in detail the effects of flow parameters on entrainment. The experimental apparatus and conditions were similar to those in Yonomoto and Tasaka (1988). By using the empirical modifications, the break flow rate for different flow conditions in the main duct were correlated to an accuracy of ±30%.

Micaelli and Memponteil (1989) studied two-phase steam-water stratified flow in a horizontal pipe with a single branch. The diameter of the main pipe in the experiments varied from 102 to 284 mm while the branch diameter varied from 4 to 34 mm. The branch was oriented vertically upwards, horizontally, or vertically downwards. The system pressure was varied from 0.2 to 7 MPa. Correlations for predicting the OGE and OLE, as well as the quality in the branch, were given for each branch orientation. In a similar fashion to Smoglie and Reinmann (1986), the correlations for the branch quality were given in terms of the dimensionless interface level and the density ratio.

Hassan et al. (1998) presented experimental data for the quality and mass flow rate of two-phase air-water flow in a small branch (6.35-mm I.D.) located on the side of a large reservoir under stratified conditions. The pressure of the test section P_o ranged from 316 to 517 kPa and the interface levels varied between those at OGE and OLE. The test-

section-to-separator pressure difference ΔP ranged from 40 to 235 kPa and the hydraulic resistance R_l in the line connecting the test section and the separator was varied from 1000 to 3000 $(kg \cdot m)^{-0.5}$. Each set of tests in the experiment contained data points covering interface levels between those at OGE and OLE while P_o, ΔP, and R_l were held constant. The values of P_o, ΔP, and R_l were varied among the data sets to allow for the individual assessment of the influence of each independent parameter on the two-phase mass flow rate and quality. Empirical relations were developed for the prediction of the two-phase mass flow rate and quality based on the normalized interface level. In the case of quality, the relation also involved the density ratio of the two phases.

2.3 Multiple-Discharge Investigations

The above studies investigated two-phase flows through a single branch in a channel or reservoir containing stratified flow. The following studies considered two-phase flow from more than one branch in a channel containing stratified flow. Kowalski and Krishnan (1987) and Kowalski and Hanna (1989) studied two-phase steam-water flow in a large manifold typical of a CANDU reactor header-feeder system. The test facility consisted of inlet and outlet headers connected by 30 feeders. The inlet and outlet headers had dimensions typical of CANDU systems, but with half the normal length (0.325-m I.D. and 4.2-m length). Vertical turrets attached to the top of the inlet header supplied a mixture of steam and water. Each header was connected to six banks of feeders. Each bank had five feeders, two of which were attached to the header horizontally, two were at 45° downwards from the horizontal and one was attached vertically downwards. The test conditions were such that the total water injection flow rates used were 30, 45, and 60

kg/s, while the steam injection flow rate was varied from 0.05-2.4 kg/s. The inlet-header pressures used were 1, 2, and 5 MPa. The apparatus was instrumented extensively. Three differential-pressure transmitters and three conductivity-probe assemblies were used to infer the water level at three locations along the header. The void fraction and volumetric flow rate were measured at three out of the six banks of feeders along the header. Visualization of the flow structure in the header was not possible due to the high pressures and temperatures involved thereby requiring a metallic (non-transparent) test section.

Based on the void-fraction and volumetric-flow-rate measurements at the three banks of feeders, the authors (1987 and 1989) detected flow stratification in the headers both in the case of one-turret and two-turret modes of injections. In general, the water level in the header decreased as the injection quality increased. In the one-turret injection tests, the water level was low near the injection turret and rose considerably with distance downstream from the turret. In the case of two–turret injection, the water level was highest between the two turrets. Kowalski and Hanna (1989) also compared their experimental results with simulation results from an in-house computer program for the analysis of a loss-of-coolant accidents (LOCAs).

Rong and Kawaji (1995) performed experiments to study two-phase air-water flow distribution in multiple channels that are connected in parallel as in the case of a stacked-plate heat exchanger. Adiabatic experiments were carried out in a parallel-flow assembly consisting of three to seven flat flow channels with round fins and common transparent

inlet header. The maximum mass flow rate of either fluid was 0.039 kg/s and the maximum flow quality was 0.22. The channels were tested in both vertically upward and vertically downward flow directions. The outlet air and water volumetric flow rates were measured from each channel separately. Highly non-uniform flow distribution was observed in the channels under most test conditions, especially for the vertically downward flow orientation. The inlet flow rate and quality, flow channel orientation, and geometry of the channel inlet port also affected the flow distribution in the channels. The two-phase flow patterns in the transparent header were identified by visual observation for different test conditions. The study also showed that partial flow blockages placed in the inlet port of each channel could improve the flow distribution.

Hassan (1995) performed an experimental investigation on two-phase flow for two side horizontal branches (6.35-mm I.D.) with centrelines falling in the same horizontal or vertical plane. The branches were mounted on a vertical wall on the side of a high-pressure reservoir containing stratified air and water. The separation distance of the branches examined were l/d=1.5, 2.0, 3.0, and 8.0. The following ranges were covered: P_o = 316 and 516 kPa, ΔP = 37 to 229 kPa, and R_l = 900 to 3000 $(kg.m)^{-0.5}$, where P_o is the test-section pressure, ΔP is the test-section-to-separator pressure drop, and R_l is the hydraulic resistance in the lines connecting the test section to the separators. Empirical correlations were given for the two-phase mass-flow rate and quality in the branches for the different centreline orientations on the vertical wall. The author also conducted experiments with three branches installed on a semi-circular wall where the dimensions of the wall-branches assembly were selected to be in direct proportion to the CANDU

header-feeder system. No attempt was made to derive correlations for the branches on the semicircular wall.

2.4 Closure

The above literature review shows that some information on two-phase flow in single- and multiple-branch-discharge conditions is available. However, the amount of information available on multiple discharge from headers is especially limited in scope. The results from these single- and multiple-discharge studies cannot be extrapolated to provide all the necessary information on the two-phase flow distribution in complex-geometry manifolds of which the CANDU inlet header is one example. Further efforts are obviously needed to develop more understanding of the two-phase flow from headers with multiple branches. These efforts can provide the necessary information for flow situations encountered in many applications, such as in heat exchangers, cooling systems of nuclear reactors under LOCA, flow-distribution systems, and boilers.

CHAPTER 3

EXPERIMENTAL INVESTIGATION

3.1 Introduction

This chapter describes the experimental apparatus used including the flow loop, test section, and instrumentation. As well, the experimental conditions and procedure are discussed. Finally, a summary of the experimental uncertainty is given.

3.2 Test Facility

The experimental facility described in this thesis is located at the Department of Mechanical and Industrial Engineering, University of Manitoba. The facility consists of a well-instrumented gas-liquid flow loop, and a simulated CANDU header-feeder system as the test section.

3.2.1 Test Section

The test section consists of a header that has two inlet turrets and 30 outlet feeders arranged in six banks of five feeders around the header. The header itself was bored out from an acrylic cylinder. The turrets and feeders were also bored out from acrylic rods and attached to the main body of the header. The feeders are spaced out uniformly along the length of the header. Each bank of five feeders consists of two feeders that emerge horizontally from the header, two that emerge at 45 degrees downwards from the horizontal and one that emerges vertically downwards. The header, turrets and feeders

have internal diameters of 38.1 mm (1.5 in.), 36.2 mm (1.425 in.), and 6.4 mm (0.25 in.), respectively. The length of the header is 484.8 mm. The two ends of the header were sealed with end caps which were held in place with a clamp-like arrangement. The detailed dimensions of the different parts of the header are shown in Figures 3.1 and 3.2.

3.2.2 Notation

A matrix-type system in the form of (i,j) was used to identify the feeders, as shown in Figure 3.3. The feeders that emerge from the header horizontally have an i-value of 1. The feeders that emerge from the header at 45 degrees from the horizontal have an i-value of 2, and the feeders that emerge vertically downwards from the header have an i-value of 3. The banks of feeders from the left end of the header to the right end each have a j-value of 1 through 6, respectively.

3.2.3 Flow Loop

A schematic diagram of the flow loop is shown in Figure 3.4. The flow loop consists of a water pumping station with a by-pass line, a compressed air line with a pressure controller, two mixers, the header-feeder system, a measuring separation tank, a residual separation tank and several instruments for pressure, temperature and flow-rate measurement. The measuring separation tank and the residual separation tank are hereafter referred to as the measuring tank and the residual tank, respectively. Detailed sketches of the measuring and residual tanks are shown in Figure 3.5 and a schematic diagram of the mixers is shown in Figure 3.6.

Distilled water was pumped from a water tank and the desired flow rate was measured using rotameters before it was directed into the mixers. The water in the tank was maintained at approximately room temperature using a cooling coil that was submerged in the tank. A separate rotameter was used for each mixer. A by-pass line directed the remaining water back to the water tank. Air was supplied from a central compressing station in another campus building. Some of the air was released into the atmosphere through a by-pass line while the rest was measured using rotameters before it entered the mixers. Again, each mixer had its own set of rotameters. The two-phase flow from the mixers was then injected into the header through one or two turrets. During the one-turret experiments, only the mixer that injects flow into turret A was operated while the mixer that injects flow into turret B was completely shut off (see Figure 3.4). During two-turret experiments, identical flow rates were fed into each of the two mixers. The inlet flow left the header through the feeders. A series of on/off ball valves were used to direct the flow from each feeder into either one of the separation tanks. The flow from the feeder being measured was directed into the measuring tank while the flow from all remaining feeders was directed into the residual tank. The two-phase mixture that entered the measuring tank was separated into water and air. The air was measured by a bank of rotameters before it was released into the atmosphere. The water from the measuring tank was also measured by a bank of rotameters before it was returned to the water tank. The air that went into the residual tank was exhausted into the atmosphere through one or two gate valves in parallel. The water that went into the residual tank was returned to the water tank through a gate valve at the bottom of the residual tank.

A differential-pressure transmitter was used to measure the pressure difference between the measuring tank and the residual tank. Another differential-pressure transmitter was used to measure the pressure difference between the header and the residual tank. The pressures in the inlet and outlet air rotameters, header and separation tanks were all measured using Bourdon pressure gauges. Thermocouples were used to measure the temperature of the inlet and outlet air.

3.3 Instrumentation

Several instruments were used to measure and control different variables in the flow loop. Air and water flow rates into the test section and out of the test section were measured using rotameters. Rotameters with different capacities were used to measure the different flow rates. The flow rate through the rotameters was controlled using needle valves. The needle valves on the air side were located upstream of the rotameters. The needle valves on the water side were located downstream of the rotameters. Inlet and outlet air temperatures were measured using iron-constantan thermocouples. The pressures at the inlet-air rotameters, header, and both separation tanks were measured using Bourdon gauges. The pressure difference between the header and the residual tank, as well as the pressure difference between the measuring and residual tanks were measured using Rosemount differential-pressure transmitters. A submersible circulating pump was used to pump water from the water tank to the test section. A feedback pressure controller (Fisher 4160K series) and a regulator were used to minimize fluctuations in the air supply pressure. The specifications and the duty of each instrument in the flow loop are listed in Tables 3.1 through 3.4. The location of the flow meters, Bourdon gauges and

thermocouples in the flow loop are shown in Figure 3.4. All the measuring devices were calibrated, as discussed in Section 3.6.

Table 3.1 Specification and Duty of the Pressure-Measurement Instruments

Instrument	Specification	Measured Variable
Pressure transmitter No. 1	Rosemount differential-pressure transmitter Model: 1151DP3A22GCSA Range: 0-30 in. H_2O (0-76.2 cm)	Difference in pressure between the measuring tank and the residual tank
Pressure transmitter No. 2	Rosemount differential-pressure transmitter Model: C1151DP3E22B1C6 Range: 0-30 in. H_2O (0-76.2 cm)	Difference in pressure between the residual tank and the header
Pressure gauge No. 1	USG Bourdon gauge Range: 0-200 psig (0-1379.5 kPa gauge)	Pressure of air supply before the pressure controller
Pressure gauge No. 2	Marshall town Bourdon gauge Range: 0-100 psig (0-689.8 kPa gauge)	Pressure of air supply after the pressure controller
Pressure gauge No. 3	USG Bourdon gauge Range: 0-100 psig (0-689.8 kPa gauge)	Pressure in measuring separation tank
Pressure gauge No. 4	USG Bourdon gauge Range: 0-100 psig (0-689.8 kPa gauge)	Pressure in residual separation tank
Pressure gauge No. 5	Marshall town Bourdon gauge Range: 0-60 psig (0-413.9 kPa gauge)	Pressure at the air inlet rotameters (line A)
Pressure gauge No. 6	USG Bourdon gauge Range: 0-100 psig (0-689.8 kPa gauge)	Pressure in the header
Pressure gauge No. 7	USG Bourdon gauge Range: 0-15 psig (0-103.5 kPa gauge)	Pressure of air in the outlet air rotameters
Pressure gauge No. 8	Marshall town Bourdon gauge Range: 0-100 psig (0-689.8 kPa gauge)	Pressure at the outlet of the submersible water pump
Pressure gauge No. 9	WIKA Bourdon gauge Range: 0-60 psig (0-413.9 kPa gauge)	Pressure at the air inlet rotameters (line B)

Water manometer	Range: 0-18 in. H_2O (0-45.7 cm)	Pressure of air in the outlet air rotameters

Table 3.2 Specification and Duty of the Air-Flow-Rate-Measurement Instruments

Instrument	Specification	Measured Variable
Rotameter AM1	Brooks rotameter Model: 1355EZ186 Range: 6.47-64.7 SLPM Float Type: Ball	Flow rate of inlet air (line A)
Rotameter AM2	Brooks rotameter Model: 1307EZ80 Range: 38-381 SLPM Float Type: Conventional	Flow rate of inlet air (line A)
Rotameter AM3	Brooks rotameter Model: 1307EZ84 Range: 200-2004 SLPM Float Type: Conventional	Flow rate of inlet air (line A)
Rotameter AM4	Brooks rotameter Model: 1355EZ186 Range: 6.47-64.7 SLPM Float Type: Ball	Flow rate of inlet air (line B)
Rotameter AM5	Brooks rotameter Model: 1307EZ80 Range: 38-381 SLPM Float Type: Conventional	Flow rate of inlet air (line B)
Rotameter AS1	Brooks rotameter Model: 1355EZ185 Range: 0.17-1.69 SLPM Float Type: Ball	Flow rate of outlet air
Rotameter AS2	Brooks rotameter Model: 1355EZ184 Range: 0.87-8.68 SLPM Float Type: Ball	Flow rate of outlet air
Rotameter AS3	Brooks rotameter Model: 1307EZ83 Range: 4.64-46.4 SLPM Float Type: Ball	Flow rate of outlet air
Rotameter AS4	Brooks rotameter Model: 1307EZ82 Range: 21.4-214 SLPM Float Type: Conventional	Flow rate of outlet air

Table 3.3 Specification and Duty of the Water-Flow-Rate-Measurement Instruments

Instrument	Specification	Measured Variable
Rotameter WM1	Brooks rotameter Model: 1307EZ84 Range: 300-3912 kg/hr Fluid specific gravity = 1.0 Float Type: Conventional	Flow rate of inlet water (line A)
Rotameter WM2	Brooks rotameter Model: 1307EZ97 Range: 142.6-1426 kg/hr Fluid specific gravity = 1.0 Float Type: Conventional	Flow rate of inlet water (line B)
Rotameter WS1	Brooks rotameter Model: 1355EZ183 Range: 8.54-85.4 cm^3/min Float Type: Ball	Flow rate of outlet water
Rotameter WS2	Brooks rotameter Model: 1355EZ182 Range: 49.14-491.4 cm^3/min Float Type: Ball	Flow rate of outlet water
Rotameter WS3	Brooks rotameter Model: 1307EZ81 Range: 250-2955 cm^3/min Float Type: Conventional	Flow rate of outlet water
Rotameter WS4	Brooks rotameter Model: 1307EZ80 Range: 1230-12300 cm^3/min Float Type: Conventional	Flow rate of outlet water

Table 3.4 Specification and Duty of the Temperature-Measurement Instruments

Instrument	Specification	Measured Variable
Thermocouple No. 1	Iron-constantan thermocouple	Temperature of inlet air (line A)
Thermocouple No. 2	Iron-constantan thermocouple	Temperature of inlet air (line B)
Thermocouple No. 3	Iron-constantan thermocouple	Temperature of outlet air

3.4 Experimental Conditions

The tests were divided into two groups: one-turret-injection and two-turret-injection tests. Table 3.5 shows the nominal conditions for the test matrix used in each type of injection. The inlet gas flow rates were varied in each liquid-flow-rate group so that similar inlet qualities were achieved. Inlet quality in this thesis is defined as the inlet gas mass flow rate divided by the sum of the inlet mass flow rates of gas and liquid. In the case of two-turret-injection experiments, the flow rates indicated in Table 3.5 were split equally between the two turrets.

Table 3.5 Nominal Conditions for Experimental Test Matrix

Inlet conditions		
Liquid Flow Rate *(kg/min)*	Gas Flow Rate *(kg/min)*	Quality (%)
15	0.465	3
	0.2325	1.5
	0.11625	0.75
	0.05813	0.375
30	0.93	3
	0.465	1.5
	0.2325	0.75
	0.11625	0.375

Table 3.6 shows the list of tests and the corresponding actual inlet gas flow rate, inlet liquid flow rate, and inlet quality for each test. A total of 16 experiments were performed. The first 8 tests, namely, R-2 through R-5 and R-7 through R-10 are one-turret-injection tests. Tests R-11 through R-18 are two-turret tests. For each type of injection, two inlet liquid flow rates and four inlet gas flow rates were used, allowing coverage over the desired range of operating conditions. Two repeatability tests were also performed. Test RPT-8 was performed under the same nominal inlet conditions as test R-8 and was used

as a repeatability test for the one-turret experiments. Similarly, test RPT-16 was performed under the same nominal inlet conditions as test R-16 and was used as a repeatability test for the two-turret experiments. Both repeatability tests were performed after the completion of all the regular experiments.

In tests R-2 through R-5 and R-11 through R-14, the nominal inlet liquid flow rate was 15 kg/min. For tests R-7 through R-10 and R-15 through R-18, the nominal inlet liquid flow rate was 30 kg/min. For each liquid flow rate in the two groups of experiments, the inlet gas flow rate was varied so that nominal percentage inlet qualities of 3.0, 1.5, 0.75, and 0.375 were achieved.

Table 3.6 Actual Inlet Conditions for Each Test

	Test No.	Inlet Gas Flow Rate (kg/min)	Inlet Liquid Flow Rate (kg/min)	Inlet Quality (%)
One-Turret Injection	R-2	0.460	15.19	2.9
	R-3	0.237	15.19	1.5
	R-4	0.115	15.21	0.75
	R-5	0.0583	15.17	0.38
	R-7	0.969	29.27	3.2
	R-8	0.453	29.33	1.5
	R-9	0.241	29.33	0.81
	R-10	0.1138	29.28	0.39
	RPT-8	0.453	29.36	1.5
Two-Turret Injection	R-11	0.471	15.71	2.9
	R-12	0.231	15.72	1.4
	R-13	0.1177	15.74	0.74
	R-14	0.0578	15.72	0.37
	R-15	0.920	30.16	3.0
	R-16	0.470	30.20	1.5
	R-17	0.2293	30.20	0.75
	R-18	0.1155	30.20	0.38
	RPT-16	0.468	30.24	1.5

3.5 Experimental Procedure

The following numbered steps were followed in performing each of the 16 regular tests and the two repeatability tests.

1. Initially, all valves that led flows from the header to the measuring tank were closed while all valves leading to the residual tank were opened.
2. All valves leading to the air and water outlet rotameters were closed.
3. The desired flow rate of inlet air was injected through line A for one-turret-injection tests by adjusting the inlet needle valve while no flow went through line B. In the case of two-turret-injection tests, equal amounts of flow were injected through rotameters in both lines A and B.
4. The pressure in the header was maintained at an absolute value of 170.3 kPa (24.7 psia) by controlling the amount of air that leaves the residual tank through one of two gate valves.
5. One of the valves that led flows from the header to the measuring tank was momentarily opened until the measuring tank was pressurized to about 170 kPa absolute.
6. The desired flow rate of inlet water was injected through line A for one-turret-injection tests by adjusting the inlet needle valve while no flow went through line B. In the case of two-turret-injection tests, equal amounts of flow were injected through rotameters in both lines A and B.
7. A steady level of water was maintained in the residual tank by adjusting the gate valve at the bottom of the tank.

8. All the flow from any one feeder (or a pair of feeders in the case of horizontal and 45° feeders) was directed into the measuring tank while the flow from all the other feeders was directed into the residual tank.
9. The outlet flow rates of air and water from the measuring tank were adjusted using the appropriate valves so that an approximate steady water level was achieved.
10. The outlet air valves on both tanks were adjusted so that the pressure difference between the measuring and residual tanks was near zero.
11. Once the pressure difference was adjusted to near zero, the setting of the outlet water valve was fine-tuned to keep the water level in the measuring tank steady.
12. The adjustments in the above two steps were done repeatedly and the level of water in the residual tank was monitored so that it did not overflow or get drained completely. The header pressure was also monitored and kept near 170.3 kPa absolute.
13. A steady-state condition was achieved when the header pressure remained steady near 170.3 kPa absolute, the pressure difference between the residual and measuring tanks remained near zero and the water level in the measuring tank was steady.
14. Once a steady-state condition was achieved, the level of water in the measuring tank was recorded. Subsequently, the following readings were taken: the pressure at the pressure controller, control valve height, inlet air and water rotameters, inlet air temperature, header pressure, pressure difference between the header and residual tank, the pressure difference between the residual and measuring

tanks, the pressure at the outlet of the water pump, the pressure in both separation tanks, outlet air and water rotameters, outlet air temperature, and finally the height of the water level in the measuring tank was recorded again. This data-gathering process took approximately 1.5 minutes to complete.

15. Flow from the vertical feeders in each bank of feeders was measured one feeder at a time. The flows from both the 45° feeders in each bank of feeders were combined and measured together. Similarly, the flows from both the horizontal feeders in each bank of feeders were also combined and measured together. The combined flow rates were taken for the 45° and horizontal feeders with the assumption that each pair of two feeders that are located in the same bank and at the same orientation (45° or horizontal) received equal amounts of flow.
16. All the flow from a particular feeder (or set of two feeders) which had just been measured was now directed into the residual tank. At the same moment, the flow from the next feeder (or set of two feeders) was directed into the measuring tank.
17. Steps 10-16 were repeated until the flow from all 30 feeders was measured. The average time required to complete each experiment according to the procedure described here was about 12 continuous hours.

3.6 Calibration of Measuring Devices

All measuring devices used in this experiment were calibrated in-house and compared with the manufacturer's data. The two differential-pressure transmitters that were used in the experiment were calibrated against a water manometer using a digital voltmeter. The digital voltmeter that was used in the calibration of the differential-pressure transmitters

was also used in the normal running of the experiments. The sensitivity of the digital voltmeter was approximately 10.5 mV per mm of water for both calibration and subsequent experiments. The discrimination on the voltmeter was ±1 mV. The Bourdon pressure gauges were calibrated using a dead-weight tester. Thermocouples were tested using a standard mercury-in-glass thermometer. Air rotameters were calibrated using wet test meters and venturi meters (in turn the calibrations of which are traceable to NIST standards). Air rotameters that have ball-type floats were calibrated at two different pressures since the density correction used in converting the actual flow rates to standard conditions is not as accurate for these rotameters as it is for air rotameters with conventional-type floats. The results of the calibrations at pressures that were closest to the experimental conditions were used in tests that involved air rotameters with ball-type floats. The water rotameters were calibrated using a weigh-and-time method. The calibration results are shown in Appendix A.

The in-house calibration values of the measuring instruments were used in the data analysis. Linear interpolation between two consecutive calibration points was used in the case of air and water rotameters as well as pressure gauges. A linear fitted curve was used in the case of the differential-pressure transmitters.

3.7 Estimates of Experimental Uncertainty

The method of Kline and McClintock (1953) was used in estimating the uncertainties in the experimental data. All the uncertainties quoted here are at "odds" of 20 to 1. The

following sources were identified and taken into consideration in estimating the uncertainties:

1) Experimental fluctuation.
2) Discrimination in the scale of the measuring device.
3) Uncertainties due to the calibration process.
4) Errors associated with fitting mathematical functions to the calibration data.

The principles of the uncertainty analysis and a sample uncertainty calculation are shown in Appendix B. The uncertainties in the inlet mass flow rate of gas and liquid into the header and the outlet mass flow rates of gas and liquid from each feeder are also tabulated in Appendix B for all test runs.

There was significant variation in the flow rate of gas and liquid among the feeders. Some feeders would have mostly gas flow and others would have mostly liquid flow. A summary of the results of the uncertainty analysis follows.

3.7.1 Inlet Gas Flow Rate

The uncertainty in the inlet gas flow rate in both the one-turret-injection and two-turret-injection tests ranged from ±2.4% to ±6.3%.

3.7.2 Gas Flow Rate Through the Feeders

The uncertainty in the gas flow rate for the one-turret-injection tests ranged from ±1.9% to ±6.0% for 88.3% of the data points. Uncertainties outside ±6.0% were all in feeders

(except for one feeder) that had the lowest gas flow rate for the particular test. The uncertainty in the two-turret-injection tests ranged from ±1.9% to ±6.0% for 84.6 % of the data points. Again, with the exception of one feeder, uncertainties that are outside ±6.0% were in feeders that had the lowest gas flow rate for the particular test.

3.7.3 Inlet Liquid Flow Rate

The uncertainty in the inlet liquid flow rate in both the one-turret-injection and two-turret-injection tests ranged from ±1.2% to ±3.0%.

3.7.4 Liquid Flow Rate Through the Feeders

The uncertainty in the liquid flow rate for 81.5% of the data points ranged from ±1.2% to ±6.0% for the one-turret-injection tests. The uncertainties for the two-turret-injection tests ranged from ±1.2% to ±6.0% for 74.1% of the data points. In both the one-turret- and two-turret-injection tests, uncertainties greater than ±6.0% were mostly in feeders that carried the least amount of liquid flow rate for the particular test and the vertical feeders; the relatively low gas flow rate in the vertical feeders made it difficult to attain steady conditions in the measuring separation tank.

All dimensions are in millimetres

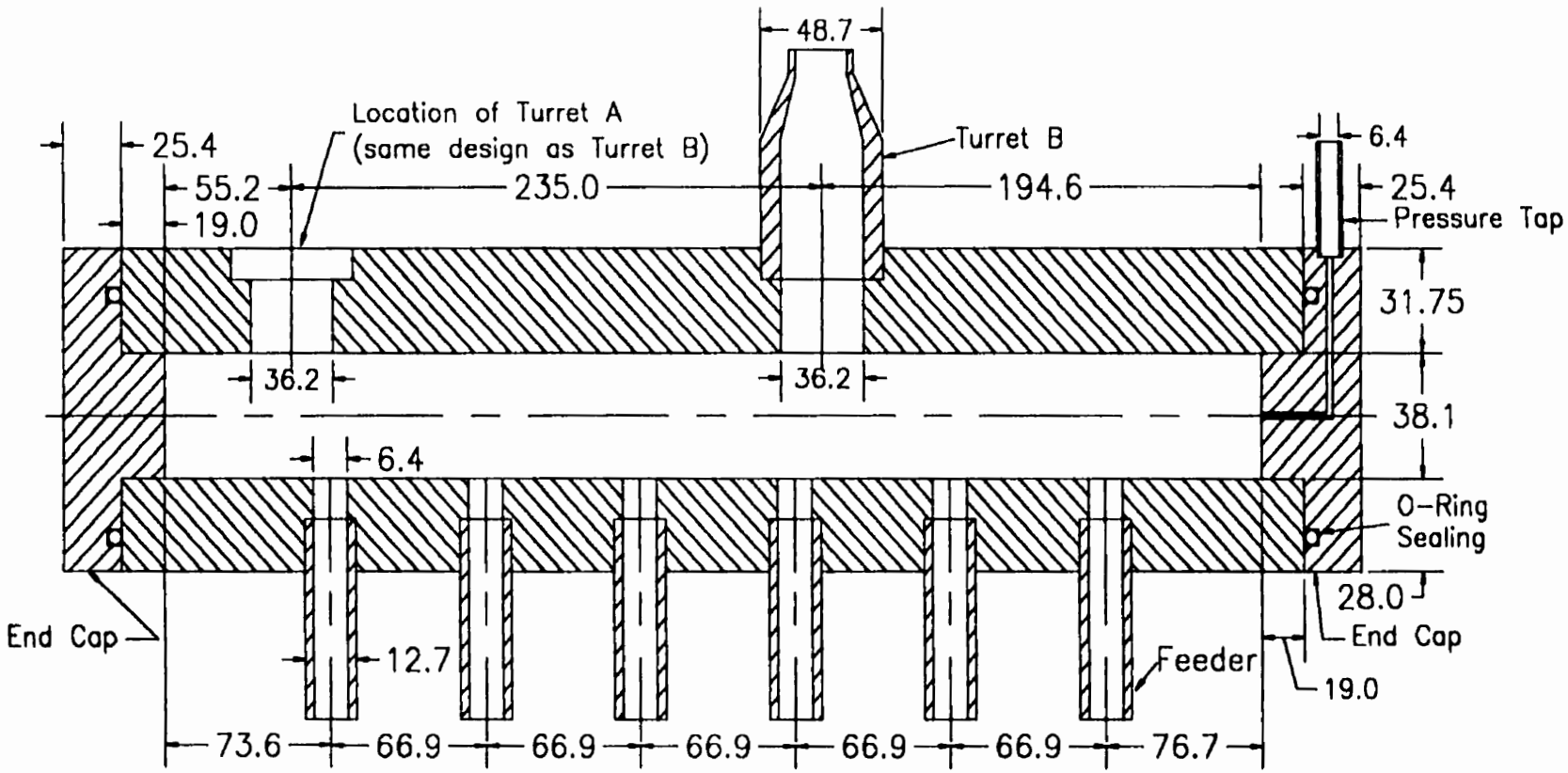

Figure 3.1 Cross-sectional View Along the Axis of the Test Section

All dimensions are in millimetres

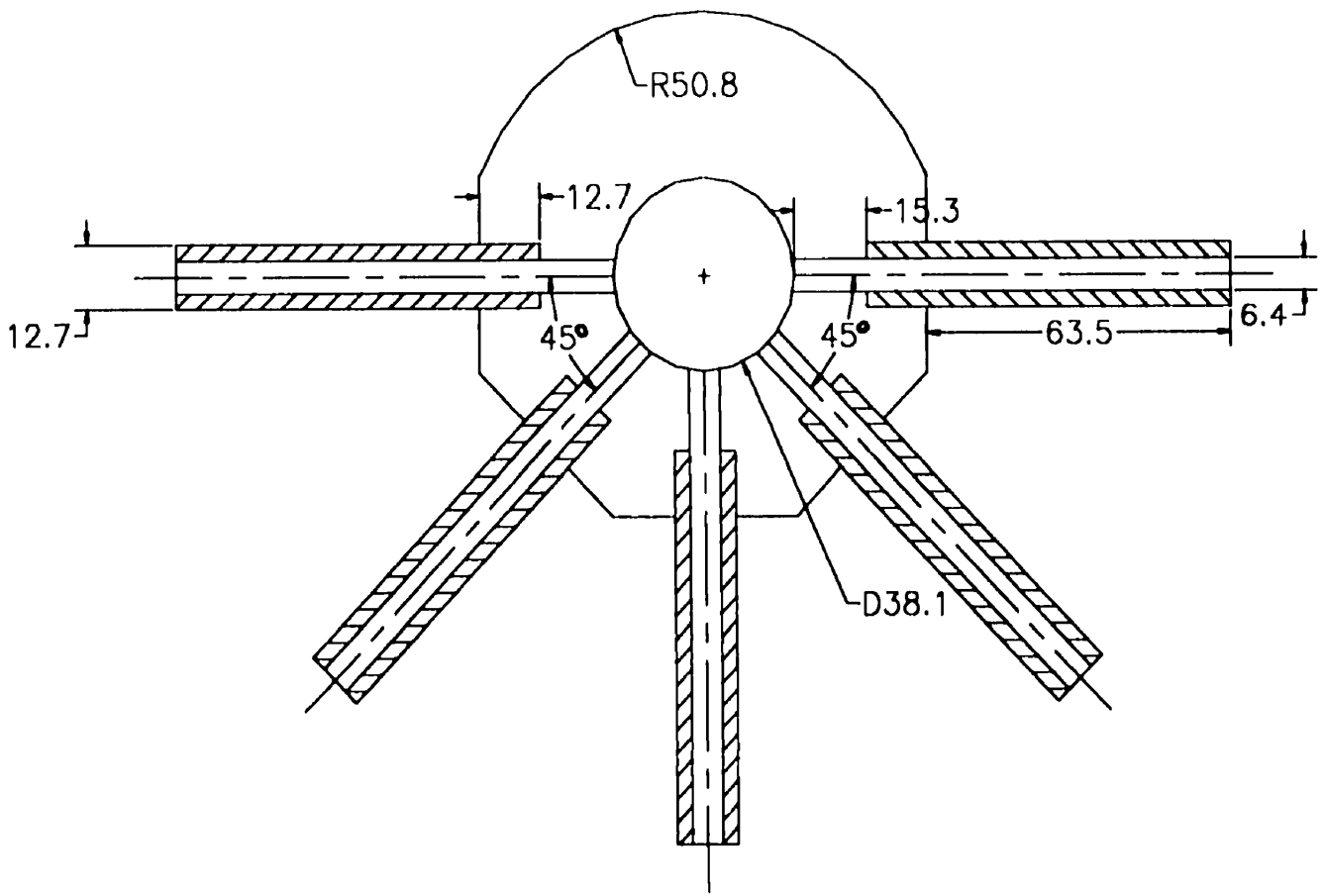

Figure 3.2 Cross-sectional View Normal to the Axis of the Test Section at a Feeder Bank

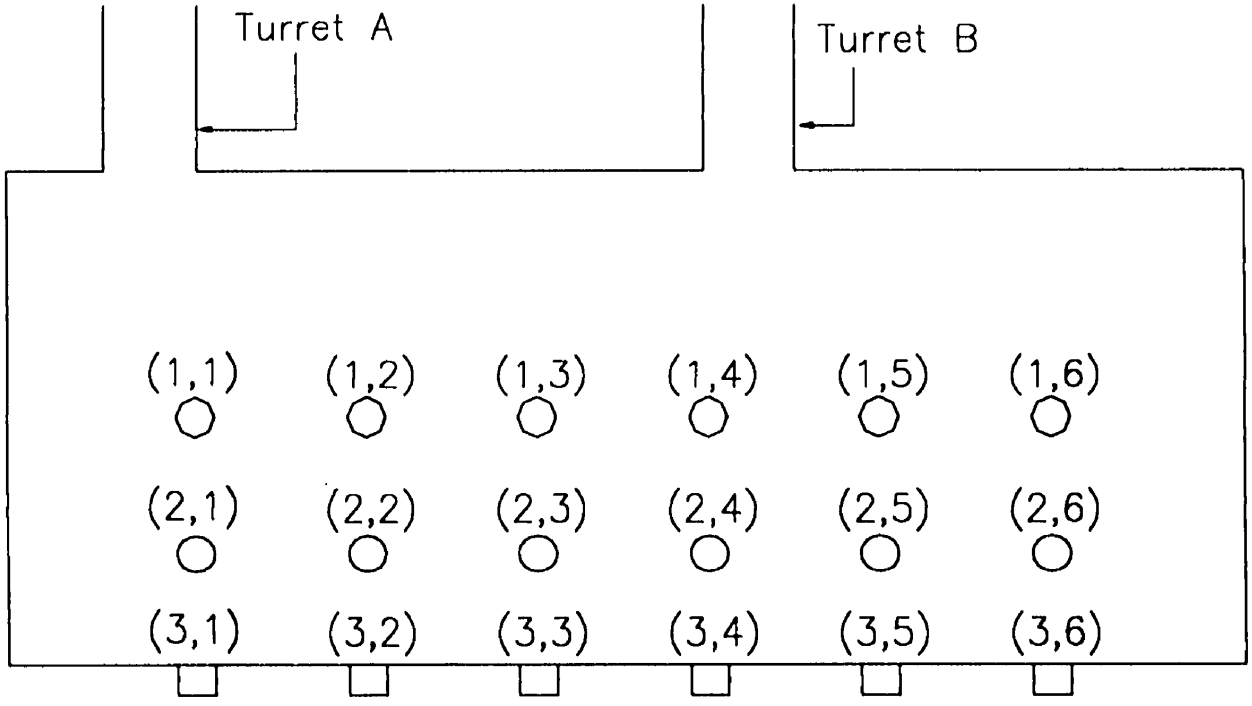

Figure 3.3 Feeder Identification System

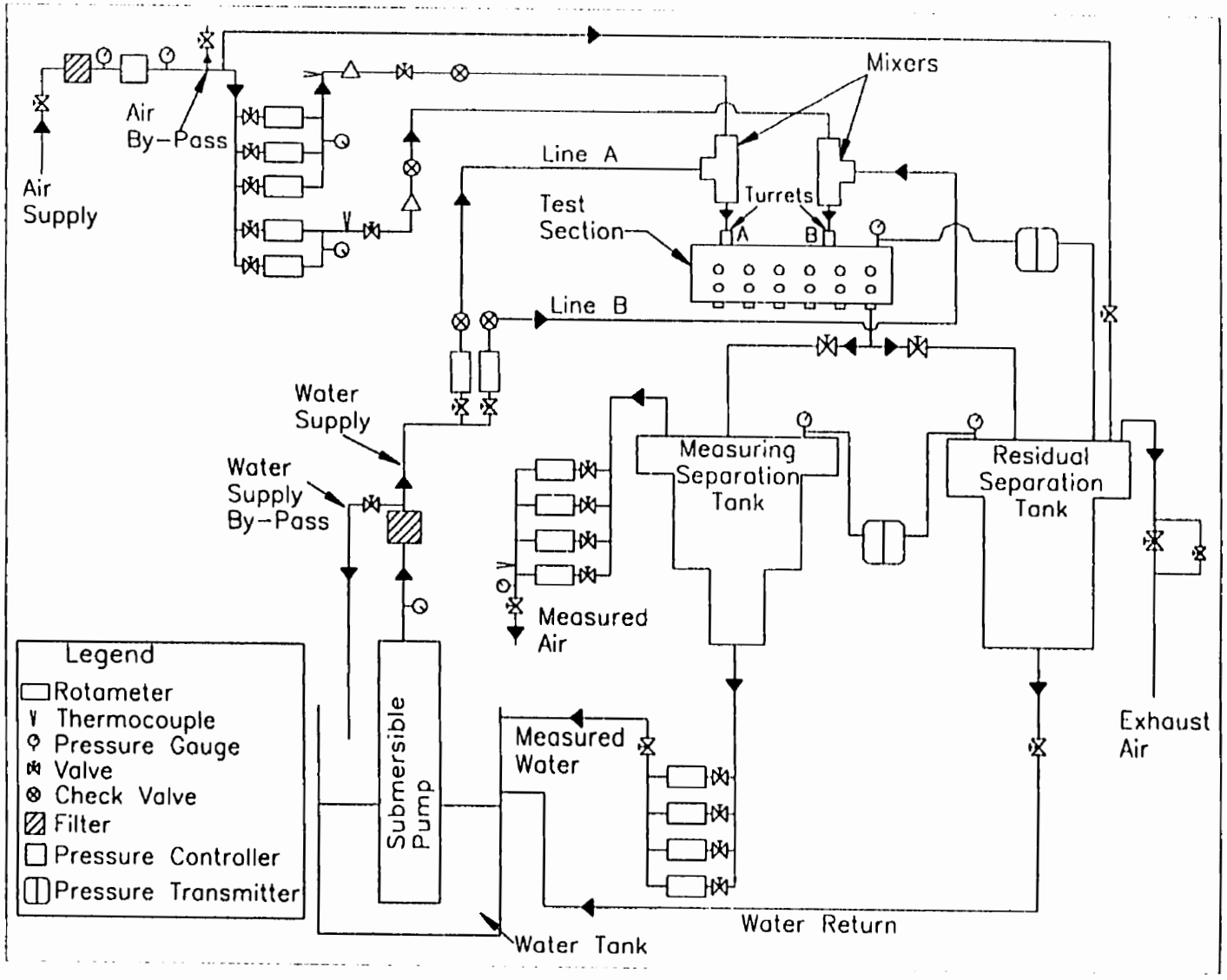

Figure 3.4 Schematic Diagram of the Flow Loop

All dimensions are in centimetres
Drawing not to scale

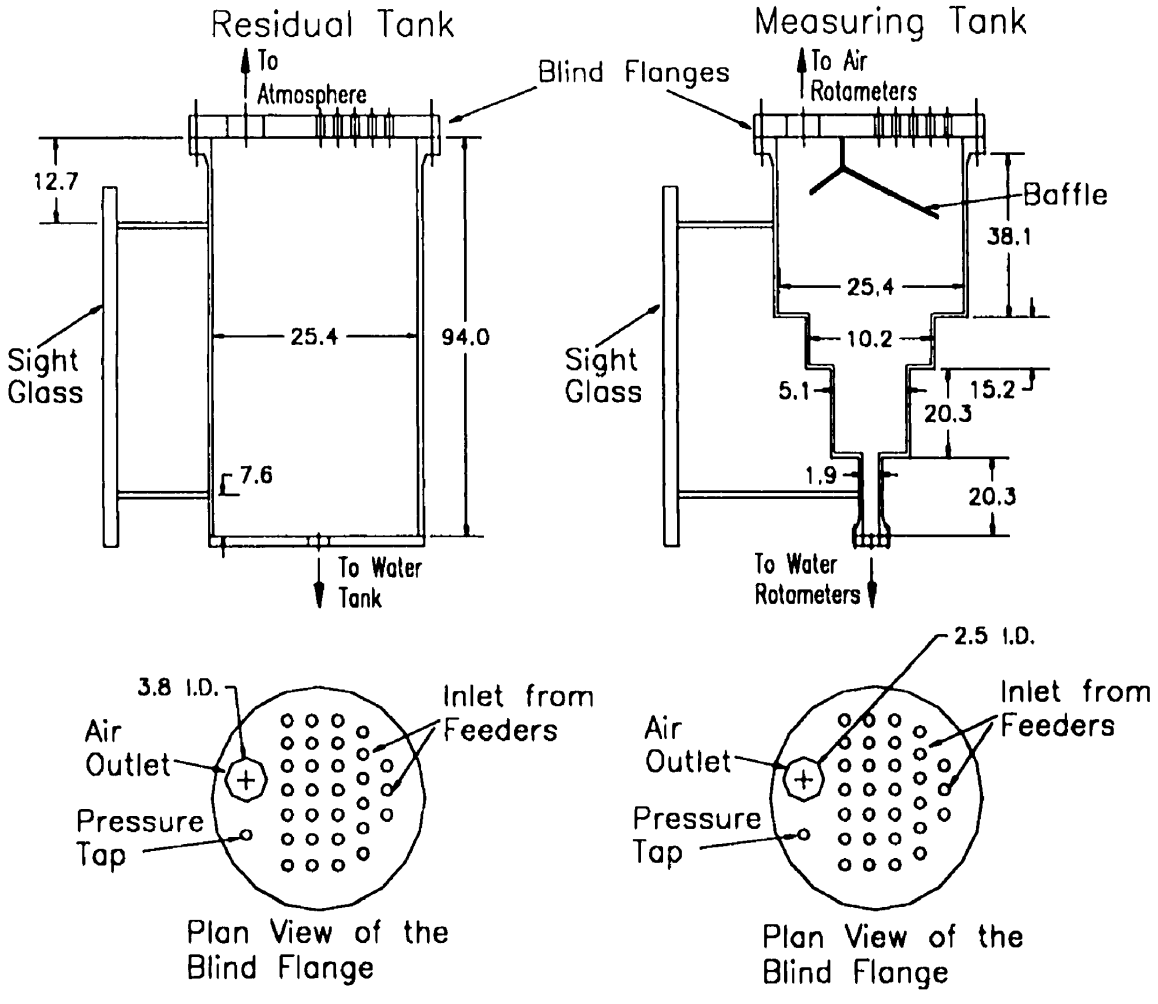

Figure 3.5 Details of the Separation Tanks

All dimensions are in millimeters

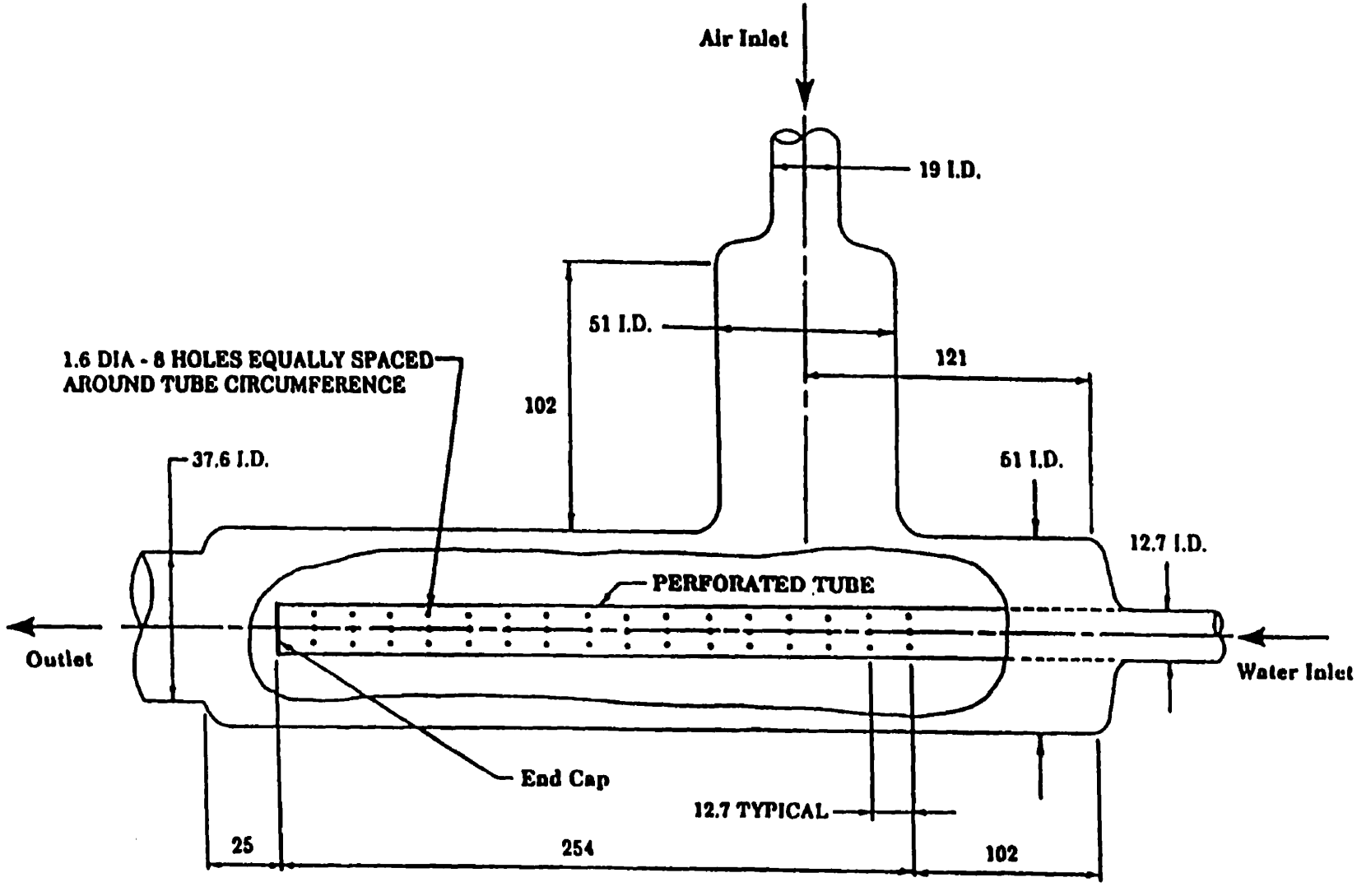

Figure 3.6 Schematic Diagram of the Two-Phase Mixer

CHAPTER 4

RESULTS AND DISCUSSION

4.1 Introduction

The results for all the 16 tests are listed in Tables C.1 to C.16 of Appendix C. The table for each test includes the test number, type of injection, inlet flow rates of gas and liquid, inlet quality, header-to-separator pressure difference, the mass balance error on the gas and liquid sides, as well as the gas flow rate, liquid flow rate and quality in each feeder. Symmetry was assumed for the 45° and horizontal feeders; therefore, only one set of values is listed for each of these feeders. The mass balance error for both gas and liquid is defined by

$$mass\ balance\ error(\%) = \frac{inlet\ flow\ rate - total\ outlet\ flow\ rate}{inlet\ flow\ rate} \times 100$$

For 14 out of the 16 tests, the mass balance error for the water was within ± 2.1% and the maximum error was 5.17%. For inlet air flow rates higher than 0.23 kg/min, the mass balance error was consistently within ±5% (10 of the 16 runs). For the remaining six runs with inlet air flow rates lower than 0.12 kg/min, the mass balance error was within ±7% for four runs and within ±15% for the other two runs. These values are acceptable (some are remarkably good) keeping in mind that the outlet flow rate is the sum of 18 individual readings. The gas mass balance quoted would change by approximately 1% (typically

improving) if corrections for the vapour content at the outlet gas measuring station were introduced (inlet measurement is for dry air containing essentially no water vapour). Two repeatability tests were performed and the results are given in Appendix D.

The results of the experimental investigation are presented in this chapter. As well, the trends in the mass flow rate and quality in the branches are discussed in relation to the effects of the independent parameters and the experimental observations of the flow pattern in the header. This is followed by a discussion on the header-to-separator pressure drop in the tests. Finally, an approach for correlating the data is presented and discussed.

4.2 Mass Flow Rates and Quality in the Feeders

The trends in the mass flow rates as well as the quality in the feeders are discussed in this section and these trends are related to the sketches of the actual flow conditions in the header. The quality in a feeder is defined as the gas mass flow rate in that feeder divided by the sum of the mass flow rates of gas and liquid in the same feeder. The tests are divided into groups of four depending on the type of injection and the inlet liquid flow rate.

4.2.1 One-Turret-Injection Tests: Low Liquid Flow Rate (Test Nos. R-2 to R-5)

In these tests, the air-water mixture was injected into the header through Turret A while Turret B was completely shut off. The gas flow rate, the liquid flow rate and the quality in each feeder for these tests with an inlet liquid flow rate of 15 kg/min and decreasing air flow rate are shown in Figures 4.1 to 4.4.

The general observation from the figures is that qualitatively, the shapes of flow and quality distribution in the feeders do not change markedly with decreasing inlet gas flow rate. There is, though, a significant axial and circumferential variation in the absolute flow rates of gas and liquid as well as in the quality in the feeders.

From these figures, it is seen that the horizontal feeders receive the highest gas flow rate followed by the 45° feeders. The vertical feeders receive the smallest gas flow rate. Some tests show a slight deviation from this trend with some "overlap" in gas flow rates at bank 1 ("overlap" in this discussion will mean that gas flow rates at a given bank do not decrease in the order of horizontal, 45° and vertical orientations; or, in the case of liquid flow rates at a given bank, they do not decrease in the order of vertical, 45° and horizontal orientations). However, when this overlap occurs, the difference in the flow rates is so small that it is fair to state that the general trend mentioned earlier is valid. The gas flow rates from the horizontal feeders and 45° feeders gradually increase from the left end of the header to the right end of the header until it reaches a peak around bank 4 or 5 (bank 5 most of the time) beyond which it drops sharply to the value at bank 6. However, the gas flow rate in the vertical feeders does not show a clear common trend and the axial variation of gas flow rate in these feeders is generally small compared with the other feeders. As one would expect, the magnitude of the gas flow rate in the feeders decreases with decreasing inlet gas flow rate (a behaviour seen with the other groups of tests).

The general trend of the liquid flow rate in the feeders is the reverse of the trend in the gas-flow-rate distribution. At any feeder bank, the vertical feeders receive the highest

liquid flow rates and the horizontal feeders receive the least. Figures 4.1 to 4.4 show that liquid flow rate in the vertical feeders initially drops from bank 1 to bank 2 followed by a gradual increase until it reaches a maximum at bank 6. The liquid flow rate in the horizontal and 45° feeders show relatively small axial variation except for a sharp increase from bank 5 to bank 6.

As regards quality, as shown in Figures 4.1 to 4.4, the horizontal feeders have the highest flow quality, followed by the 45° feeders. The vertical feeders have the least flow quality. The circumferential and axial variation in the quality in the 45° and vertical feeders is relatively small. The horizontal feeders have the highest quality with the maximum always at bank 5 and are accompanied by a larger axial variation than the other feeders. The magnitude of the peak increases with decreasing gas flow rate.

In the initial stages, it was planned to perform video and photographic studies of the flow pattern in the header; however, these were not done because of time limitations. Instead, sketches were prepared based on visual observation of the flow in the header during each test. The main features of the sketches in each group of four tests corresponding to the same type of injection and the same inlet liquid flow rate had similar features and therefore, only one sketch will be presented for each of the four test groups.

The sketch of the flow pattern in the header corresponding to this test group (corresponding to Figures 4.1 to 4.4) is shown in Figure 4.5. The flow near the injection turret is highly turbulent and some bubbles can be seen in the upper left end of the

header. Between turret A and bank 4, an interface is distinguishable, but it is rough, highly turbulent and with some splashing. The flow becomes less turbulent starting near bank 4 up to the right end of the header and the interface becomes relatively smooth and steady. The height of this interface line from the bottom of the header is at its lowest around bank 5, which corresponds to the peak in the gas flow rates in the horizontal feeders, and to a lesser extent in the 45° feeders, in Figures 4.1 to 4.4. Figure 4.5 also shows that there is an accumulation of nearly stagnant water at the right end of the header, which again corresponds to the high liquid flow rate in bank 6 in Figures 4.1 to 4.4. As the inlet gas flow rate is decreased from one test to the next in the same group, between turret A and bank 4, there is less and less gas apparent in the gas-liquid mixture beneath the interface and the height of the visible interface level in Figure 4.5 decreases.

4.2.2 One-Turret-Injection Tests: High Liquid Flow Rate (Test Nos. R-7 to R-10)

The gas flow rate, the liquid flow rate and the quality in each feeder for those tests with one-turret injection and an inlet liquid flow rate of 30 kg/min are shown in Figures 4.6 to 4.9 in order of decreasing inlet gas flow rate.

With the exception of the vertical feeders in tests R-9 and R-10, the general trend in these figures is that the feeders in banks 2, 3 and 4 of all the tests receive higher gas flow rates than other banks for any given feeder orientation. However, unlike the trend in tests R-2 to R-5, there is overlap in that some 45° feeders receive more gas flow than the horizontal feeders in the same bank, and some vertical feeders receive more gas flow than the 45° feeders (or indeed the horizontal feeders) in the same bank. This overlapping is observed

in tests with the higher inlet gas flow rates (R-7 and R-8) but not in the tests with the lower inlet gas flow rates (R-9 and R-10). The feeder bank where the maximum gas flow rate occurs in any of the feeder orientations varies from bank 2 to bank 4.

Figures 4.6 to 4.9 show that there is some overlap with the liquid flow rates in tests R-7 and R-8 (where there was overlap in the gas flow rates in the same bank) and no overlap in the tests R-9 and R-10 (where there was no overlap in the gas flow rate). The liquid flow rate in the vertical feeders initially decreases to a minimum at bank 2 or 3 after which it rises to a maximum at bank 6; in the 45° feeders, there is a decrease to a minimum at banks 2 to 4 and then an increase to a maximum at bank 6. With the horizontal feeders, there is a gentle decrease in the liquid flow rate up to bank 4 beyond which it increases up to bank 6.

The quality distribution in the feeders in this group of tests follows the same trend as the gas flow rate in the feeders. In each test, the feeders that have a high gas flow rate also have a high quality and *vice versa*.

Figure 4.10 is a sketch of the typical flow pattern in this test group. The flow in the header is more turbulent than the flow in the tests R-2 to R-5 and has no interface. The flow in the header near banks 1, 2 and 3 is highly turbulent and emulsified making it difficult to make visual observation of the flow in that area. The figure also shows some liquid swirling near the top of banks 4 and 5 as well as gas bubbles near the top of banks 4 to 6. There is an accumulation of nearly stagnant water at the right end of the header,

which again corresponds to the high liquid flow rate and low gas flow rate in bank 6 in Figures 4.6 to 4.9. Excepting for the comment on gas and liquid flow rates in bank 6, the visual observations do not help to explain the flow rate behaviour seen in Figures 4.6 to 4.9. As the inlet gas flow rate decreases within the same group, the area in the header that the swirling liquid and gas bubbles occupy expands while the flow becomes less turbulent.

In terms of the effect of reducing the inlet gas flow rate within this test group, the circumferential variation increases with decreasing inlet gas flow rate. Also, as mentioned earlier, the overlap in gas and liquid flow rates at the higher inlet gas flow rates (tests R-7 and R-8) is not seen at the lower inlet gas flow rates (tests R-9 and R-10).

The effects of increasing the inlet liquid flow rates can be seen by comparing Figures 4.6 to 4.9 with Figures 4.1 to 4.4. The circumferential variation in gas and liquid flow rates in individual feeders decreases with increasing inlet liquid flow rate. This effect could possibly be explained by a tendency towards homogeneity with the higher inlet liquid flow rate tests, particularly in tests with higher inlet gas flow rates (R-7 and R-8).

4.2.3 Two-Turret-Injection Tests: Low Liquid Flow Rate (Test Nos. R-11 to R-14)

In these tests, the air-water mixture was injected into the header through both Turret A and Turret B. The gas flow rate, the liquid flow rate and the quality in each feeder for tests with two-turret injection and an inlet liquid flow rate of 15 kg/min are shown in Figures 4.11 to 4.14 in order of decreasing inlet gas flow rates.

The general trend in these figures is that the horizontal feeders receive more air flow than the 45° feeders while the vertical feeders receive the least. The only exceptions to this trend are tests R-13 and R-14 where there are overlaps with some vertical feeders receiving more air flow than the 45° feeders at some banks (R-13) or more gas flow than both the 45° and horizontal feeders at the same bank (R-14). The gas flow rate in the horizontal feeders in all tests shows a slight increase from bank 1 to bank 2 after which it drops to a minimum at bank 4. The gas flow rate then increases sharply from bank 4 to bank 5; it increases from bank 5 to bank 6 with the exception of test R-11 where it decreases slightly. As shown in Figures 4.11 to 4.14, the gas flow rate in the 45° feeders increases slightly from bank 1 to bank 2 (with the exception of test R-14) after which it drops to a minimum at bank 3; the gas flow rate increases gradually from bank 3 to bank 5 in all tests in this group with a slight drop at bank 6. The vertical feeders show little axial variation in the air flow rate with the exception of test R-14 where there is a larger axial variation.

Figures 4.11 to 4.14 also show that, in any bank of feeders, the vertical feeders receive more liquid flow than the 45° feeders and the horizontal feeders receive the least. The liquid flow in the vertical feeders increases from bank 1 to bank 2 with the exception of test R-11 where there is very little liquid flow change between these banks; in all tests in the present group, the liquid flow then increases from bank 2 to a maximum at bank 3; the liquid flow then gradually drops from bank 3 to a minimum at bank 5 and finally rises sharply to bank 6. The behaviour of the liquid flow rate in the 45° feeders generally

follows that of the vertical feeders. There is very little axial variation in liquid flow in the horizontal feeders.

The quality distribution in the horizontal feeders in this group follows a similar trend to the gas flow rate in the horizontal feeders. A close examination of the tabulated data reveals that there are significant axial and circumferential variations in the quality in the 45° and vertical feeders. However, there is even a larger circumferential variation in the quality between the horizontal feeders and both the 45° and vertical feeders.

Figure 4.15 is a sketch of the typical flow pattern in this test group. As is evident on the sketch, the injection jets from both turrets impinge on the bottom of the header and spread out. Some swirling of the liquid is visible at the top left end of the header as well as near bank 3. An interface is visible in the area between the two turrets and near the right end of the header. As in the previous test groups, the sketch shows that there is an accumulation of nearly stagnant water at the right end of the header. There is mainly liquid and very little gas in the bottom half of the right end of the header. Possibly as a result, the vertical feeder in bank 6 receives lower gas and higher liquid flow rates. The interface to the right of Turret B drops partially below the horizontal feeders in banks 5 and 6 which corresponds to the higher gas flow rates in these feeders. The interface between the two turrets also partially drops below the horizontal feeders in banks 2 and 3 resulting in more gas flow in these feeders as shown in Figures 4.11 to 4.15. As the inlet gas flow rate is reduced within this group, the flow in the header becomes less turbulent and the height of the interface decreases.

In regards to the effect of reducing the inlet gas flow rate within this test group, the general shape of the gas and liquid distribution in the feeders is preserved. However, the gas flow rate in the horizontal feeders in banks 1 and 5 decreases as the inlet gas flow rate is decreased. As mentioned earlier, the behaviour of the quality in the feeders is the same as the gas flow rate with decreasing inlet gas flow rate.

The effect of using two-turret injection compared with one-turret injection (for the same inlet gas and liquid flow rates) can be seen by comparing Figures 4.11 to 4.14 (two-turret injection) with Figures 4.1 to 4.4 (one-turret injection). It is seen that using two-turret injection rather than one-turret injection changed the axial flow distribution of gas and liquid in the feeders very significantly. The two-turret-injection tests have two banks of feeders where the gas and liquid flow rates reach a peak or a maximum value. However, the one-turret-injection tests typically have only one feeder bank where gas and liquid-flow rates reach a peak or a maximum value.

4.2.4 Two-Turret-Injection Tests: High Liquid Flow Rate (Test Nos. R-15 to R-18)

In these tests, the air-water mixture was injected into the header through both Turret A and Turret B. The gas flow rate, the liquid flow rate and the quality in each feeder for the two-turret injection and a liquid flow rate of 30 kg/min tests are shown in Figures 4.16 to 4.19 in order of decreasing inlet gas flow rate.

The general observation from these figures (with two exceptions) is that the horizontal feeders receive the highest gas flow rate followed by the 45° feeders; the vertical feeders

receive the least gas flow rate. The gas flow rate in the feeders in a given orientation increases from bank 1 to 2 and then drops to a minimum at bank 3. It then gradually rises to a maximum at bank 5 and finally drops sharply to bank 6. Only one feeder deviates from this trend but the magnitude of the deviation is very small.

Figures 4.16 to 4.19 also show that the liquid flow distribution in the feeders has an opposite sense to the gas-flow distribution. In any given bank (with one exception), the vertical feeders receive the highest liquid flow followed by the 45° feeders; the horizontal feeders receive the least amount of liquid flow. The liquid flow rate in all feeders in a given orientation decreases from bank 1 to 2 then increases to a maximum at bank 3. It then gradually drops to a minimum at bank 5 and finally rises sharply to bank 6.

The quality distribution in the feeders in this group is also shown in Figures 4.16 to 4.19. It is seen that the quality follows the same trend as the distribution of gas.

Figure 4.20 is a sketch of the typical flow pattern in this test group. Increasing the inlet gas flow rate increases the level of turbulence in the header and no interface is visible. Some swirling and air bubbles can be seen on top of the area between the two turrets (banks 2 and 3) as well as the top left and top right (bank 6) corners of the header. The sketch also shows that there is an accumulation of nearly stagnant water at the right end of the header, which could explain the relatively low gas and high liquid flow rates in the 45° and vertical feeders of bank 6. As the inlet gas flow rate decreases within the same

group, the area in the header that the swirling liquid and gas bubbles occupy expands and the flow becomes less turbulent.

With respect to decreasing the inlet gas flow rate within this group of tests, it is seen that the circumferential variation in the gas and liquid flow rates as well as quality increases with decreasing inlet gas flow rate. The shape of the axial distribution of flow rates and quality does not change as the inlet gas flow rate is decreased.

The effect of the inlet liquid flow rate in the two-turret-injection tests can be seen by comparing Figures 4.16 to 4.19 with Figures 4.11 to 4.14 (low inlet liquid flow rate). The circumferential variation in the gas and liquid flow rates at any given bank decreases as the inlet liquid flow rate is increased. Possibly, this is due to the tendency towards homogeneity of the flow in the header as the inlet liquid flow rate is increased. This reduction in the circumferential variation was also observed in one-turret experiments on increasing the inlet liquid flow rate. At bank 6, the gas flow rate in the horizontal feeder is markedly reduced on increasing the inlet liquid flow rate. This reduction is associated with the flow conditions in the vicinity of bank 6; for the case of low inlet liquid flow rate, the horizontal feeder is exposed essentially to gas (see Figure 4.15) while in the case of high inlet liquid flow rate that feeder is exposed to a two-phase mixture (see Figure 4.20). On increasing the inlet liquid flow rate, there are some minor shifts in the banks at which maximum and minimum values of the gas and liquid flow rates as well as quality appear.

The effect of using two-turret injection compared with one-turret injection (for the same inlet gas and liquid flow rates) can be seen by comparing Figures 4.16 to 4.19 (two-turret injection) with Figures 4.6 to 4.9 (one-turret injection). The observations are similar to those with the lower inlet liquid flow rate, specifically, the axial distribution of the gas and liquid in the feeders changes significantly on changing from one-turret to two-turret injection.

4.3 Header-to-Separator Pressure Drop

As discussed in Chapter 3, the header-to-separator pressure drop was measured during each test. The relationship between the header-to-separator pressure drop and the inlet gas flow rate for each combination of inlet liquid flow rate and type of injection is shown in Figure 4.21.

As shown in the figure, the header-to-separator pressure drop increases almost linearly as the inlet gas flow rate increases. For the high inlet liquid flow rate, Figure 4.21 shows a marked effect of the type of injection; the one-turret results lie clearly above the two-turret results, suggesting a higher level of turbulence associated with one-turret injection for otherwise the same conditions. For the low inlet liquid flow rate, the absolute differences between the one-turret- and the two-turret-injection data are small, although the one-turret results lie consistently above the two-turret results. For the same inlet liquid flow rate, the one-turret-injection tests show a larger pressure drop than the two-turret-injection tests suggesting that there is more turbulence in the header in the one-turret-injection tests. Finally, the figure demonstrates that increasing the inlet liquid flow

rate while keeping the same type of injection also increases the header-to-separator pressure drop.

4.4 Data Correlation

Steps taken to correlate the data are discussed in this section and the actual correlating equations are presented. A Lockhart-Martinelli-type parameter, defined as

$$(\Phi_g)^2 = \frac{\Delta P_{tp}}{\Delta P_{sp}} \tag{4.1}$$

was adopted in correlating the data, where ΔP_{tp} is the pressure drop from the header to the separator measured during the two-phase tests (see Section 4.3), and ΔP_{sp} is the pressure drop between the header and the separator if the gas flows alone in the feeder (the amount of gas being that measured in the feeder under consideration during the two-phase test). A separate single-phase test described next was performed to determine ΔP_{sp} as a function of gas flow rate.

Air (no water) was injected into the header through turret A. The valve from one feeder was open to the measuring tank while valves from all other feeders were shut off. The inlet air flow was varied to obtain a wide range of pressure drops. The pressure drop was measured using a pressure transducer and ranged from 19.1 mm (0.75 in.) of water to 483.6 mm (19.04 in.) of water. For each outlet air flow rate, the corresponding pressure drop was recorded. The following simple correlation was obtained from a plot of the pressure drop versus outlet air flow rate,

$$\Delta P_{sp} = 2260.1(\dot{m}_g)^2 \tag{4.2}$$

where ΔP_{sp} is the single-phase pressure drop in cm of water and $\dot{m}_g$ is the air mass flow rate in kg/min.

Since $\dot{m}_g$ in each feeder and ΔP_{tp} in each test were known, $(\Phi_g)^2$ was calculated for each feeder in each test and plotted against (1-x)/x, where x is the quality in the feeder. In developing the correlation, tests with deviations greater than 5% between the inlet and outlet gas flow rates were eliminated. Thus, tests R-4, R-5, R-13 and R-14 (i.e., four out of 16 tests) were eliminated. The data were correlated using an equation of the form

$$(\Phi_g)^2 = 1 + a\left(\frac{1-x}{x}\right)^b \tag{4.3}$$

For tests R-2 and R-3 (one-turret injection, low inlet liquid flow), the data are correlated with

$$(\Phi_g)^2 = 1 + 0.27\left(\frac{1-x}{x}\right)^{1.2} \tag{4.4}$$

and are shown against Equation (4.4) in Figure 4.22. The data for tests R-7 to R-10 (one-turret injection, high inlet liquid flow) are shown in Figure 4.23 to be nicely correlated with

$$(\Phi_g)^2 = 1 + 0.49\left(\frac{1-x}{x}\right)^{1.2} \tag{4.5}$$

while Figure 4.24 shows the data of tests R-11 and R-12 (two-turret injection, low inlet liquid flow) to be well correlated with

$$(\Phi_g)^2 = 1 + 0.27\left(\frac{1-x}{x}\right)^{1.2} \tag{4.6}$$

Finally, Figure 4.25 shows the data of tests R-15 to R-18 (two-turret injection, high inlet liquid flow) correlated with

$$(\Phi_g)^2 = 1 + 0.36\left(\frac{1-x}{x}\right)^{1.2} \tag{4.7}$$

Table 4.1 summarizes the *a* and *b* of Equation (4.3) for the various test conditions.

Table 4.1 Summary of the Values of *a* and *b* in Equation (4.3)

Description of Test Conditions	Tests	*a*	*b*	Correlating Equation Number
One-turret injection, low inlet liquid flow	R-2 and R-3	0.27	1.2	4.4
One-turret injection, high inlet liquid flow	R-7 to R-10	0.49	1.2	4.5
Two-turret injection, low inlet liquid flow	R-11 and R-12	0.27	1.2	4.6
Two-turret injection, high inlet liquid flow	R-15 to R-18	0.36	1.2	4.7

In order to assess the agreement between the eliminated data and the above correlation, the data of tests R-4 and R-5 were compared with Equation (4.4) and the data of tests R-13 and R-14 were compared with Equation (4.6). The results of the comparison are shown in Figures 4.26 and 4.27. It is clear from these figures that the trends in the data and correlating equations are similar; however, there is much more scatter in the data compared with that seen in Figures 4.22 to 4.25. A possible reason for the scatter is the higher imbalance between the inlet and the outlet air flow rates.

Equation (4.3) that was used in the correlation converges to the right limit, $(\Phi_g)^2 = 1$, as the quality x approaches 1 (gas only). It is also worth noting that all the correlations have the same value for the exponent, b=1.2.

The coefficient 0.49 in Equation (4.5) for one-turret injection and high inlet liquid flow (tests R-7 to R-10) is higher than the coefficient 0.36 in Equation (4.7) for the two-turret injection and the same high inlet liquid flow rate (tests R-15 to R-18). This is consistent with the observation (see Section 4.3) that the level of turbulence in the header is higher in the one-turret-injection case compared with the two-turret-injection case, as implied from the magnitude of the header-to-separator pressure differences shown in Figure 4.21. The coefficients in Equations (4.4) and (4.6) are the same (0.27), indicating that, for the low inlet liquid flow rates, the type of injection essentially does not matter.

Finally, all the correlated data in Figures 4.22 to 4.25 were plotted on the same graph. Figure 4.28 shows the predicted value of $(\Phi_g)^2$ using the constants in Table 4.1 plotted against the measured (experimental) value of $(\Phi_g)^2$. This figure shows excellent agreement with approximately 89% of the correlated experimental data falling within ±30% of the predicted values. The root-mean-square deviation in Figure 4.28 is 22.2% and the arithmetic-mean deviation is –1.4%. The success of the correlation suggests good accuracy in the experimental data.

It is important to note that the correlating equations cannot be used to predict the individual flow rates of gas and liquid in each feeder. The correlating scheme, however,

does show that the highly irregular data of the flow rates in the individual feeders can be regularized in the fashion described. The present work will hopefully help in ultimately achieving prediction techniques for the flow rates in the individual feeders in this extremely complex flow situation.

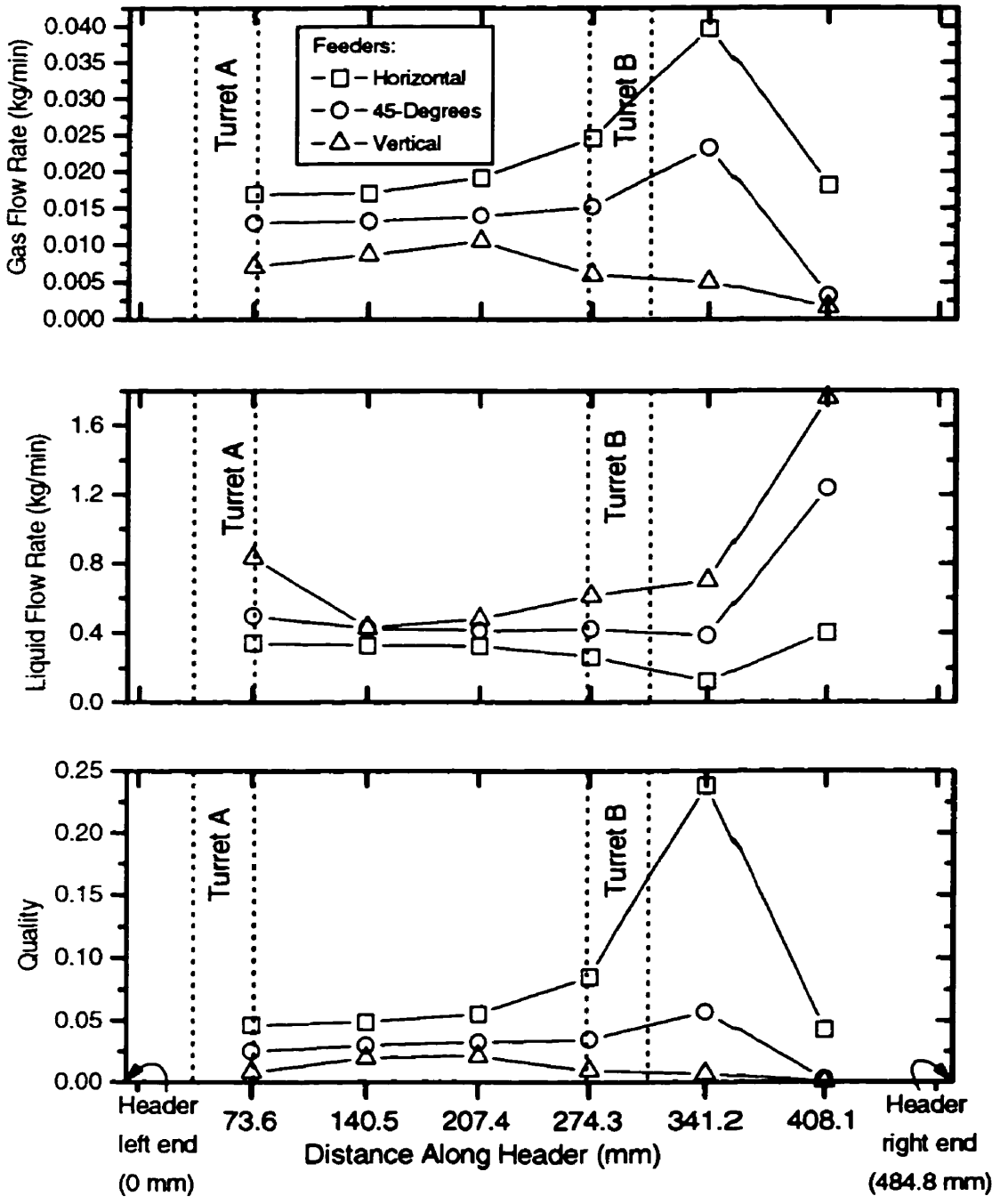

Figure 4.1 Quality, Gas and Liquid Flow Rate in Individual Feeders for Test No. R-2

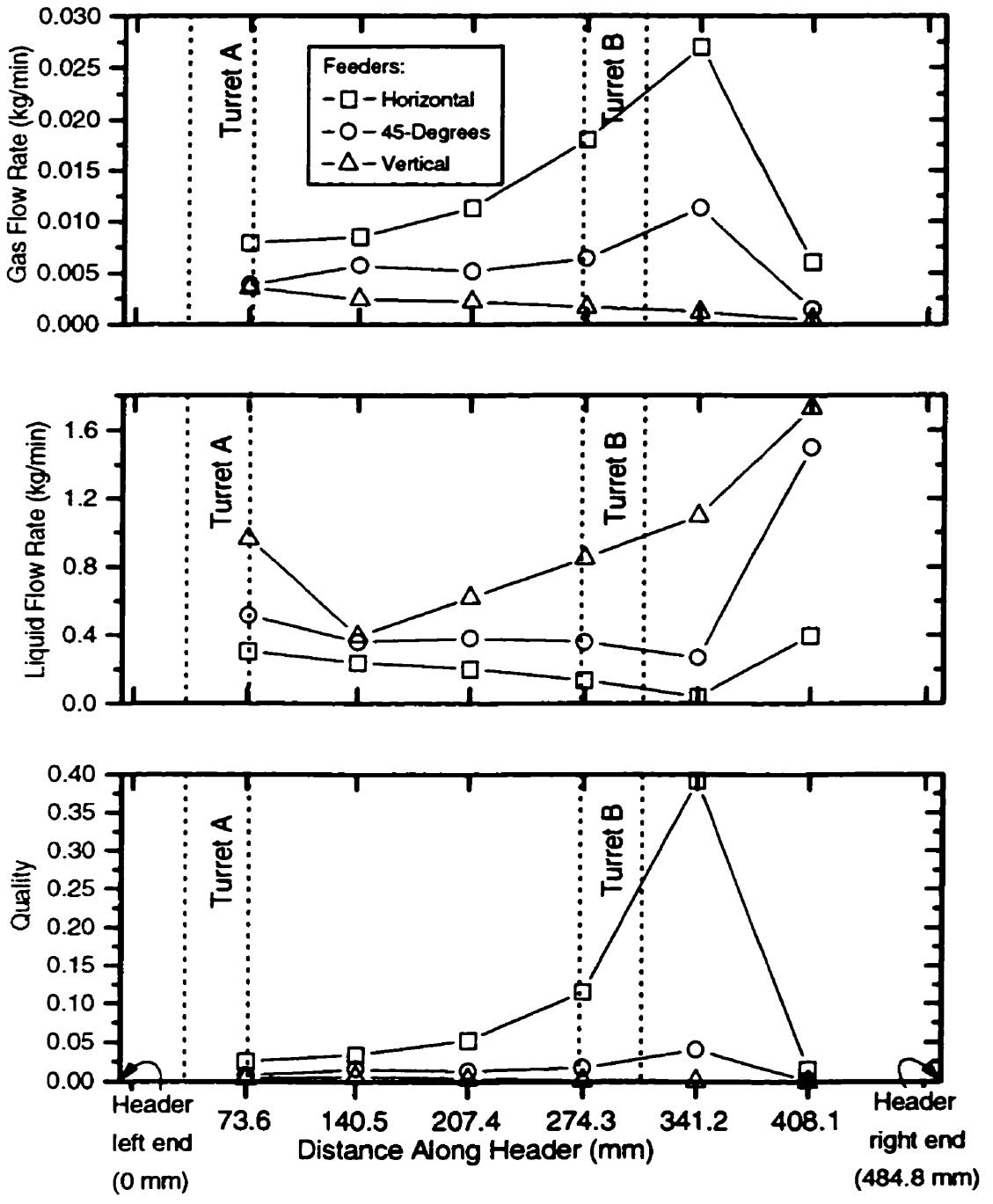

Figure 4.2 Quality, Gas and Liquid Flow Rate in Individual Feeders for Test No. R-3

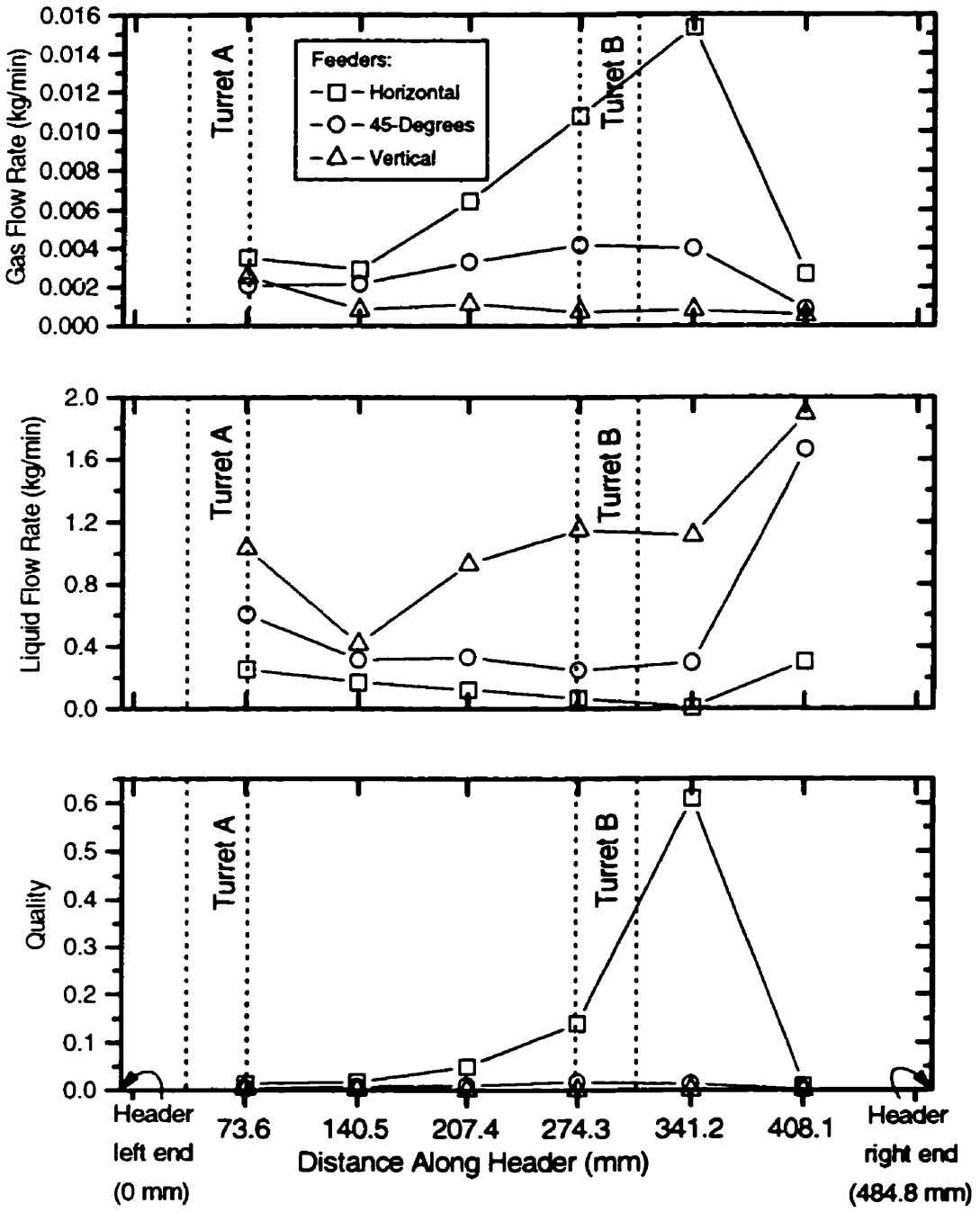

Figure 4.3 Quality, Gas and Liquid Flow Rate in Individual Feeders for Test No. R-4

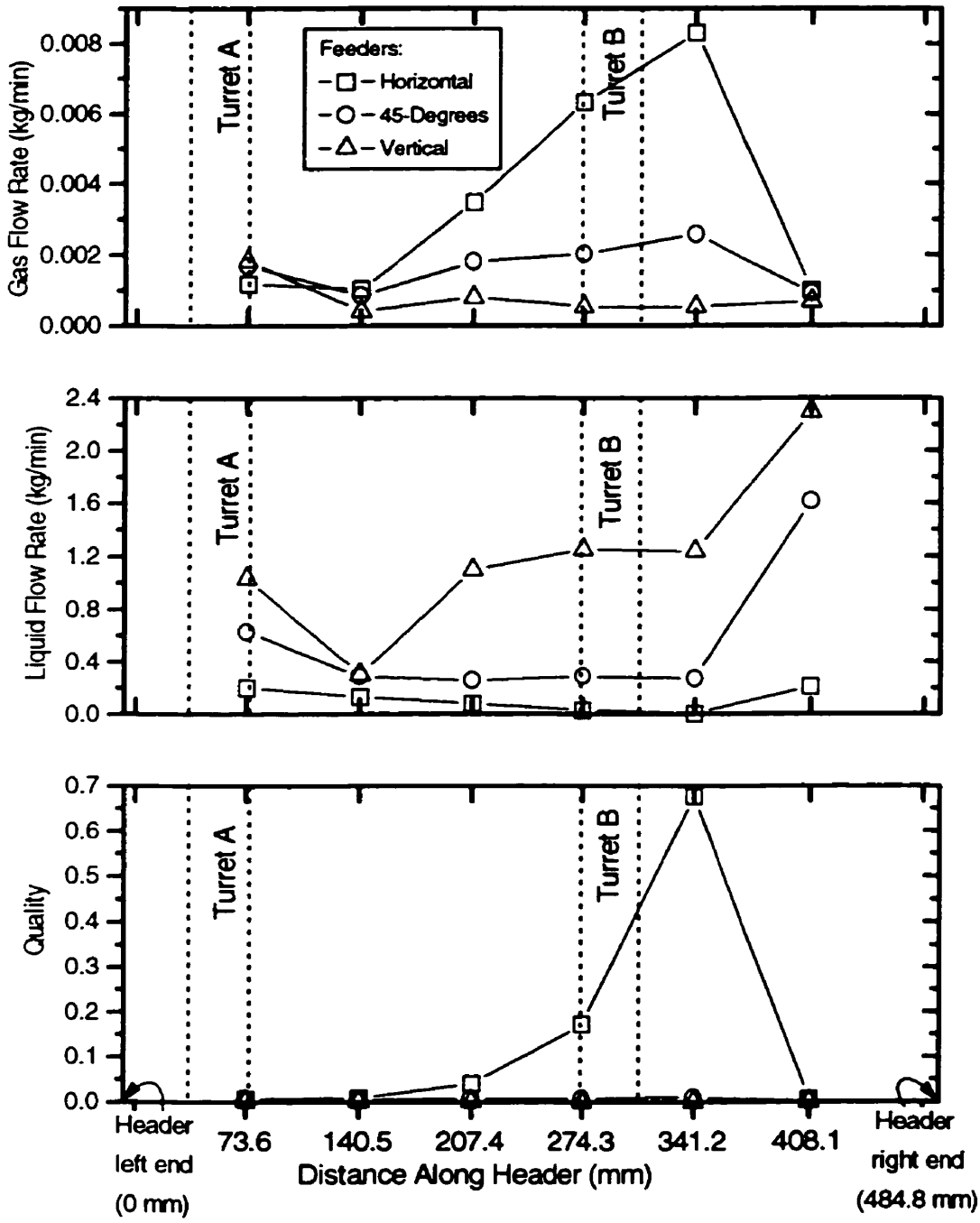

Figure 4.4 Quality, Gas and Liquid Flow Rate in Individual Feeders for Test No. R-5

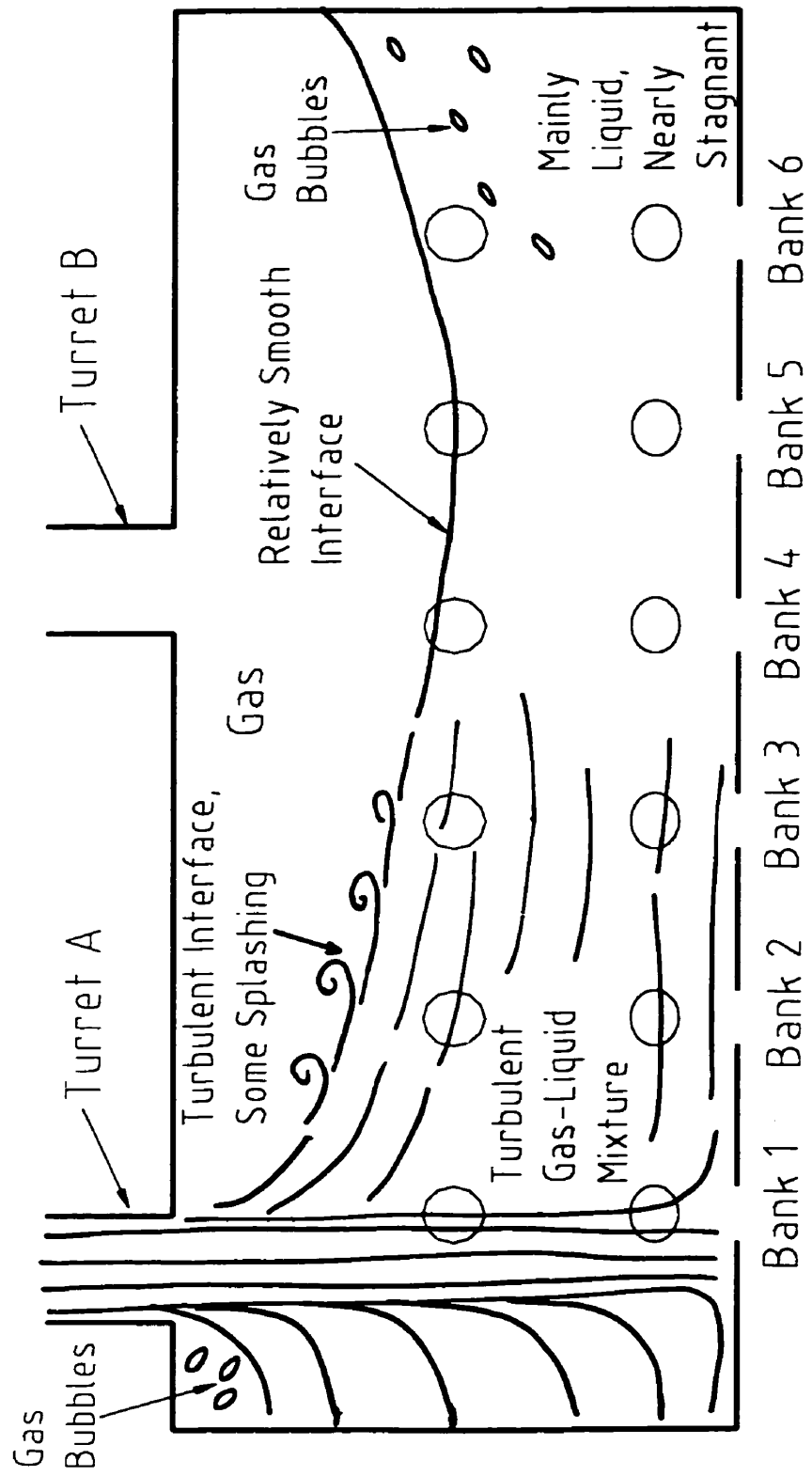

Figure 4.5 Sketch of the Flow Pattern in the Header for Test Nos. R-2 to R-5

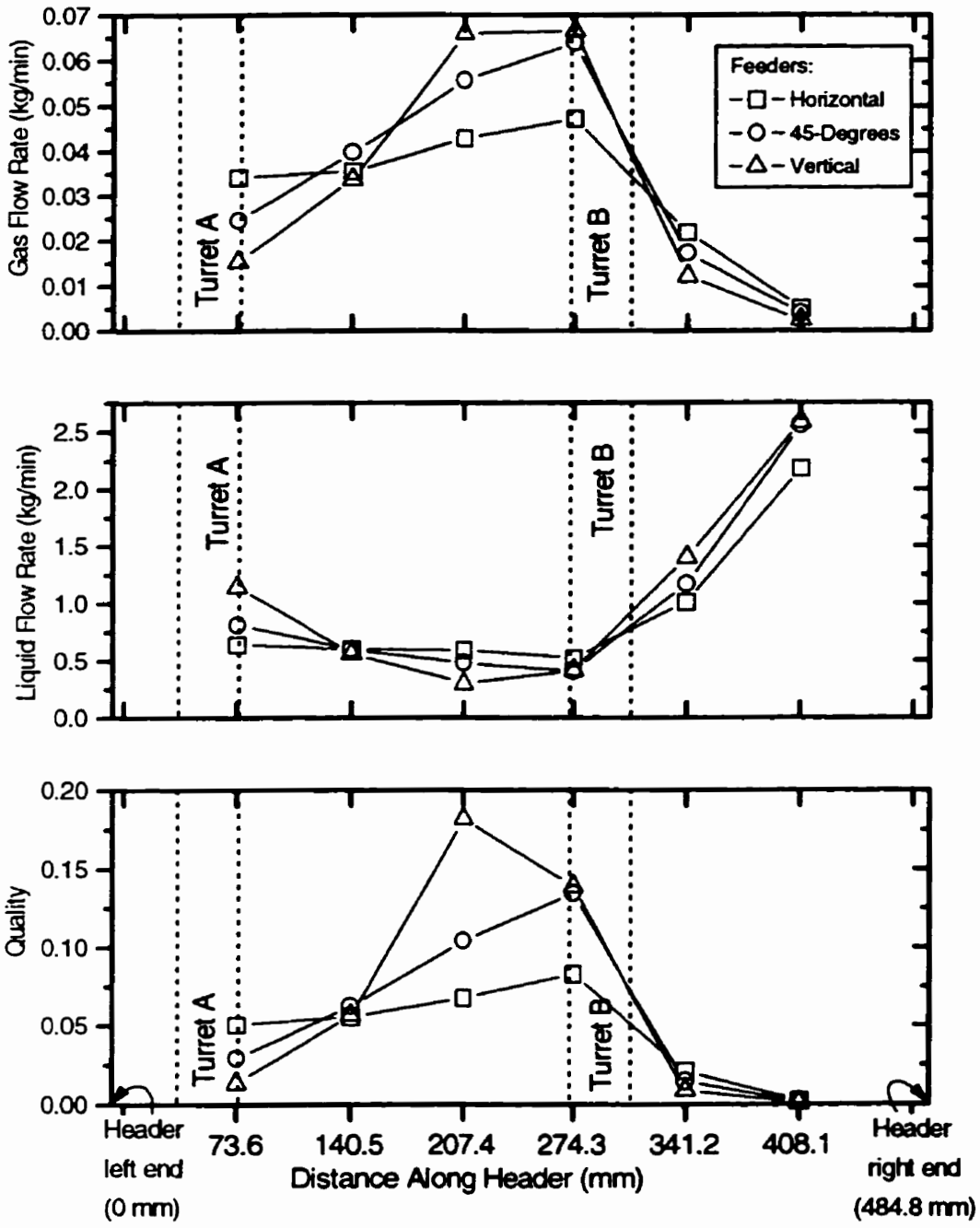

Figure 4.6 Quality, Gas and Liquid Flow Rate in Individual Feeders for Test No. R-7

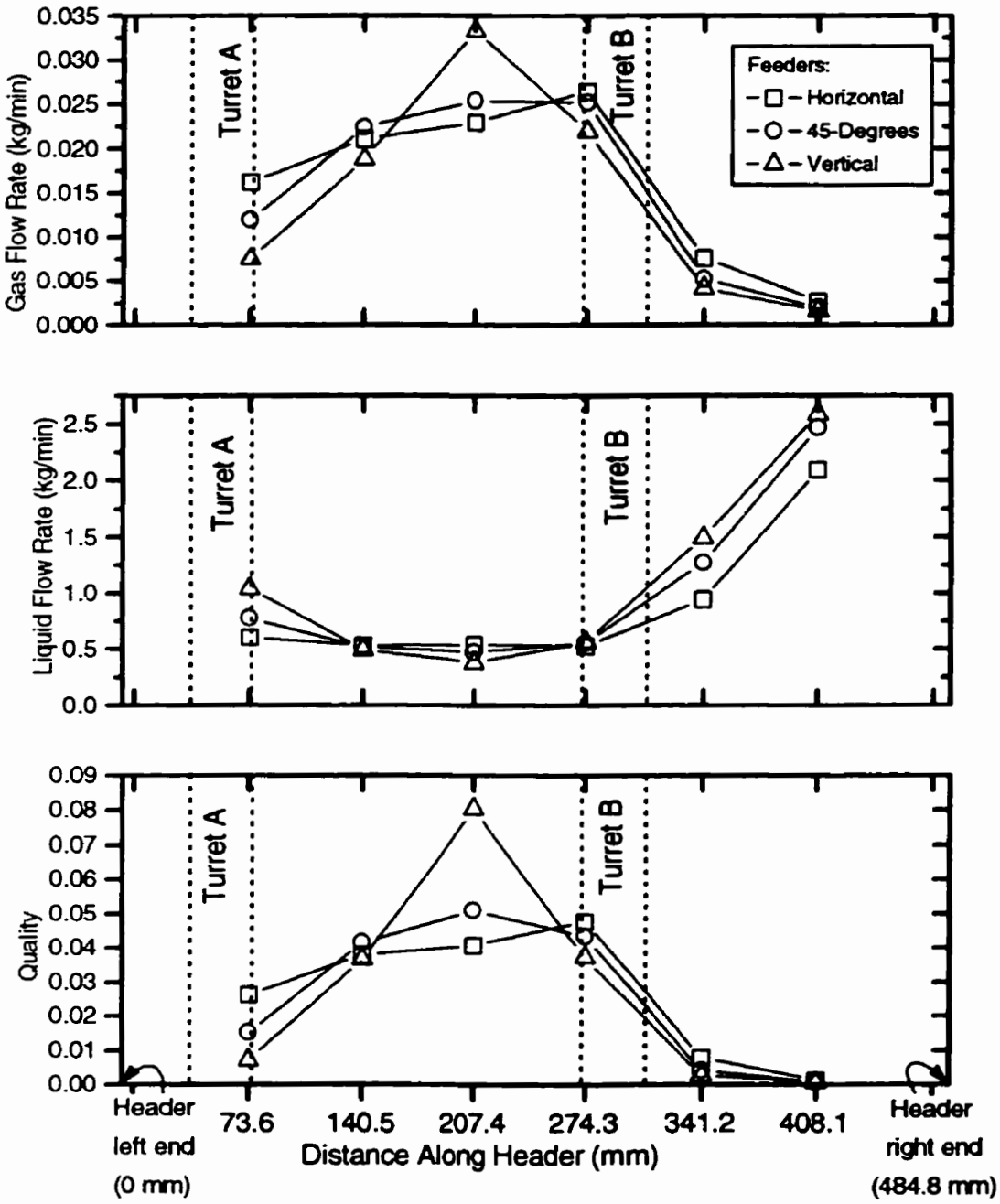

Figure 4.7 Quality, Gas and Liquid Flow Rate in Individual Feeders for Test No. R-8

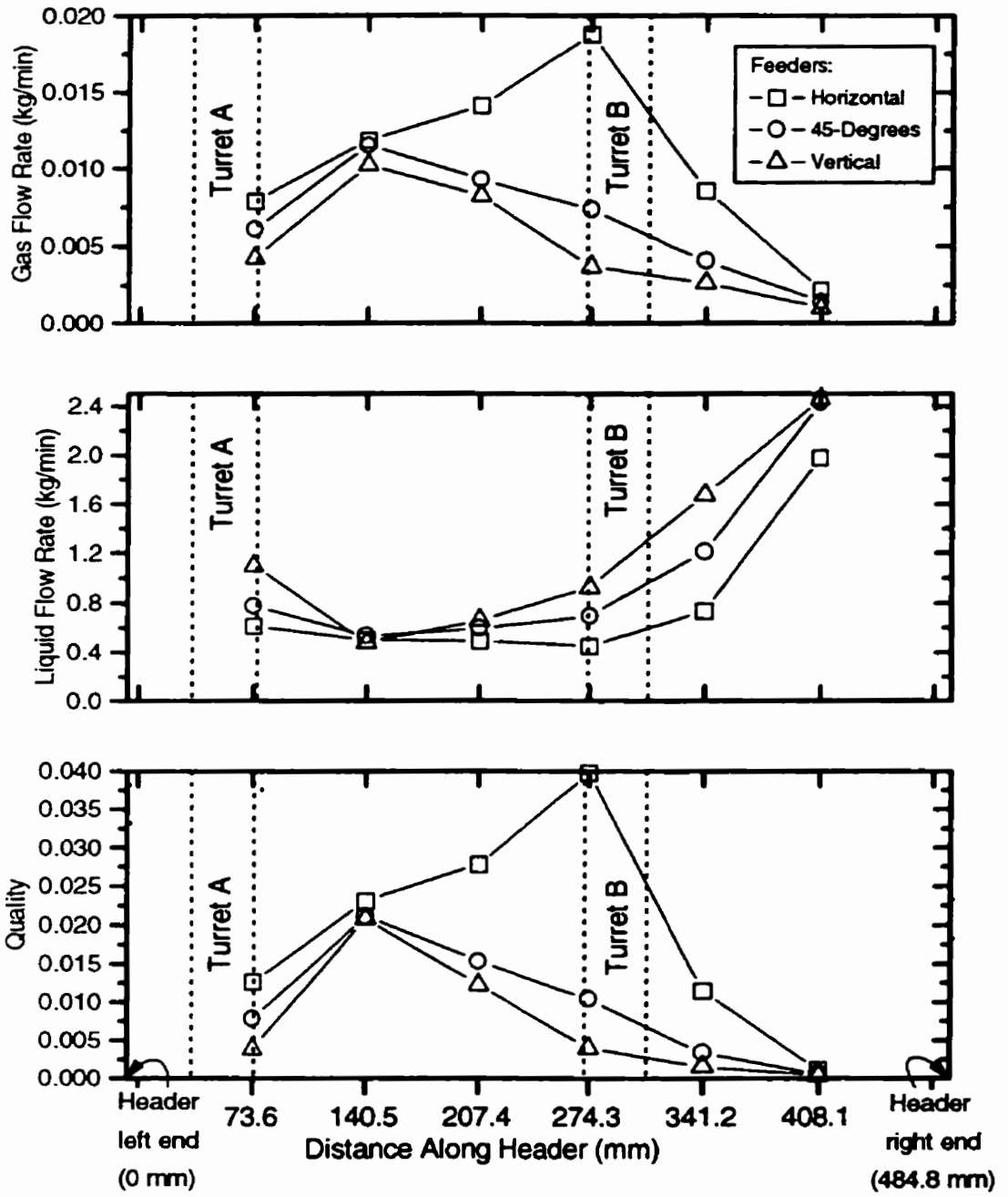

Figure 4.8 Quality, Gas and Liquid Flow Rate in Individual Feeders for Test No. R-9

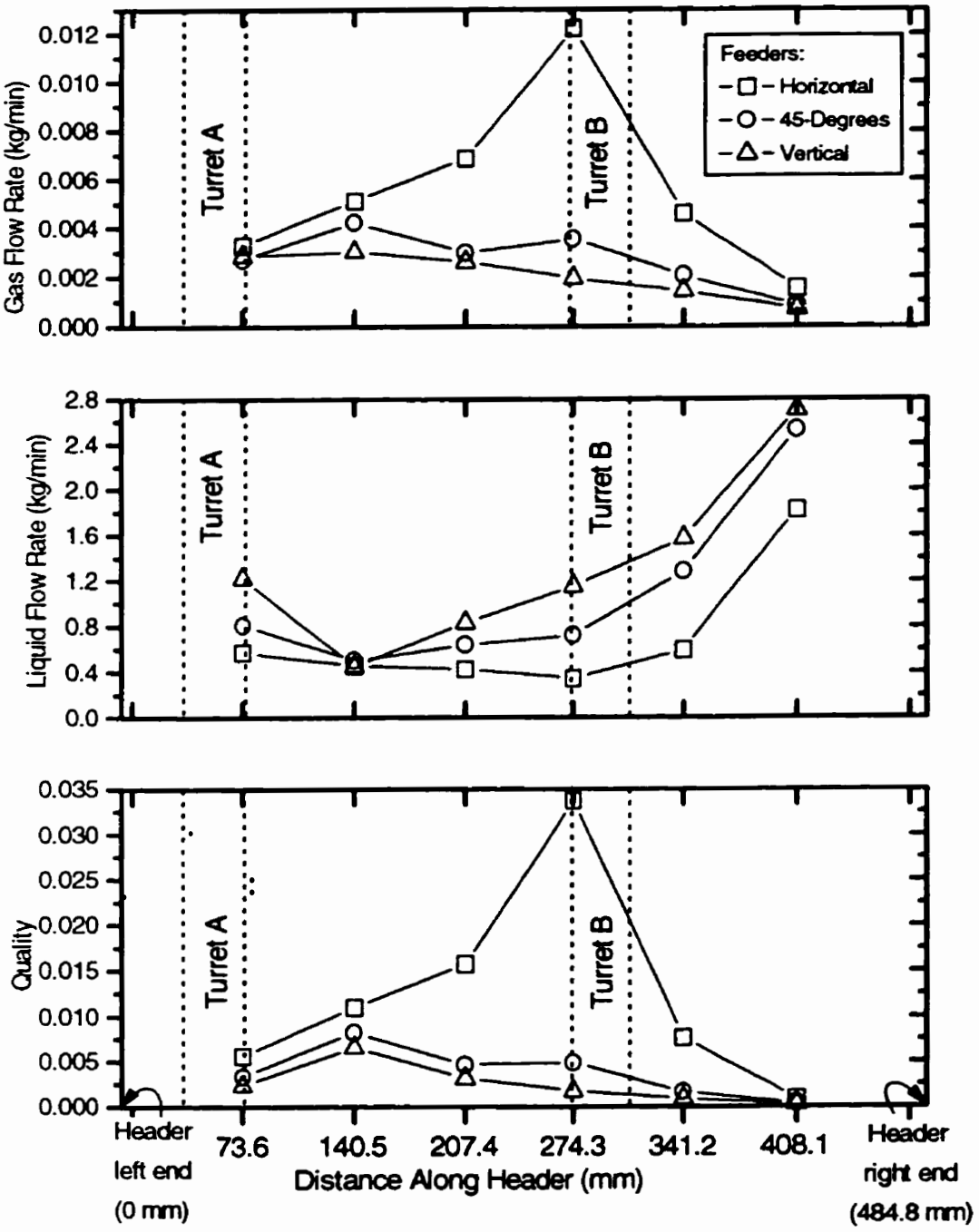

Figure 4.9 Quality, Gas and Liquid Flow Rate in Individual Feeders for Test No. R-10

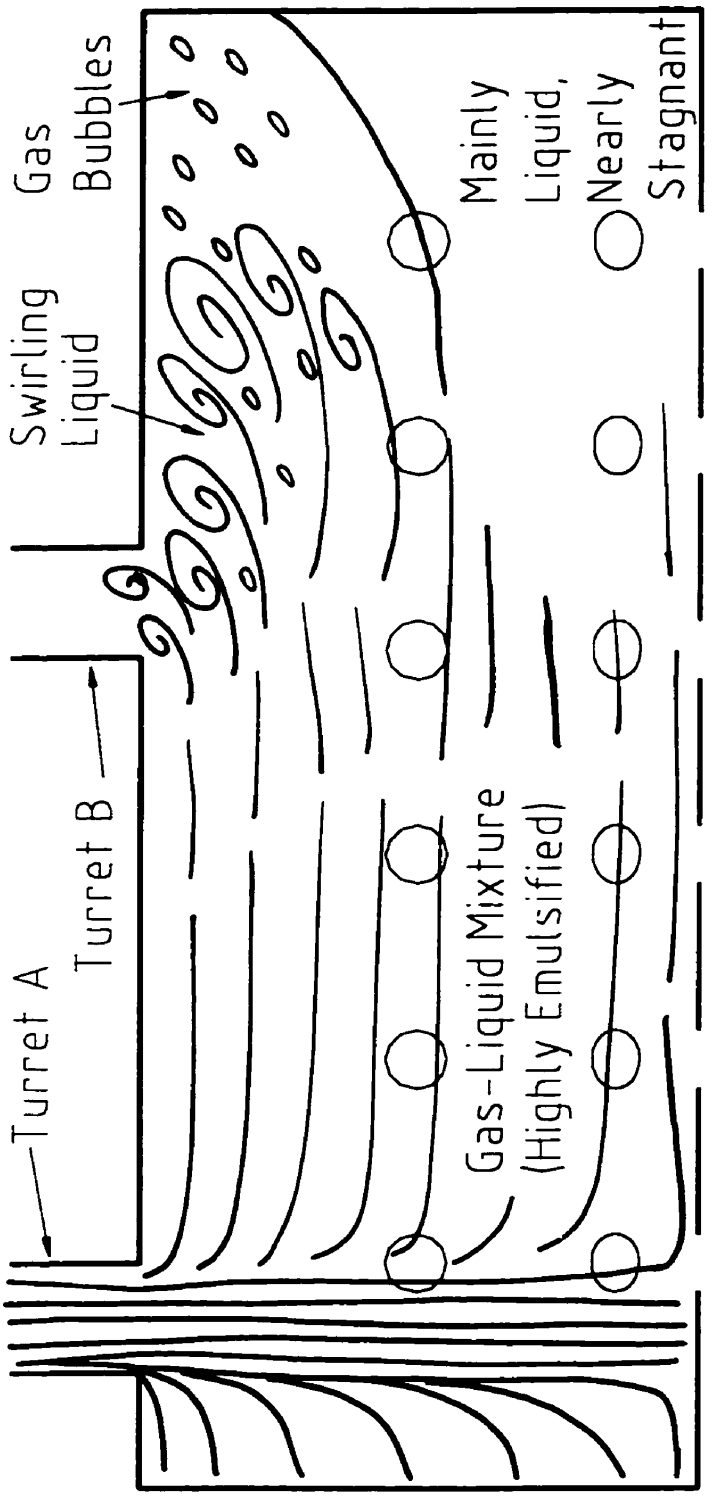

Figure 4.10 Sketch of the Flow Pattern in the Header for Test Nos. R-7 to R-10

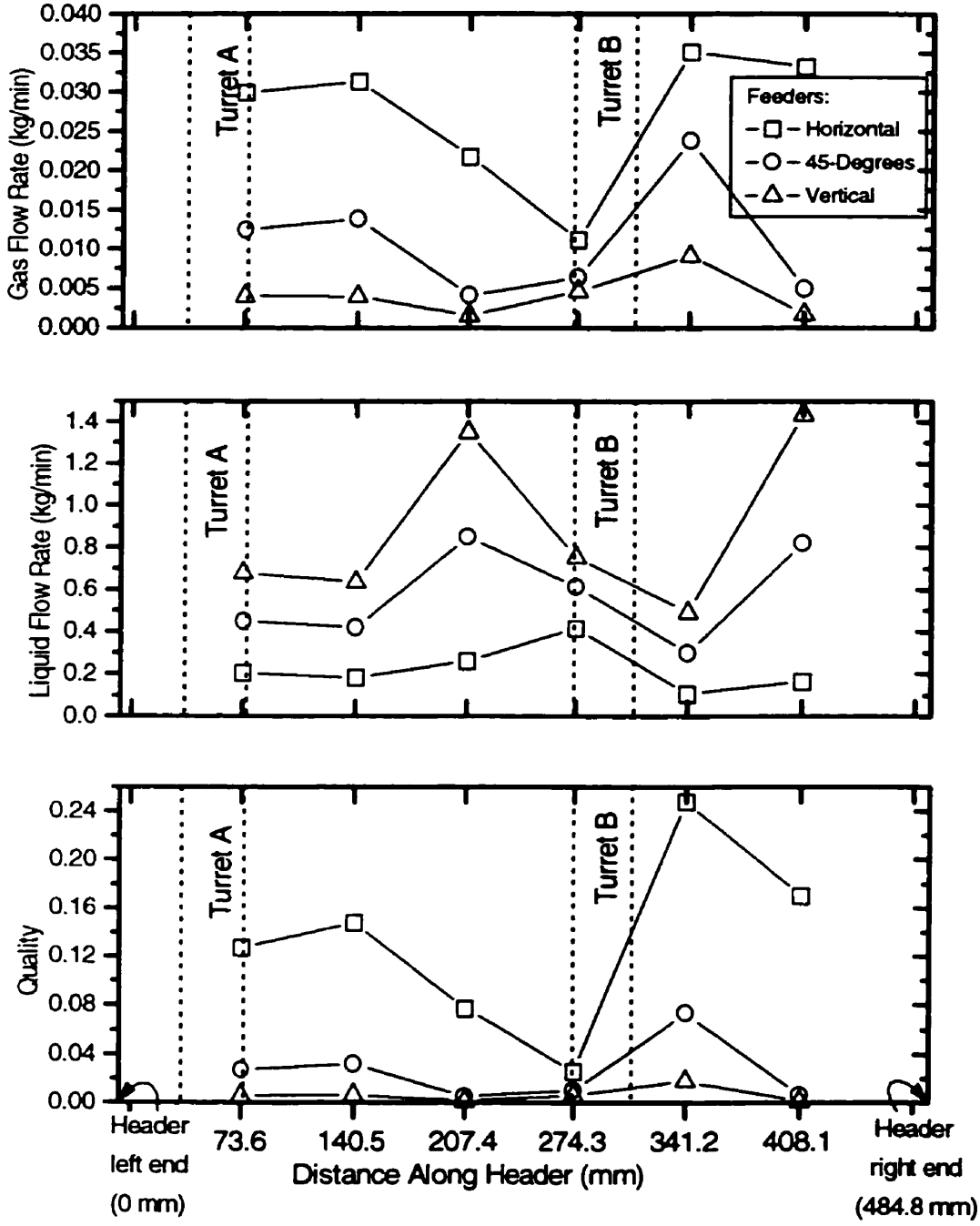

Figure 4.11 Quality, Gas and Liquid Flow Rate in Individual Feeders for Test No. R-11

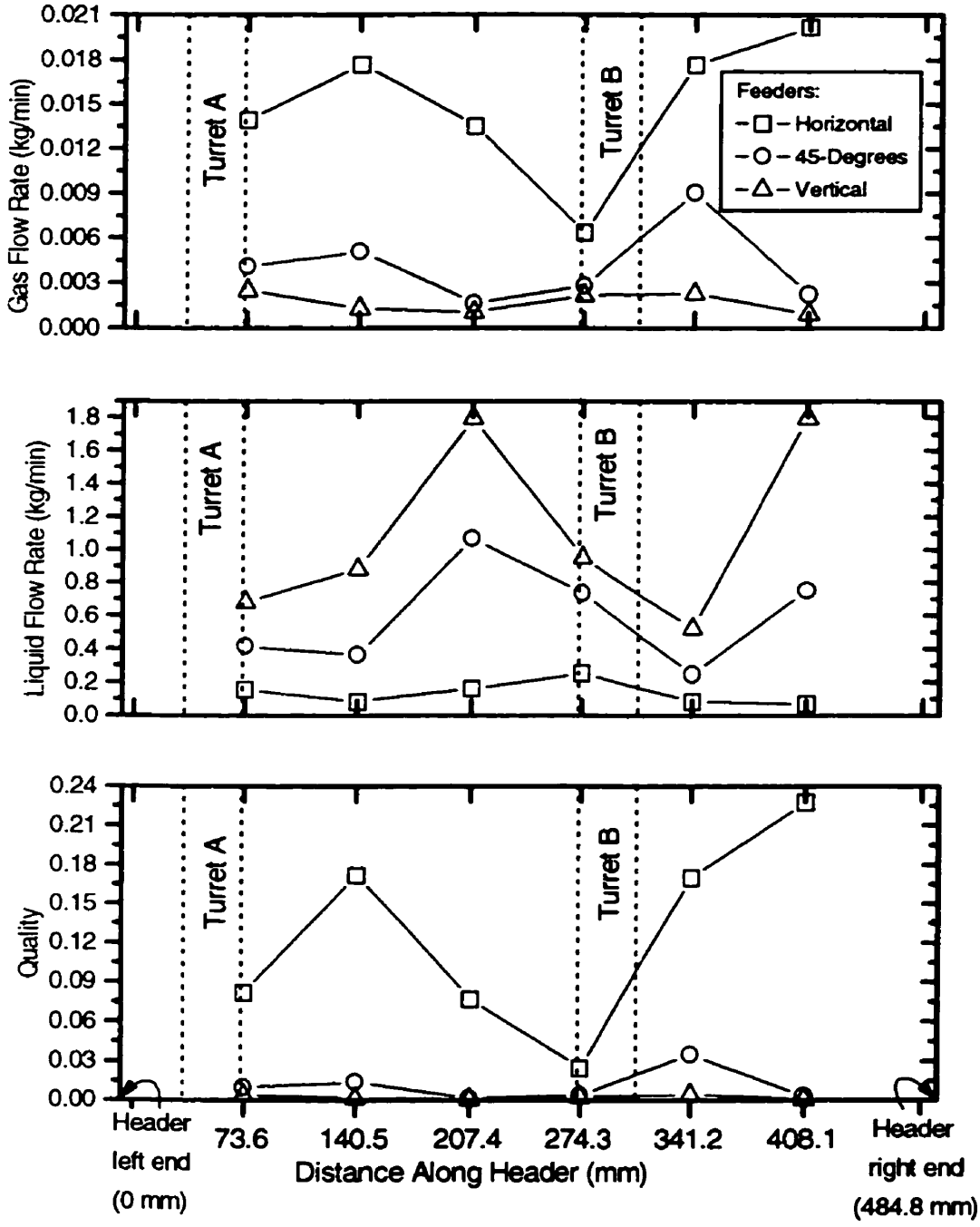

Figure 4.12 Quality, Gas and Liquid Flow Rate in Individual Feeders for Test No. R-12

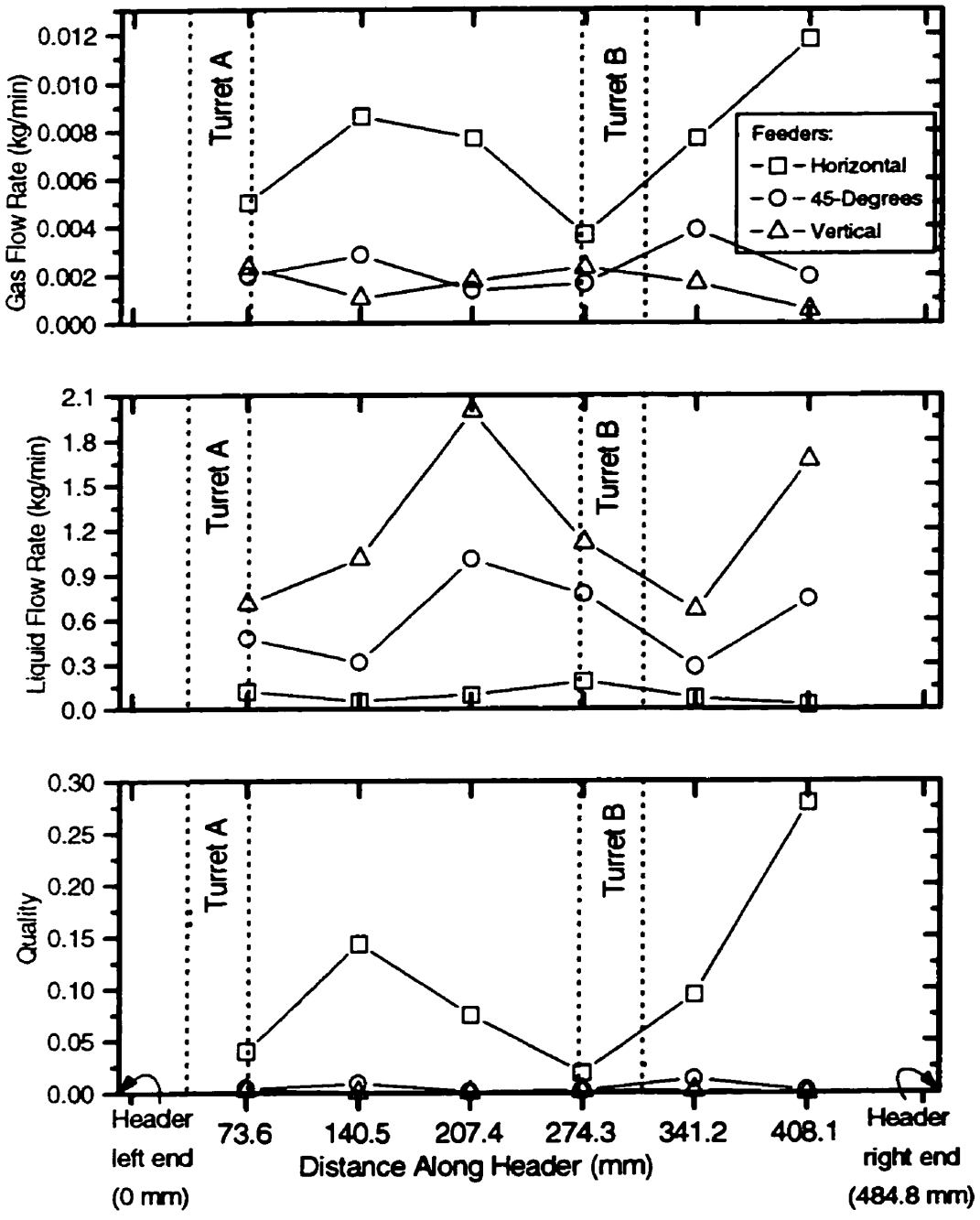

Figure 4.13 Quality, Gas and Liquid Flow Rate in Individual Feeders for Test No. R-13

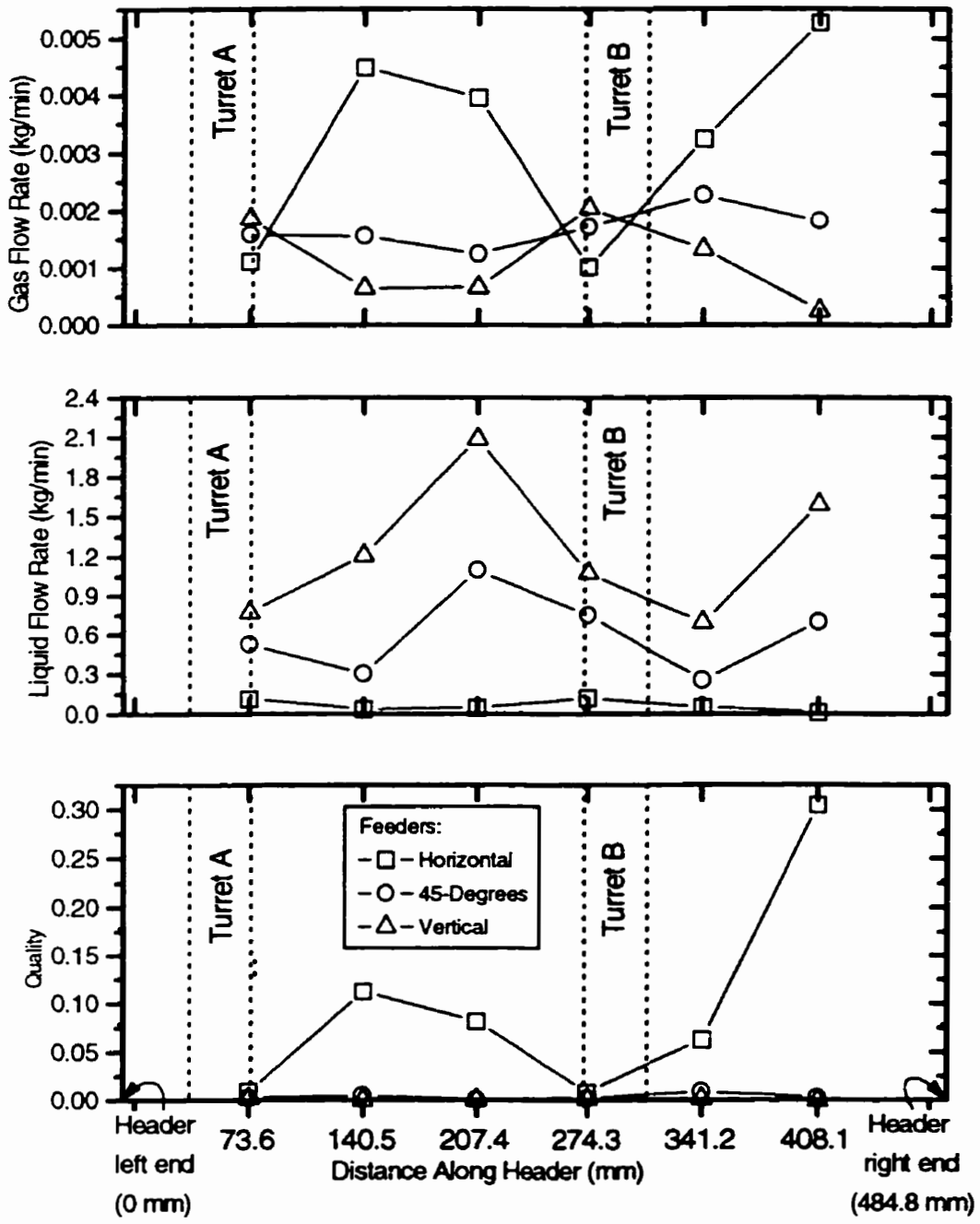

Figure 4.14 Quality, Gas and Liquid Flow Rate in Individual Feeders for Test No. R-14

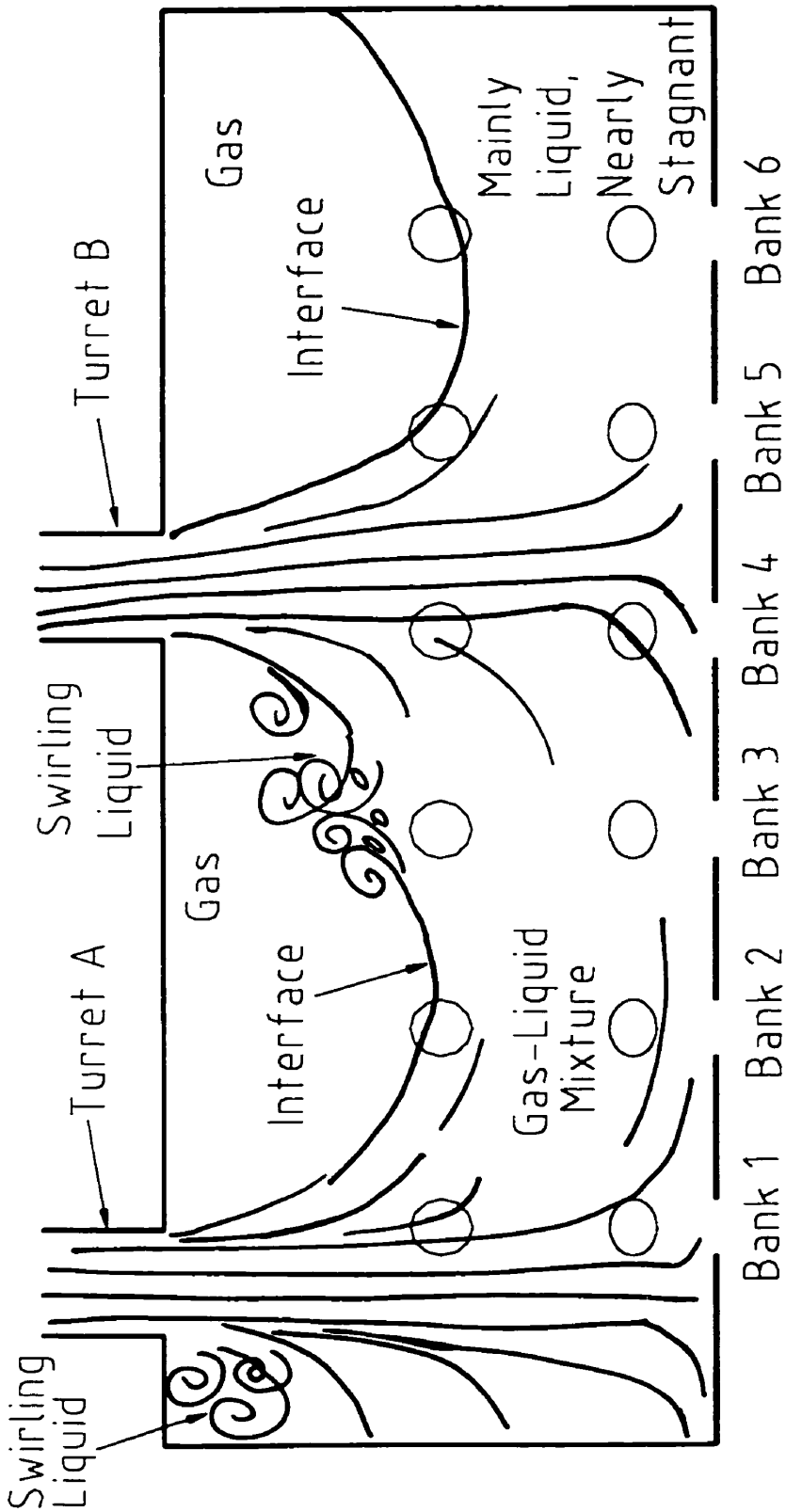

Figure 4.15 Sketch of the Flow Pattern in the Header for Test Nos. R-11 to R-14

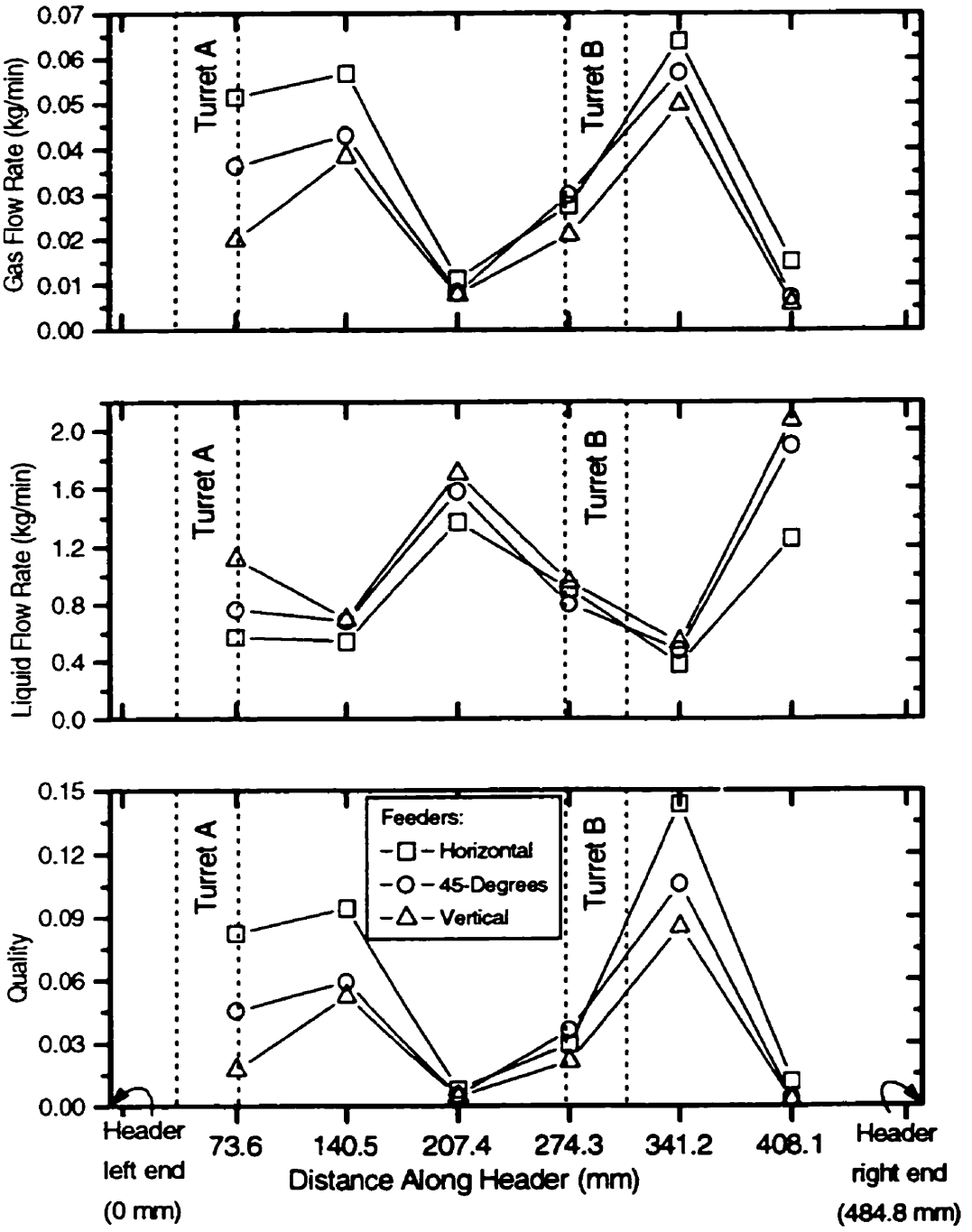

Figure 4.16 Quality, Gas and Liquid Flow Rate in Individual Feeders for Test No. R-15

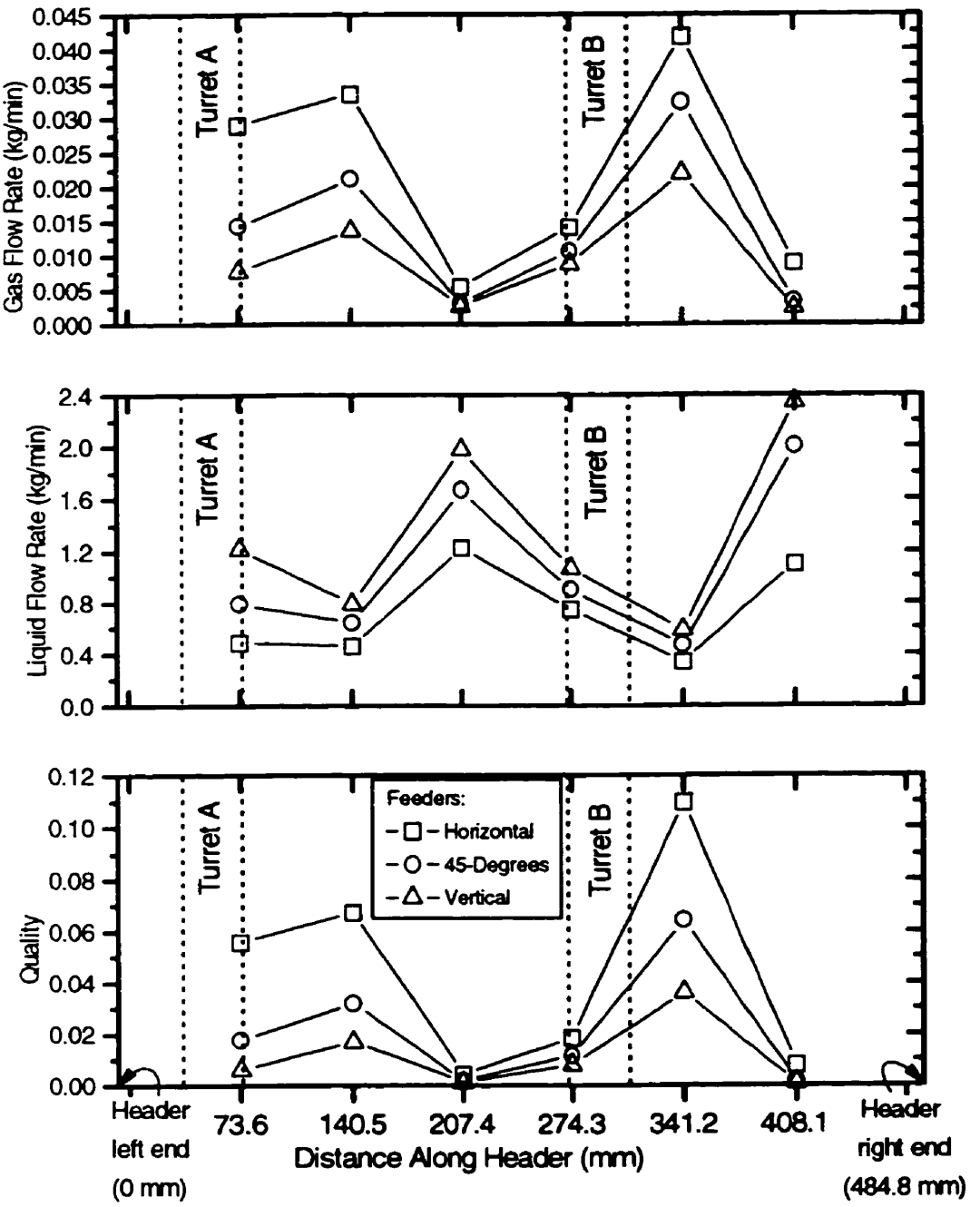

Figure 4.17 Quality, Gas and Liquid Flow Rate in Individual Feeders for Test No. R-16

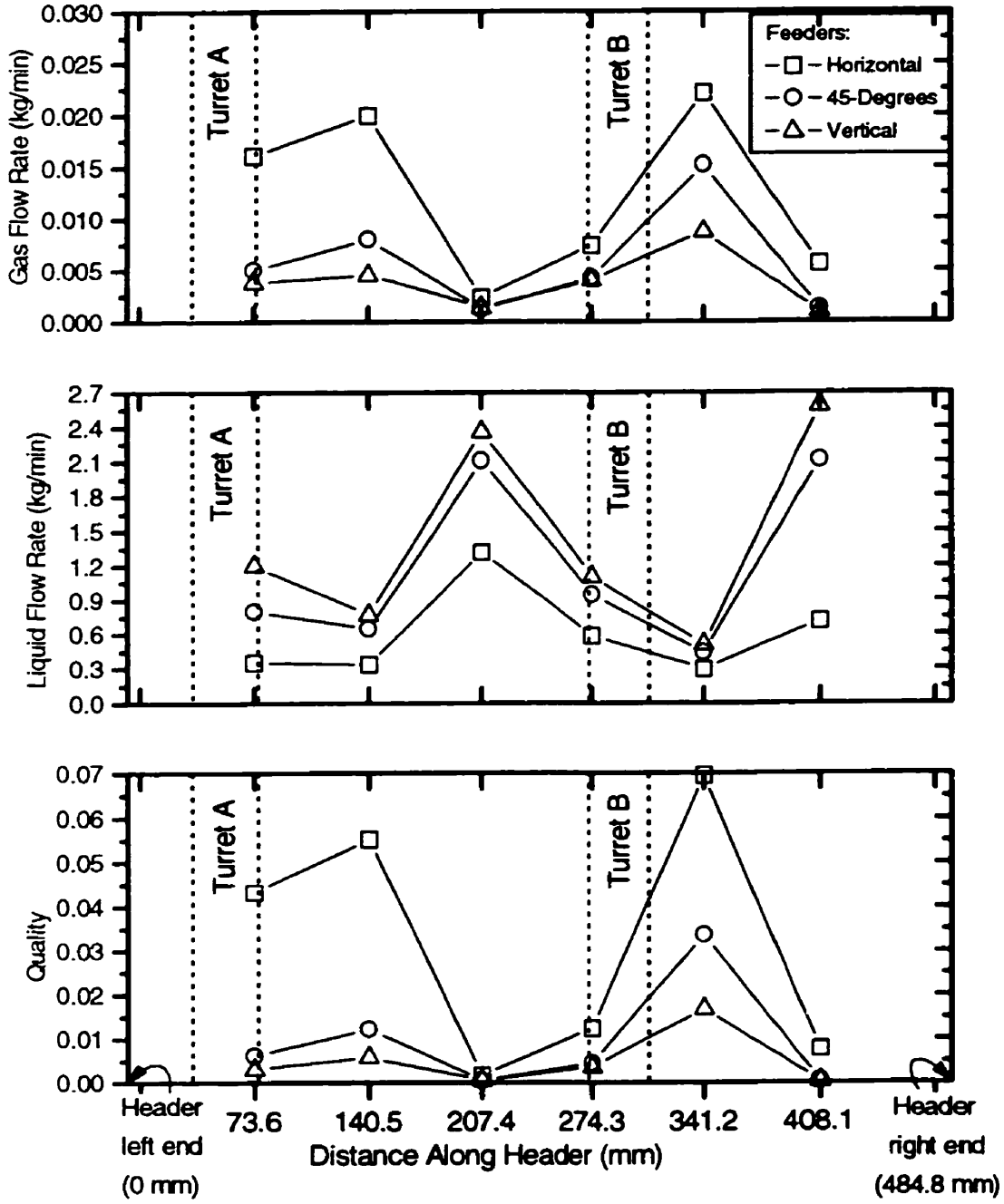

Figure 4.18 Quality, Gas and Liquid Flow Rate in Individual Feeders for Test No. R-17

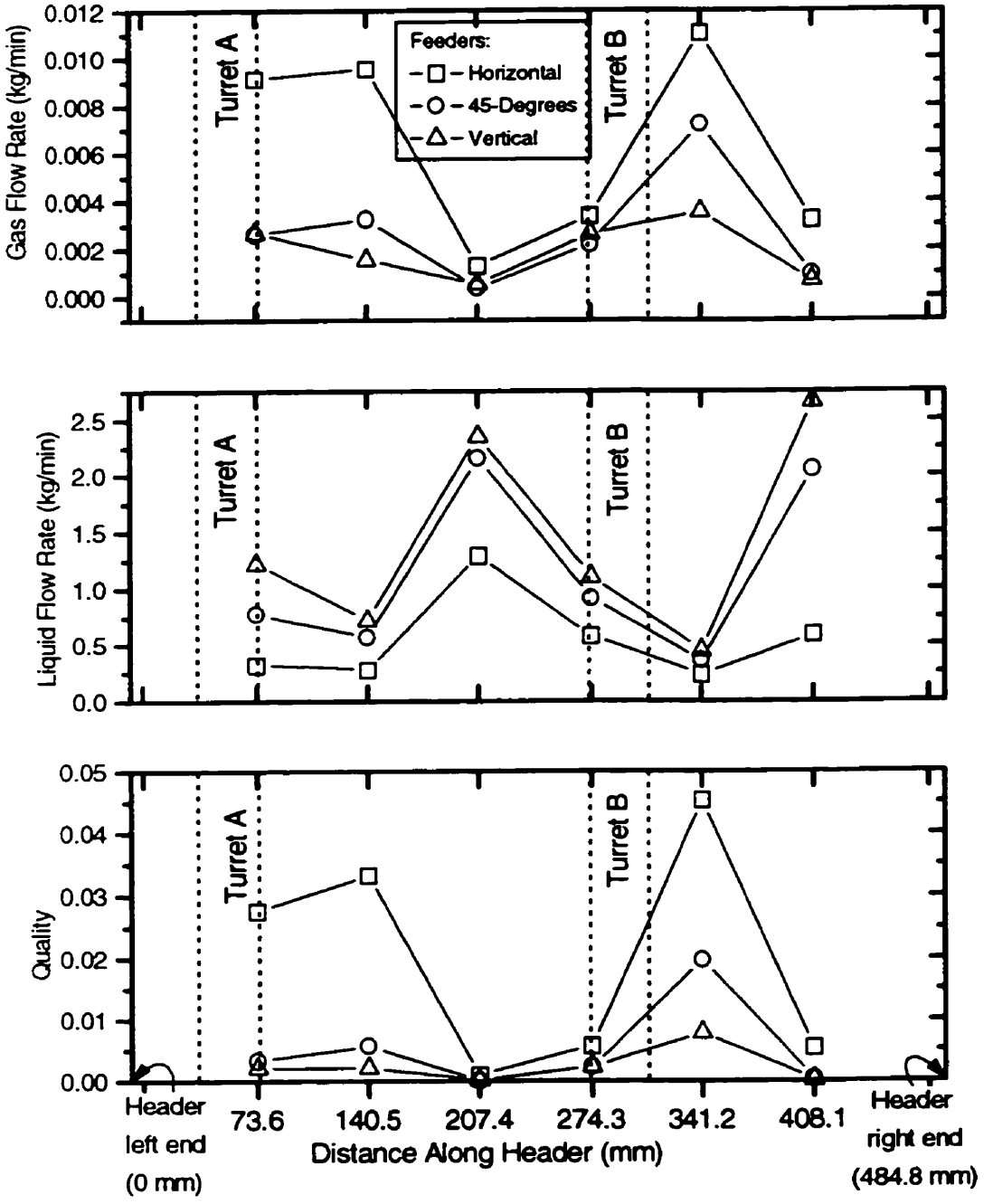

Figure 4.19 Quality, Gas and Liquid Flow Rate in Individual Feeders for Test No. R-18

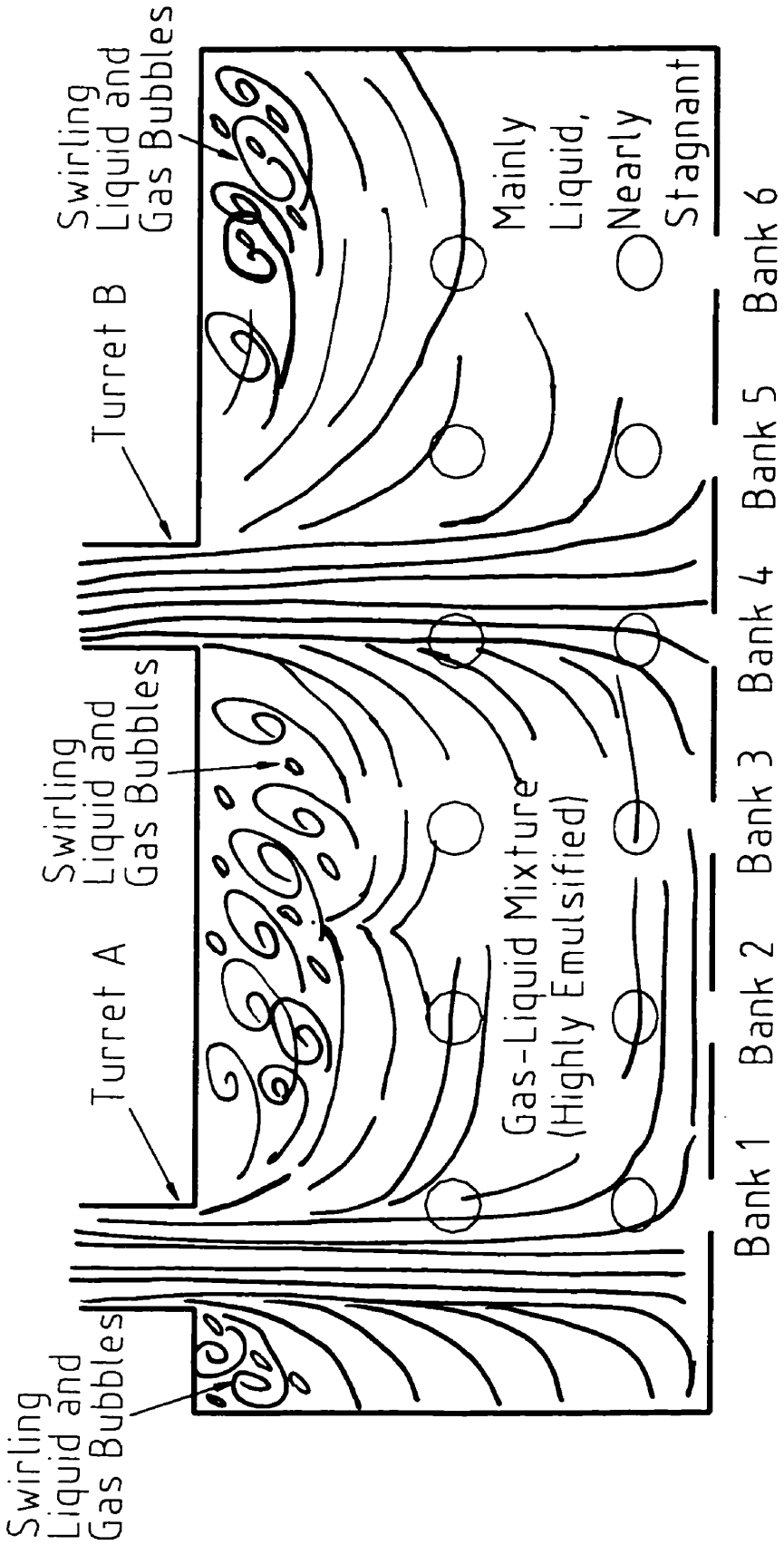

Figure 4.20 Sketch of the Flow Pattern in the Header for Test Nos. R-15 to R-18

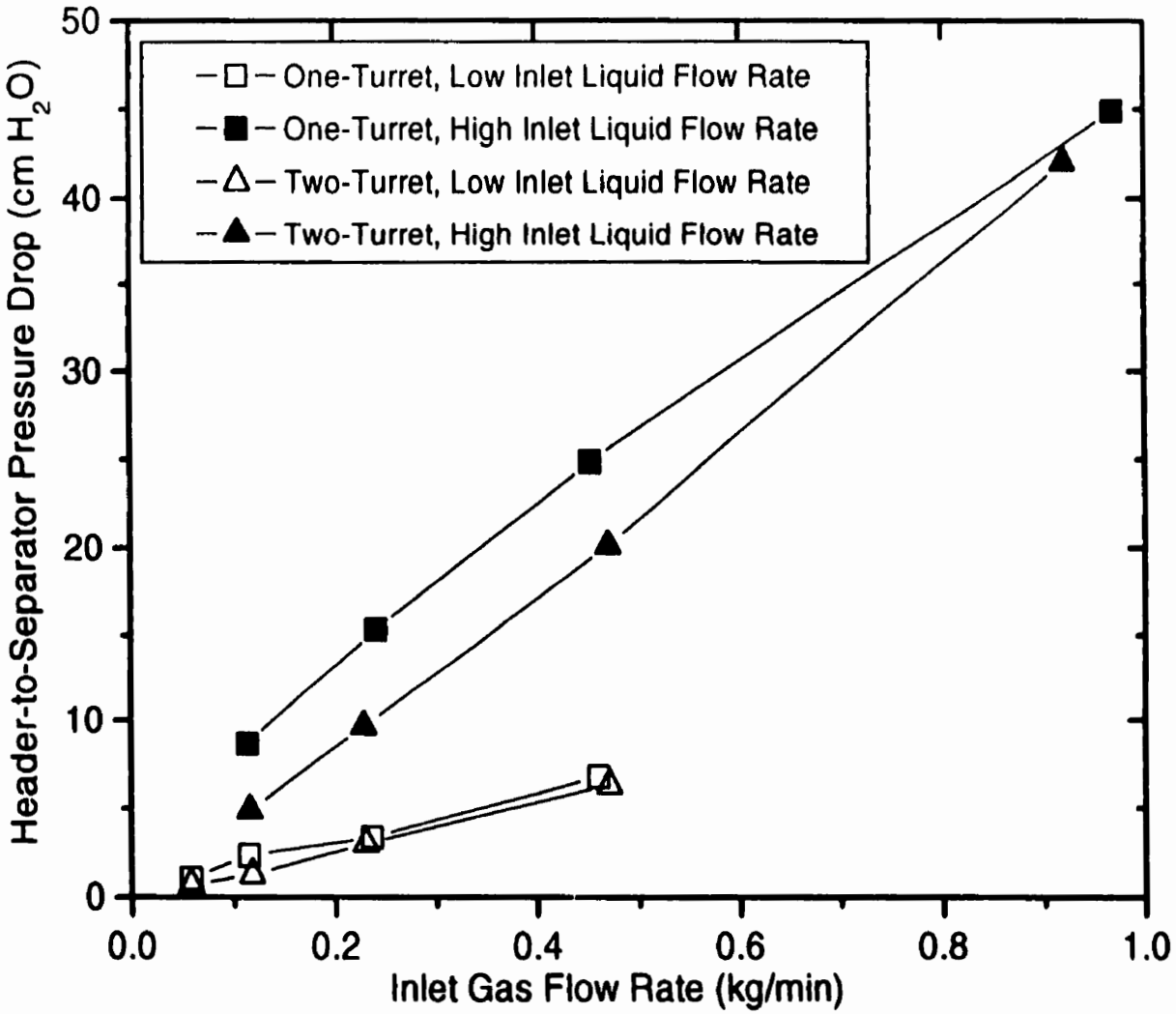

Figure 4.21 Header-to-Separator Pressure Drop vs. Inlet Gas Flow Rate

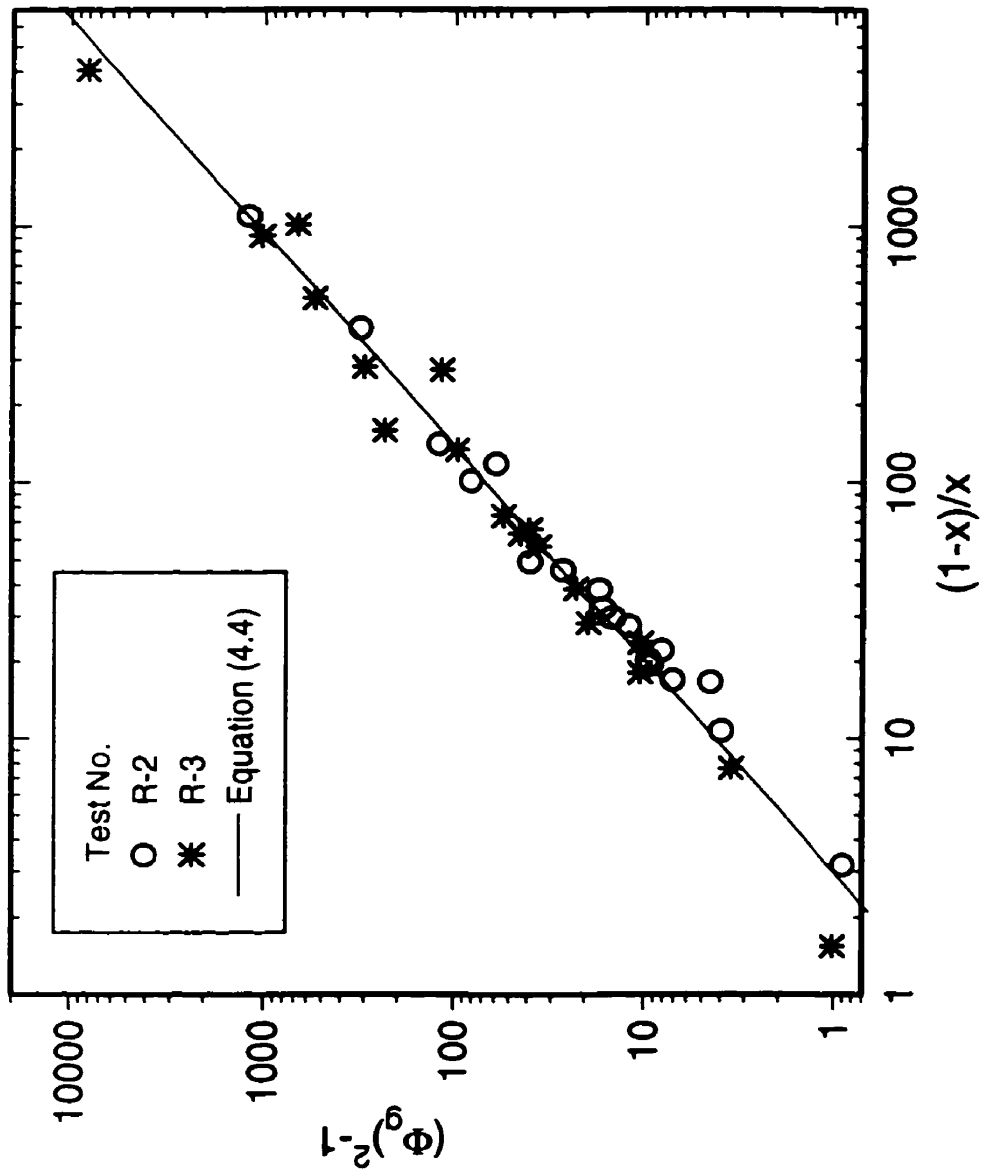

Figures 4.22 $(\Phi_g)^2$-1 vs. (1-x)/x for Test Nos. R-2 and R-3

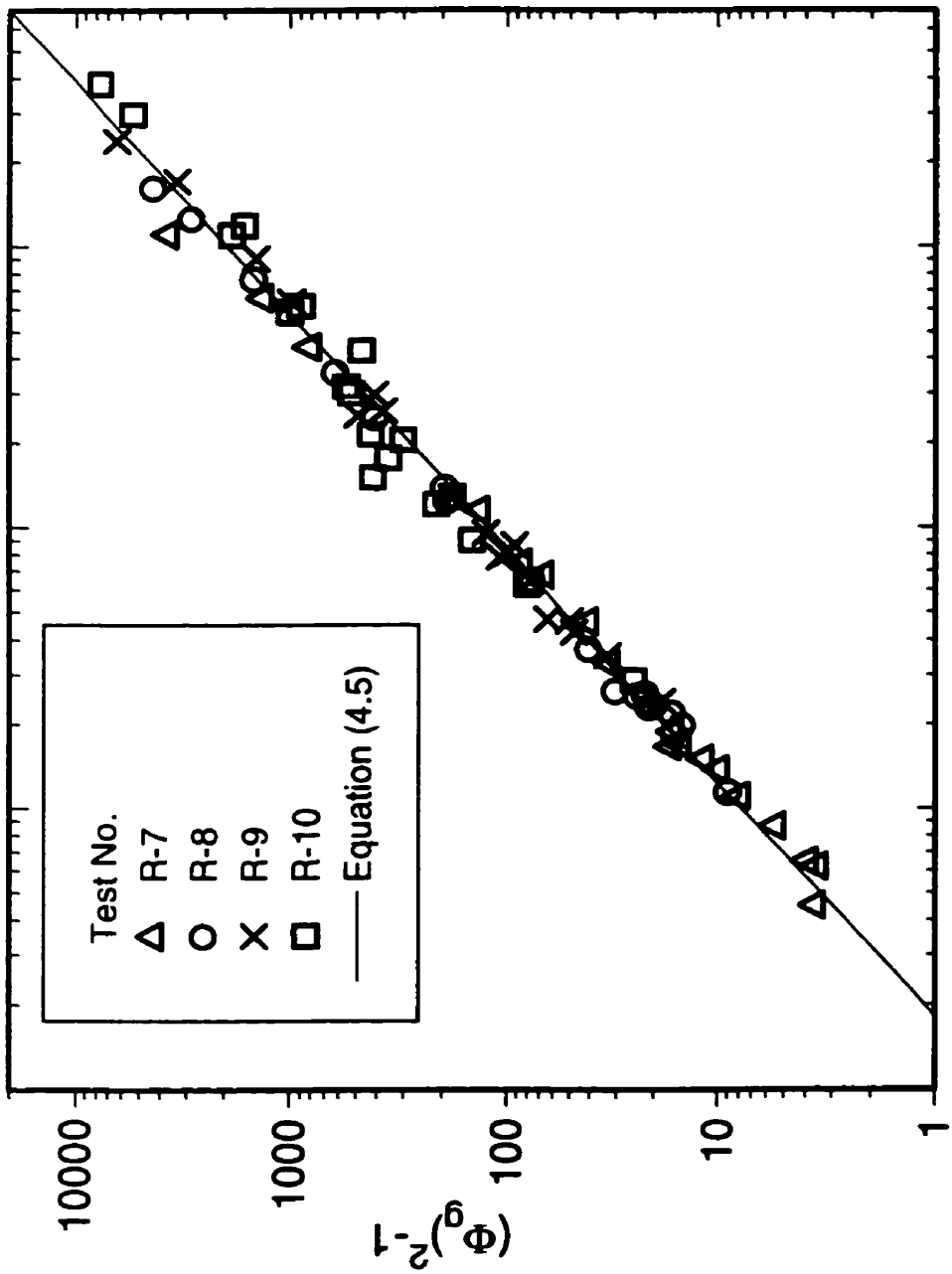

Figures 4.23 $(\Phi_g)^2$-1 vs. (1-x)/x for Test Nos. R-7 to R-10

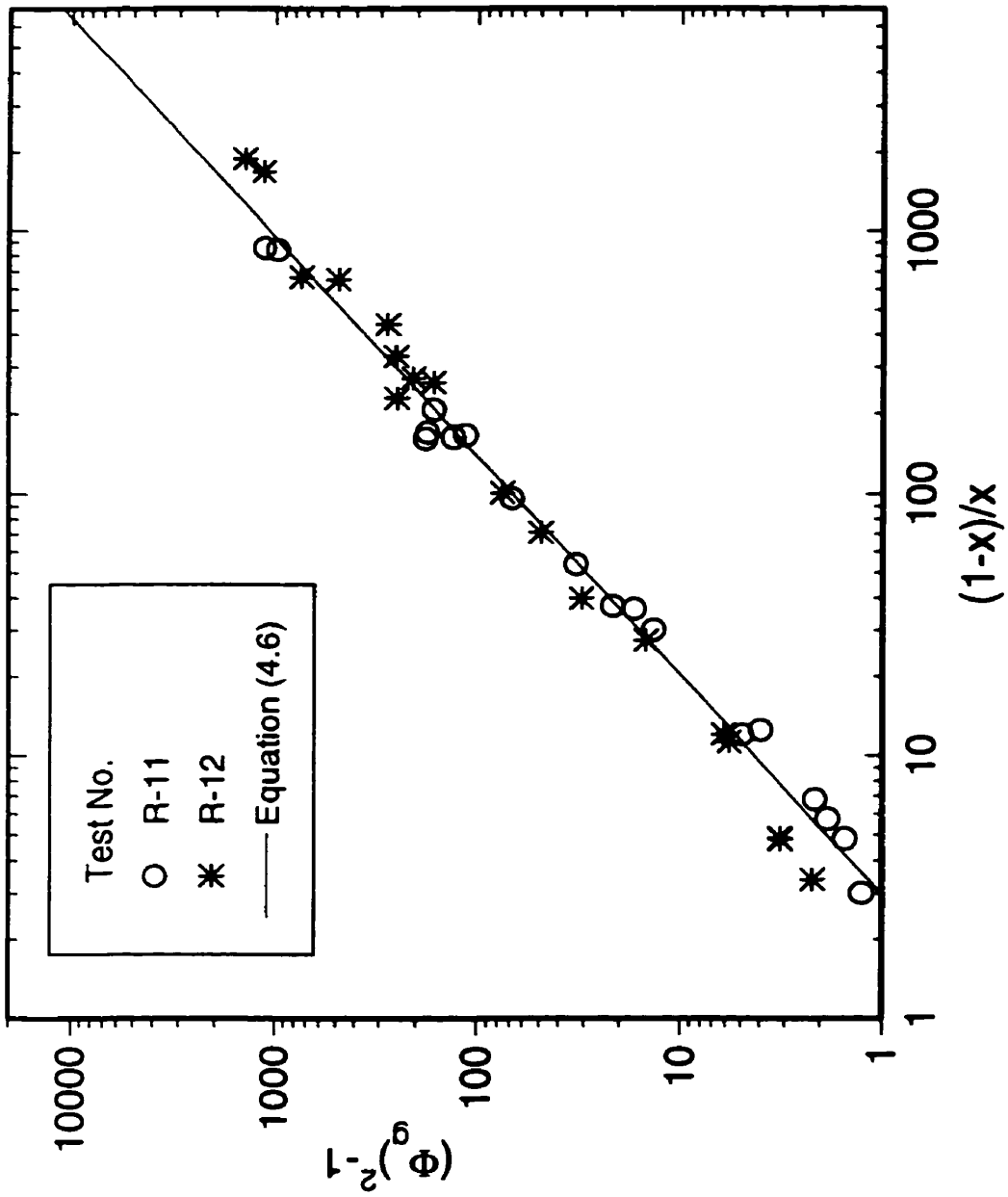

Figures 4.24 $(\Phi_g)^2$-1 vs. (1-x)/x for Test Nos. R-11 and R-12

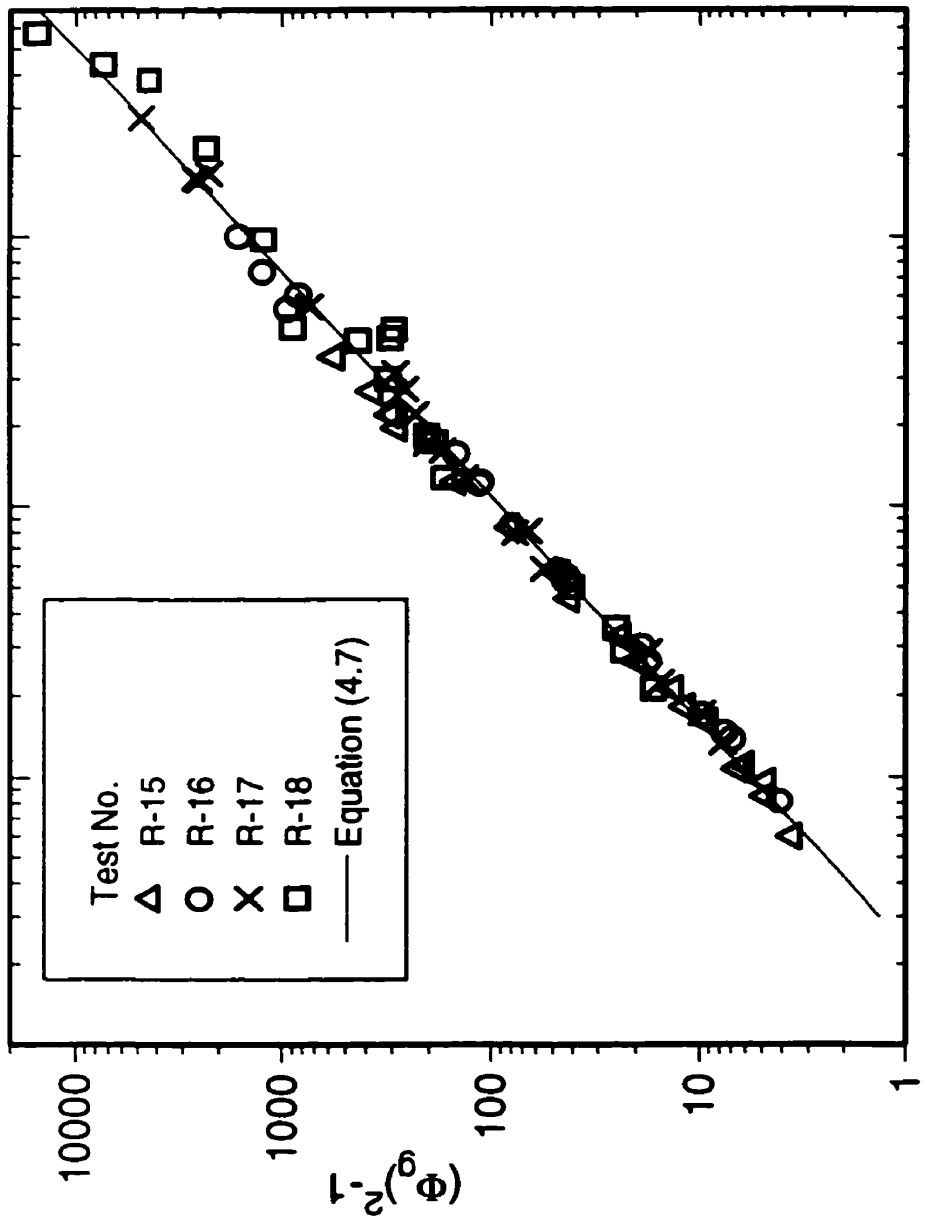

Figures 4.25 $(\Phi_g)^2$-1 vs. (1-x)/x for Test Nos. R-15 to R-18

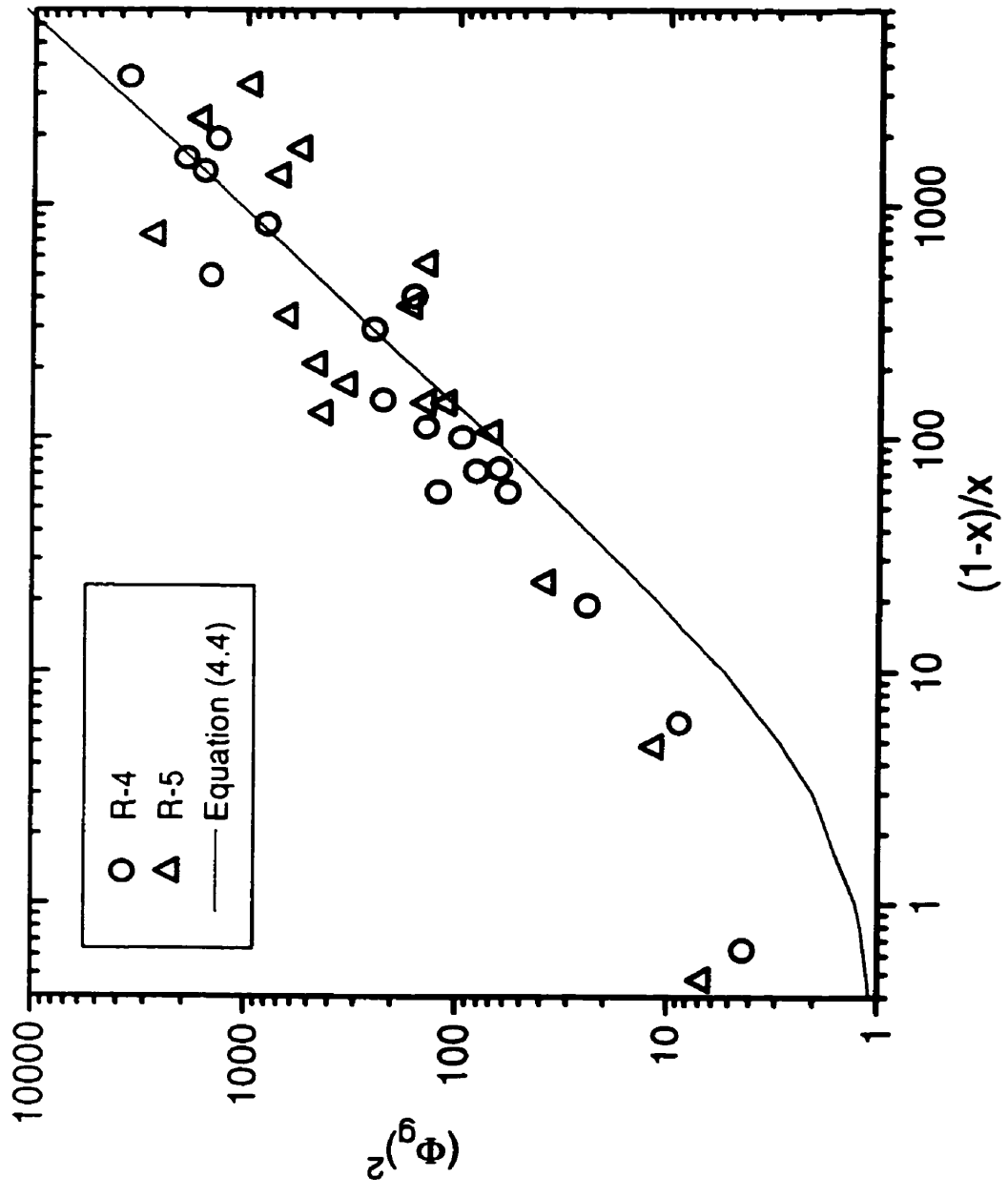

Figures 4.26 Data of Test Nos. R-4 and R-5 Compared with the Correlating Equation for Test Nos. R-2 and R-3

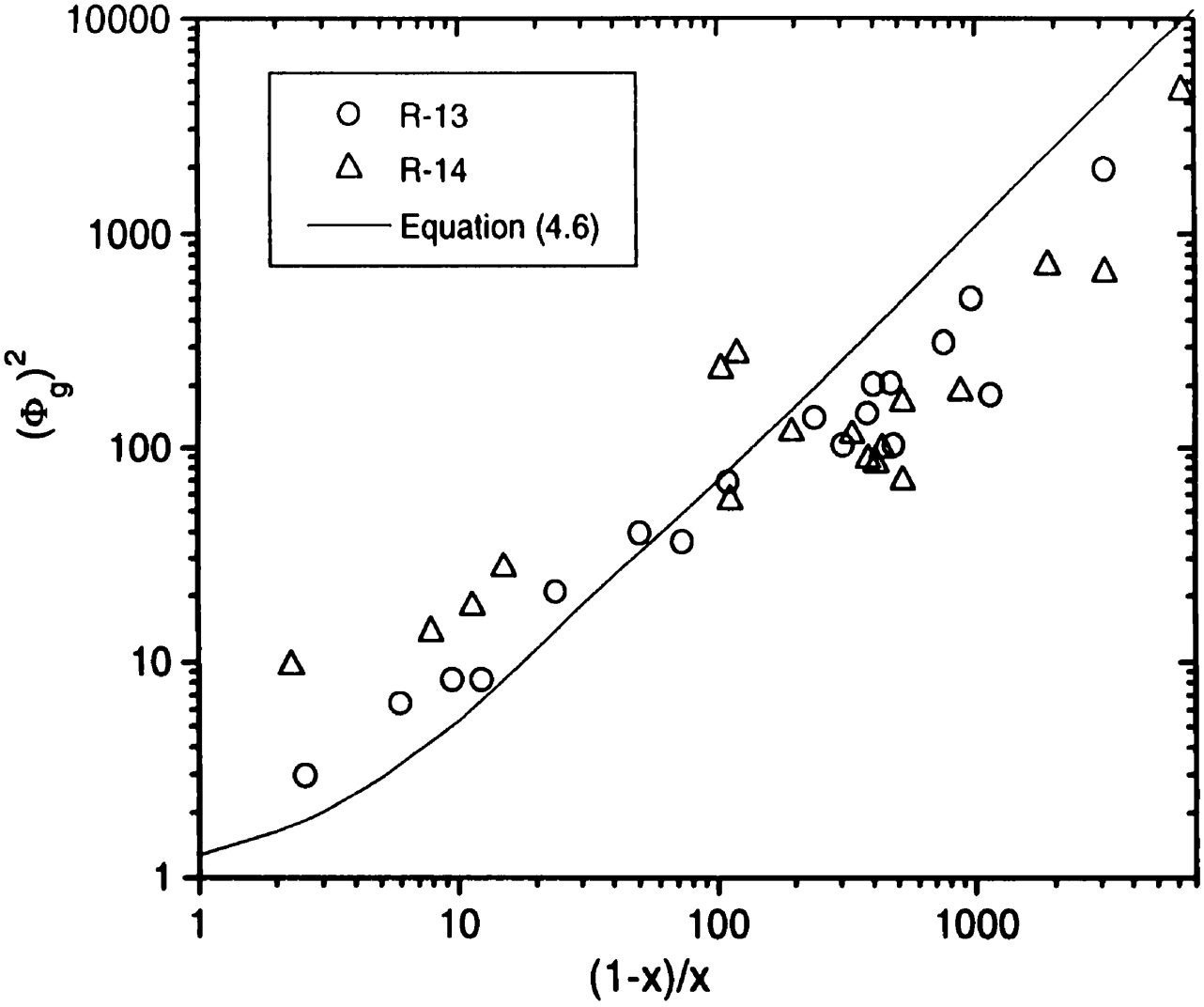

Figures 4.27 Data of Test Nos. R-13 and R-14 Compared with the Correlating Equation for Test Nos. R-11 and R-12

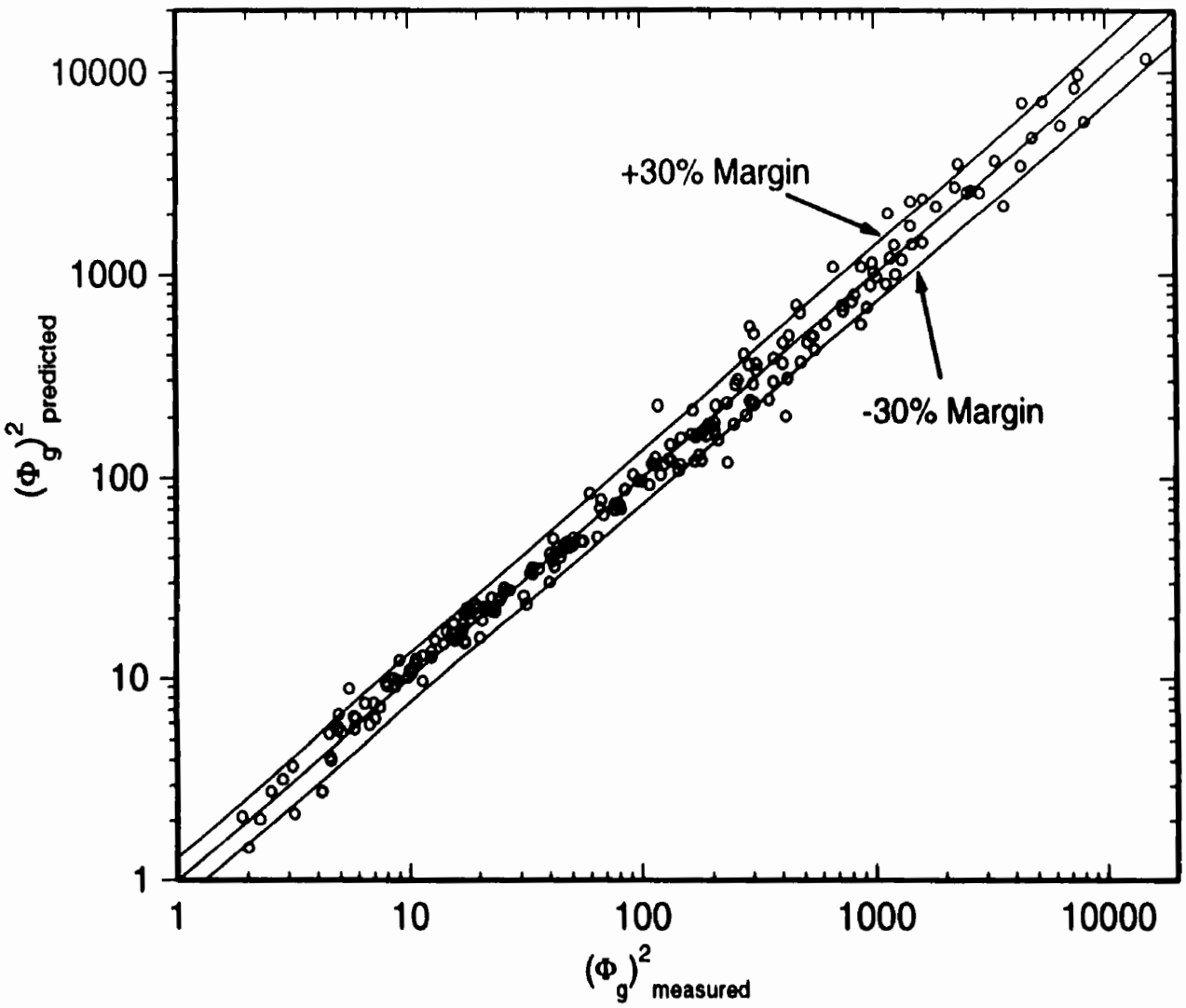

Figures 4.28 Comparison of the Predicted $(\Phi_g)^2$ vs. Measured $(\Phi_g)^2$

CHAPTER 5

CONCLUSIONS AND RECOMMENDATIONS

5.1 Conclusions

Experimental data were generated for two-phase gas-liquid flow in a scaled-down version of a CANDU-type header-feeder system. The test section consisted of a transparent header with six banks of five feeders. Air-water mixtures at room temperature were used in the experiment with a nominal absolute pressure in the header of 170.3 kPa (24.7 psi abs). A total of 16 tests were conducted using one- and two-turret injection and various inlet flow rates of gas and liquid. In each test, the individual outlet mass flow rates of gas and liquid from the feeders were measured under the condition of equal pressure drop across all 30 feeders. The following conclusions were drawn from this experimental investigation:

1. Significant variations in the gas and liquid flow rates were found among the feeders of the same bank and from bank to bank. It is believed that phase distribution in the header affected gas and liquid flows in the feeders.
2. The gas, liquid and quality distributions in the feeders were strongly affected by the inlet gas and liquid flow rates as well as the type of injection (one-turret or two-turret).
3. In some cases visual observations of flow patterns in the header during the tests could help to explain the gas and liquid flow distributions in the feeders.

4. The data from 12 out of the 16 tests that were performed were well correlated using a Lockhart-Martinelli-type parameter and the feeder quality. These correlations have trends similar to those in the data of the four remaining tests. However, the correlation method does not allow the prediction of the individual gas and liquid flow rates in the feeders.

5.2 Recommendations for Future Work

The following recommendations are made for future work:

1. Other combinations of inlet conditions different from the ones used in the present experiment could be investigated to widen the range of data available.
2. Similar experiments should be conducted on a larger-scale CANDU-type header to see how the scaling factor affects the dependent variables in this experiment.
3. Additional two-phase tests should be conducted to measure the void distribution at any cross-section and along the header. Knowledge of this parameter is no doubt essential to predict the phase and flow distribution in the feeders correctly.
4. Consideration should be given to using the present data to test and improve the computer codes developed to predict header-feeder flow conditions in postulated LOCA scenarios in CANDU nuclear reactors.

REFERENCES

Hassan, I.G., "Single, Dual and Triple Discharge from a Large Stratified, Two-Phase Region through Small Branches", Ph.D. Thesis, University of Manitoba, 1995.

Hassan, I.G., Soliman, H.M., Sims, G.E. and Kowalski, J.E., "Two-Phase Flow from a Stratified Region through a Small Side Branch", ASME Journal of Fluids Engineering, Vol. 120, pp. 605-612, 1998.

Kline, S.J. and McClintock, F.A., "Describing Uncertainties in Single-Sample Experiments", Mech. Eng., Vol. 75, pp. 3-8, 1953.

Kowalski, J.E. and Hanna, B.N., "Studies of Two-Phase Flow Distribution in a CANDU-Type Header/Feeder System", Proceedings of the Fourth International Topical Meeting on Nuclear Reactor Thermalhyraulics, Karlsruhe, Germany, Vol. 1, pp. 28-33, October, 1989.

Kowalski, J.E. and Krishnan, V.S., "Two-Phase Flow Distribution from a Large Manifold", AIChE Annual Meeting, New York, November 15-20, 1987.

Micaelli, J.C. and Memponteil, A., "Two-Phase Flow Behaviour in a Tee-Junction - The CATHARE Model", Proceedings of the Fourth International Topical Meeting on

Nuclear Reactor Thermal-Hydraulics, Karlsruhe, Germany, Vol. 2, pp. 1024-1030, October 10-13, 1989.

Rong, X. and Kawaji, M., "Two-Phase Header Flow Distribution in a Stacked Plate Heat Exchanger", Gas Liquid Flows, ASME, FED-Vol. 225, pp. 115-122, 1995.

Schrock, V.E., Revankar, S.T., Mannheimer, R., Wang, C.-H. and Jia, D., "Steam-Water Critical Flow through Small Pipes from Stratified Upstream Regions", Proceedings of the Eighth International Heat Transfer Conference, San Francisco, California, Vol. 5, pp. 2307-2311, August 17-22, 1986.

Smoglie, C. and Reimann, J., "Two-Phase Flow through Small Branches in a Horizontal Pipe with Stratified Flow", International Journal of Multiphase Flow, Vol. 12, pp. 609-625, 1986.

Yonomoto, T. and Tasaka, K., "New Theoretical Model for Two-Phase Flow Discharged from Stratified Two-Phase Region through Small Break", Journal of Nuclear Science and Technology, Vol. 25, pp. 441-455, 1988.

Yonomoto, T. and Tasaka, K., "Liquid and Gas Entrainment to a Small Break Hole from a Stratified Two-Phase Region", International Journal of Multiphase Flow, Vol. 17, pp. 745-765, 1991.

APPENDIX A

INSTRUMENT CALIBRATION

A.1 Introduction

All measuring devices used in the experimental flow loop were calibrated in-house and the calibrations were compared with the manufacturer's data. The results of the calibrations are presented in this appendix. The instruments are listed in Tables 3.1 to 3.4. Calibration results of the differential-pressure transmitters are presented first followed by the calibration results of the Bourdon pressure gauges and flow meters. The thermocouples used in the experiment were tested using a standard mercury-in-glass thermometer and were found to be in adequate working condition. The in-house calibration values were used in the data analysis. Linear interpolation between two consecutive calibration points was used in the case of air and water rotameters as well as pressure gauges. A linear fitted curve was used in the case of the differential-pressure transmitters.

A.2 Calibration of the Pressure Transmitters

The two pressure transmitters that were used in the experiment were calibrated against a water manometer using a digital voltmeter. The digital voltmeter that was used in the calibration of the pressure transmitters was also used in the normal running of the experiments. The sensitivity of the digital voltmeter was approximately 10.5 mV per mm of water for both calibration and subsequent experiments. The discrimination in the

voltmeter was ±1 mV. The results of the calibration of the two pressure transmitters are presented in Tables A.1 and A.2. The manometer pressure is shown in the first column. The corresponding actual reading on a digital voltmeter is shown in the second column. A linear relationship is expected between the range of output of the pressure transmitters and the pressure difference reading, where a reading of 2.000 V corresponds to a pressure difference of 0.0 inches of H_2O and a reading of 10.000 V corresponds to a pressure difference of 30.0 inches of H_2O. The points from the expected linear relationship that correspond to the given manometer pressure are shown in the third column.

Table A.1 Calibration Results of Differential-Pressure Transmitter No. 1

Manometer Pressure (inches H_2O)	Actual Reading (volts)	Expected Linear Reading (volts)
0.0	2.0003	2.0000
5.0	3.302	3.333
10.0	4.640	4.667
15.0	5.972	6.000
20.0	7.315	7.333
25.0	8.674	8.667
30.0		10.000

The following equation gives a linear relation between the actual pressure difference measured by the manometer and the actual voltage reading of transmitter No.1.

$$\Delta P = -7.41 + 3.74V \qquad \text{(A.1)}$$

where,

ΔP = pressure difference in inches of water, and

V = actual voltage reading in volts.

Equation (A.1) was used in the data analysis.

Table A.2 Calibration Results of Differential-Pressure Transmitter No. 2

Manometer Pressure (inches H_2O)	Actual Reading (volts)	Expected Linear Reading (volts)
0.0	1.9998	2.0000
5.0	3.318	3.333
10.0	4.649	4.667
15.0	5.983	6.000
20.0	7.321	7.333
25.0	8.650	8.667
30.0	9.991	10.000

The following equation gives a linear relation between the actual pressure difference measured by the manometer and the actual voltage reading of transmitter No. 2.

$$\Delta P = -7.47 + 3.75V \qquad \text{(A.2)}$$

where the symbols are as for Equation (A.1).

Equation (A.2) was used in the data analysis.

A.3 Calibration of the Pressure Gauges

The nine Bourdon pressure gauges used in this experiment were calibrated using a dead-weight tester. The results of the calibration are presented in tabular format in Tables A.3 through A.11. The true pressure measured by the dead-weight tester is presented in the first column of the calibration tables. The reading indicated by the pressure gauge is shown in the second column. The correction, which is defined as (True pressure –

Indicated pressure) is shown in the third column. Linear interpolation between two consecutive calibration points was used in the data analysis.

Table A.3 Calibration Results of Pressure Gauge No. 1

True Pressure		Indicated Pressure		Correction	
(psig)	(kPa)	(psig)	(kPa)	(psi)	(kPa)
0	0.0	0	0.0	0	0.0
20	137.9	22.0	151.7	-2.0	-13.8
40	275.8	41.0	282.7	-1.0	-6.9
60	413.7	61.0	420.6	-1.0	-6.9
80	551.6	81.0	558.5	-1.0	-6.9
100	689.5	100.5	692.9	-0.5	-3.4
120	827.4	120.5	830.8	-0.5	-3.4
140	965.3	140.0	965.3	0.0	0.0
160	1103.2	160.5	1106.6	-0.5	-3.4
180	1241.1	181.0	1247.9	-1.0	-6.9
200	1378.9	>200	>1378.9		

Table A.4 Calibration Results of Pressure Gauge No. 2

True Pressure		Indicated Pressure		Correction	
(psig)	(kPa)	(psig)	(kPa)	(psi)	(kPa)
0	0.0	0	0.0	0	0.0
10	68.9	12.5	86.2	-2.5	-17.2
20	137.9	22.0	151.7	-2.0	-13.8
30	206.8	32.0	220.6	-2.0	-13.8
40	275.8	42.4	292.3	-2.4	-16.5
50	344.7	52.0	358.5	-2.0	-13.8
60	413.7	62.0	427.5	-2.0	-13.8
70	482.6	72.0	496.4	-2.0	-13.8
80	551.6	82.0	565.4	-2.0	-13.8
90	620.5	92.0	634.3	-2.0	-13.8
100	689.5	>100	>689.5		

Table A.5 Calibration Results of Pressure Gauge No. 3

True Pressure		Indicated Pressure		Correction	
(psig)	(kPa)	(psig)	(kPa)	(psi)	(kPa)
0	0.0	0	0.0	0	0.0
10	68.9	10	68.9	0	0.0
20	137.9	20	137.9	0	0.0
30	206.8	29.8	205.5	0.2	1.4
40	275.8	39.9	275.1	0.1	0.7
50	344.7	49.9	344.0	0.1	0.7
60	413.7	59.9	413.0	0.1	0.7
70	482.6	69.9	481.9	0.1	0.7
80	551.6	79.9	550.9	0.1	0.7
90	620.5	89.8	619.1	0.2	1.4
100	689.5	99.8	688.1	0.2	1.4

Table A.6 Calibration Results of Pressure Gauge No. 4

True Pressure		Indicated Pressure		Correction	
(psig)	(kPa)	(psig)	(kPa)	(psi)	(kPa)
0	0.0	0	0.0	0	0.0
10	68.9	11.0	75.8	-1.0	-6.9
20	137.9	20.5	141.3	-0.5	-3.4
30	206.8	30.0	206.8	0.0	0.0
40	275.8	40.0	275.8	0.0	0.0
50	344.7	50.2	346.1	-0.2	-1.4
60	413.7	60.2	415.1	-0.2	-1.4
70	482.6	70.2	484.0	-0.2	-1.4
80	551.6	80.2	553.0	-0.2	-1.4
90	620.5	90.1	621.2	-0.1	-0.7
100	689.5	>100	>689.5		

Table A.7 Calibration Results of Pressure Gauge No. 5

True Pressure		Indicated Pressure		Correction	
(psig)	(kPa)	(psig)	(kPa)	(psi)	(kPa)
0	0.0	0	0.0	0	0.0
5	34.5	5.5	37.9	-0.5	-3.4
10	68.9	10.6	73.1	-0.6	-4.1
15	103.4	15.0	103.4	0.0	0.0
20	137.9	20.0	137.9	0.0	0.0
25	172.4	25.0	172.4	0.0	0.0
30	206.8	30.0	206.8	0.0	0.0
40	275.8	40.0	275.8	0.0	0.0
50	344.7	50.0	344.7	0.0	0.0
60	413.7	60.0	413.7	0.0	0.0

Table A.8 Calibration Results of Pressure Gauge No. 6

True Pressure		Indicated Pressure		Correction	
(psig)	(kPa)	(psig)	(kPa)	(psi)	(kPa)
0	0.0	0	0.0	0	0.0
10	68.9	10.0	68.9	0.0	0.0
20	137.9	19.0	131.0	1.0	6.9
30	206.8	29.0	199.9	1.0	6.9
40	275.8	39.0	268.9	1.0	6.9
50	344.7	49.0	337.8	1.0	6.9
60	413.7	59.5	410.2	0.5	3.4
70	482.6	69.5	479.2	0.5	3.4
80	551.6	79.5	548.1	0.5	3.4
90	620.5	89.5	617.1	0.5	3.4
100	689.5	99.5	686.0	0.5	3.4

Table A.9 Calibration Results of Pressure Gauge No. 7

True Pressure*		Indicated Pressure		Correction	
(psig)	(kPa)	(psig)	(kPa)	(psi)	(kPa)
0.99	6.8	0.8	5.5	0.19	1.3
1.19	8.2	1.0	6.9	0.19	1.3
2.17	15.0	2.0	13.8	0.17	1.2
3.19	22.0	3.0	20.7	0.19	1.3
4.29	29.6	4.0	27.6	0.29	2.0
5.12	35.3	5.0	34.5	0.12	0.8
6.19	42.7	6.0	41.4	0.19	1.3
7.15	49.3	7.0	48.3	0.15	1.0
8.27	57.0	8.0	55.2	0.27	1.9
9.27	63.9	9.0	62.1	0.27	1.9
10.32	71.2	10.0	68.9	0.32	2.2
11.23	77.4	11.0	75.8	0.23	1.6
12.36	85.2	12.0	82.7	0.36	2.5
13.28	91.6	13.0	89.6	0.28	1.9
14.25	98.2	14.0	96.5	0.25	1.7
15.25	105.1	15.0	103.4	0.25	1.7

*Tested against a mercury manometer

Table A.10 Calibration Results of Pressure Gauge No. 8

True Pressure		Indicated Pressure		Correction	
(psig)	(kPa)	(psig)	(kPa)	(psi)	(kPa)
0	0.0	0	0.0	0.0	0.0
5	34.5	5.5	37.9	-0.5	-3.4
10	68.9	10.5	72.4	-0.5	-3.4
20	137.9	20.5	141.3	-0.5	-3.4
30	206.8	30.5	210.3	-0.5	-3.4
40	275.8	41.0	282.7	-1.0	-6.9
50	344.7	50.5	348.2	-0.5	-3.4
60	413.7	60.5	417.1	-0.5	-3.4
70	482.6	70.0	482.6	0.0	0.0
80	551.6	80.0	551.6	0.0	0.0
90	620.5	89.0	613.6	1.0	6.9
100	689.5	99.5	686.0	0.5	3.4

Table A.11 Calibration Results of Pressure Gauge No. 9

True Pressure		Indicated Pressure		Correction	
(psig)	(kPa)	(psig)	(kPa)	(psi)	(kPa)
0	0.0	0.0	0.0	0.0	0.0
5	34.5	5.0	34.5	0.0	0.0
10	68.9	9.7	66.9	0.3	2.1
15	103.4	14.6	100.7	0.4	2.8
20	137.9	19.5	134.4	0.5	3.4
25	172.4	24.5	168.9	0.5	3.4
30	206.8	29.5	203.4	0.5	3.4
35	241.3	34.4	237.2	0.6	4.1
40	275.8	39.3	271.0	0.7	4.8
45	310.3	44.3	305.4	0.7	4.8
50	344.7	49.3	339.9	0.7	4.8
55	379.2	54.3	374.4	0.7	4.8
60	413.7	59.4	409.5	0.6	4.1

A.4 Calibration of the Flow Meters

The calibration results of the air and water rotameters are presented in this section. All air and water rotameters had a linear percentage scale etched on the glass tube. This percentage reading is shown in the first column of the calibration tables. The manufacturer's calibration is indicated on a scale mounted beside the rotameter tube and these readings are given in the second column of the tables. The actual measured flow rate that corresponds to the linear percentage scale reading is shown in the third column. The actual flow rates were measured using wet test meters and venturi meters for the air rotameters. A weigh-and-time method was used to measure the actual flow rates for the water rotameters.

A.4.1 Calibration of the Air Rotameters

The 11 air rotameters used in this experiment were calibrated using wet test meters and venturi meters (in turn the calibrations of which are traceable to NIST standards). Air rotameters that have ball-type floats were calibrated at two different pressures since the density correction used in converting the actual flow rates to standard conditions is not as accurate for these rotameters as it is for air rotameters with conventional-type floats. The results of the calibrations at pressures that were closest to the experimental conditions were used in tests that involved air rotameters with ball-type floats. The calibration results of the air rotameters are given in Tables A.12 through A.22.

Table A.12 Calibration Results for Rotameter AM1 at Atmospheric Pressure

Rotameter Scale Reading (%)	Indicated Flow Rate (SLPM)	Actual Flow Rate (SLPM)
10	--	5.4
20	10.4	11.1
30	16.1	17.2
40	22.2	23.7
50	28.5	30.2
60	35.8	37.5
70	42.2	45.0
80	49.2	53.4
90	56.5	62.3
100	64.3	71.6

Table A.13 Calibration Results for Rotameter AM1 at a Gauge Pressure of 206.9 kPa (30 psi)

Rotameter Scale Reading (%)	Indicated Flow Rate (SLPM)	Actual Flow Rate (SLPM)
10	--	6.1
20	10.4	12.1
30	16.1	18.3
40	22.2	24.8
50	28.5	31.4
60	35.8	38.7
70	42.2	45.7
80	49.2	53.3
90	56.5	61.2
100	64.3	68.9

Table A.14 Calibration Results for Rotameter AM2

Rotameter Scale Reading (%)	Indicated Flow Rate (SLPM)	Actual Flow Rate (SLPM)
10	44	46.0
20	82	85.4
30	120	120.6
40	155	154.6
50	192	190.7
60	226	220.1
70	261	256.2
80	298	293.4
90	337	329.9
100	373	368.8

Table A.15 Calibration Results for Rotameter AM3

Rotameter Scale Reading (%)	Indicated Flow Rate (SLPM)	Actual Flow Rate (SLPM)
10	--	156.1
20	370	375.7
30	555	560.5
40	730	753.8
50	925	936.6
60	1120	1142.6
70	1320	1366.2
80	1540	1580.9
90	1755	1831.1
100	--	--

Table A.16 Calibration Results for Rotameter AM4 at Atmospheric Pressure

Rotameter Scale Reading (%)	Indicated Flow Rate (SLPM)	Actual Flow Rate (SLPM)
10	--	5.9
20	10.6	11.5
30	16.2	17.1
40	22.4	23.5
50	28.8	30.2
60	35.9	37.2
70	42.5	44.9
80	49.4	52.3
90	56.8	60.8
100	64.7	69.6

Table A.17 Calibration Results for Rotameter AM4 at a Gauge Pressure of 96.6 kPa (14 psi)

Rotameter Scale Reading (%)	Indicated Flow Rate (SLPM)	Actual Flow Rate (SLPM)
10	--	6.0
20	10.6	11.5
30	16.2	17.7
40	22.4	23.8
50	28.8	30.4
60	35.9	37.2
70	42.5	44.7
80	49.4	51.8
90	56.8	59.3
100	64.7	67.2

Table A.18 Calibration Results for Rotameter AM5

Rotameter Scale Reading (%)	Indicated Flow Rate (SLPM)	Actual Flow Rate (SLPM)
10	47	49.3
20	87	90.5
30	123	124.7
40	158	159.4
50	195	196.4
60	230	230.6
70	266	263.8
80	303	300.8
90	342	336.3
100	379	373.0

Table A.19 Calibration Results for Rotameter AS1

Rotameter Scale Reading (%)	Indicated Flow Rate (SLPM)	Actual Flow Rate (SLPM)
10	--	0.19
20	0.27	0.36
30	0.48	0.56
40	0.69	0.75
50	0.87	0.89
60	1.05	1.07
70	1.22	1.25
80	1.38	1.43
90	1.55	1.59
100	1.69	1.76

Table A.20 Calibration Results for Rotameter AS2

Rotameter Scale Reading (%)	Indicated Flow Rate (SLPM)	Actual Flow Rate (SLPM)
10	--	0.61
20	1.50	1.64
30	2.42	2.60
40	3.30	3.50
50	4.20	4.38
60	5.10	5.32
70	6.00	6.17
80	6.90	7.04
90	7.82	7.84
100	8.68	8.79

Table A.21 Calibration Results for Rotameter AS3

Rotameter Scale Reading (%)	Indicated Flow Rate (SLPM)	Actual Flow Rate (SLPM)
10	7.3	5.4
20	12.4	10.9
30	17.1	15.9
40	22.0	20.7
50	26.5	24.9
60	30.8	29.4
70	35.5	34.0
80	39.6	38.0
90	43.5	41.2
100	--	45.3

Table A.22 Calibration Results for Rotameter AS4

Rotameter Scale Reading (%)	Indicated Flow Rate (SLPM)	Actual Flow Rate (SLPM)
10	28.0	27.1
20	49.5	48.0
30	70.5	68.3
40	90.5	87.8
50	110.5	107.0
60	130.5	126.7
70	151.0	146.5
80	171.5	165.9
90	193.0	187.8
100	--	209.9

A.4.2 Calibration of the Water Rotameters

The six water rotameters used in this experiment were calibrated using a weigh-and-time method. The calibration results of the water rotameters are given in Tables A.23 through A.28.

Table A.23 Calibration Results for Rotameter WM1 (Fluid specific gravity = 1.0)

Rotameter Scale Reading (%)	Indicated Flow Rate (kg/hr)	Actual Flow Rate (kg/hr)
10	375	397.3
20	730	749.0
30	1060	1110.0
40	1420	1473.1
50	1810	1860.4
60	2200	2247.3
70	2600	2648.2
80	2990	3070.8
90	3400	3496.3
100	3840	3946.7

Table A.24 Calibration Results for Rotameter WM2 (Fluid specific gravity = 1.0)

Rotameter Scale Reading (%)	Indicated Flow Rate (kg/hr)	Actual Flow Rate (kg/hr)
10	170	155.7
20	290	279.6
30	415	409.6
40	545	541.4
50	675	677.2
60	820	817.7
70	955	968.0
80	1105	1119.1
90	1260	1274.1
100	1413	1428.8

Table A.25 Calibration Results for Rotameter WS1

Rotameter Scale Reading (%)	Indicated Flow Rate (cm^3/min)	Actual Flow Rate (cm^3/min)
10	--	4.2
20	10.2	13.6
30	19.0	22.5
40	28.3	32.6
50	38.5	41.1
60	47.0	47.7
70	57.0	57.1
80	66.5	64.4
90	75.5	72.9
100	85.4	82.0

Table A.26 Calibration Results for Rotameter WS2

Rotameter Scale Reading (%)	Indicated Flow Rate (cm^3/min)	Actual Flow Rate (cm^3/min)
10	--	32.2
20	85	89.4
30	137	142.4
40	188	182.6
50	239	229.3
60	290	278.0
70	340	324.4
80	391	387.9
90	445	449.4
100	491.4	498.8

Table A.27 Calibration Results for Rotameter WS3

Rotameter Scale Reading (%)	Indicated Flow Rate (cm^3/min)	Actual Flow Rate (cm^3/min)
10	375	349.5
20	660	614.1
30	925	882.0
40	1175	1136.3
50	1460	1422.9
60	1725	1673.3
70	2025	1980.5
80	2325	2296.9
90	2625	2613.3
100	2955	2943.7

Table A.28 Calibration Results for Rotameter WS4

Rotameter Scale Reading (%)	Indicated Flow Rate (cm^3/min)	Actual Flow Rate (cm^3/min)
10	1.5	1.3
20	2.8	2.6
30	4.0	3.9
40	5.2	5.1
50	6.3	6.2
60	7.5	7.3
70	8.6	8.5
80	9.8	9.8
90	11.0	10.9
100	12.2	12.2

APPENDIX B

EXPERIMENTAL UNCERTAINTY

This appendix gives a discussion on the principles behind the uncertainty analysis, tabulated results of the analysis, and sample uncertainty calculations.

B.1 General

The principles behind the uncertainty analysis that was used are discussed in this section. Given a set of variables that are related by a mathematical function as follows:

$$Q = f(x_1, x_2, x_3, ...) \tag{B.1}$$

where Q is the dependent variable and x_1, x_2, x_3 are the independent variables, the uncertainty in each independent variable is expressed as $\pm\omega_{x1}$, $\pm\omega_{x2}$, $\pm\omega_{x3}$, respectively. According to Kline and McClintock (1953), propagation of these uncertainties results in uncertainties in Q of $\pm\omega_Q$ according to the relation

$$\omega_Q = \left[\left(\frac{\partial Q}{\partial x_1} \omega_{x1} \right)^2 + \left(\frac{\partial Q}{\partial x_2} \omega_{x2} \right)^2 + ... \right]^{0.5} \tag{B.2}$$

The uncertainties calculated using this method are at "odds" of 20 to 1. These odds imply that the probability any measured value is within $\pm\omega$ of the true value is approximately 95%; this holds for Q as well.

Here, it is assumed that the following factors contribute to the uncertainty in the measured variables:

- Uncertainties due to fluctuations, F
- Uncertainties due to discrimination in the instruments, D
- Uncertainties due to the calibration process, C
- Error in fitting of a mathematical function to the calibration data, I

The above are either in fractional form or in percentage, as appropriate. These factors are considered to contribute to the uncertainty ω_x in any measured variable x as follows:

$$\frac{\omega_x}{x} = \left[F_x^{\,2} + D_x^{\,2} + C_x^{\,2} + I_x^{\,2}\right]^{0.5} \tag{B.3}$$

All measuring devices were calibrated in-house and the calibrations were compared with the manufacturer's data. The results of the calibrations are shown in Appendix A.

B.2 Gas Flow Measurement

B.2.1 Inlet Gas Flow Rate

The mass flow rate of inlet gas is given by the following relation:

$$\dot{m} = \rho \dot{V} \tag{B.4}$$

where,

$\dot{V}$ = actual volumetric flow rate under the conditions in the rotameter, and

ρ = density of gas in the rotameter.

If we treat air as an ideal gas, the density can be expressed as

$$\rho = \frac{P}{RT} \tag{B.5}$$

where P is the absolute pressure in the rotameter, R is the gas constant and T is the absolute temperature of the gas. Equation (B.4) can now be written as

$$\dot{m} = \frac{P\dot{V}}{RT} \tag{B.6}$$

The application of Equation (B.2) to Equation (B.6) and division by Equation (B.6) yields

$$\frac{\omega_{\dot{m}}}{\dot{m}} = \left[\left(\frac{\omega_{\dot{V}}}{\dot{V}}\right)^2 + \left(\frac{\omega_P}{P}\right)^2 + \left(\frac{\omega_R}{R}\right)^2 + \left(\frac{\omega_T}{T}\right)^2\right]^{0.5} \tag{B.7}$$

where,

$\omega_{\dot{m}}$ = uncertainty in the mass flow rate of inlet gas,

$\omega_{\dot{V}}$ = uncertainty in the volumetric flow rate,

ω_P = uncertainty in the absolute air pressure,

ω_R = uncertainty in the gas constant, and

ω_T = uncertainty in the temperature.

The sample uncertainty calculations shown below are for inlet gas flow in test number R-2. The uncertainty in the volumetric flow rate is calculated from the following equation:

$$\frac{\omega_{\dot{V}}}{\dot{V}} = \left[F_{\dot{V}}^{\,2} + D_{\dot{V}}^{\,2} + C_{\dot{V}}^{\,2} + I_{\dot{V}}^{\,2}\right]^{0.5} \tag{B.8}$$

where,

$F_{\dot{V}}$ = the fluctuation in the float of the rotameter on the linear scale as a percentage of the actual linear scale reading,

$D_{\dot{V}}$ = discrimination in the linear scale of the rotameter as a percentage of the actual linear scale reading,

$C_{\dot{V}}$ = percentage uncertainty in the calibration, and

$I_{\dot{V}}$ = percentage error in fitting a mathematical function to the calibration data.

Rotameter (AM2) linear scale reading = 66.1,

$F_{\dot{V}}$ = (0.5/66.1)*100% = 0.756%,

$D_{\dot{V}}$ = (0.2/66.1)*100%= 0.303%,

$C_{\dot{V}}$ = 1.0%, and

$I_{\dot{V}}$ = 1.65%.

Substituting the above values into Equation (B.8), we obtain for the uncertainty in the volumetric flow rate

$$\frac{\omega_{\dot{V}}}{\dot{V}} = \left[(0.756)^2 + (0.303)^2 + (1.0)^2 + (1.65)^2\right]^{.5}$$

$$= 2.094\ \%$$

The absolute pressure P is calculated from

$$P = P_{bar} + P_g \qquad \text{(B.9)}$$

where,

P_{bar}= barometric pressure, and

P_g= gauge pressure

The uncertainty in the absolute pressure ω_P is calculated as follows:

$$\frac{\omega_P}{P} = \left[\left(\frac{\partial P}{\partial P_{bar}} \frac{\omega_{P_{bar}}}{P} \right)^2 + \left(\frac{\partial P}{\partial P_g} \frac{\omega_{P_g}}{P} \right)^2 \right]^{0.5} \tag{B.10}$$

where,

$\omega_{P_{bar}}$ = uncertainty in the barometric pressure, and

ω_{P_g} = uncertainty in the gauge pressure.

The uncertainty in the barometric pressure is negligible compared with the uncertainty in the gauge pressure, and Equation (B.10) becomes

$$\frac{\omega_P}{P} \cong \left[\left(\frac{\partial P}{\partial P_g} \frac{\omega_{P_g}}{P} \right)^2 \right]^{0.5} = \frac{\omega_{P_g}}{P} \tag{B.11}$$

The uncertainty in the gauge pressure is in turn calculated as follows:

$$\frac{\omega_P}{P} \cong \frac{\omega_{P_g}}{P} = \left[F_{P_g}{}^2 + D_{P_g}{}^2 \right]^{0.5} \tag{B.12}$$

where,

F_{Pg} = the fluctuation in the pressure gauge as a percentage of the absolute pressure,

D_{Pg} = the discrimination in the scale of the pressure gauge as a percentage of the absolute pressure.

Calibration uncertainty for the pressure gauges is negligible, as is the uncertainty due to fitting a mathematical function to the calibration data.

Again, for test number R-2:

Absolute air pressure, P = 37.82 psi,

Fluctuation in the pressure gauge = 0.5 psi, and

Discrimination on the pressure gauge = 0.2 psi.

$F_{Pg} = (0.5/37.82)*100\% = 1.322\%$, and

$D_{Pg} = (0.2/37.82)*100\% = 0.529\%$.

Substituting the above values into Equation (B.12), the uncertainty in the absolute pressure is

$$\frac{\omega_P}{P} = \left[(1.322)^2 + (0.529)^2\right]^{0.5}$$

$$= 1.424\ \%$$

$$\frac{\omega_R}{R} \cong 0 \text{ (negligible)}$$

Temperature of inlet gas:

$\omega_T = 0.2$ K,

T = 296.12 K.

The uncertainty in the inlet gas temperature is

$$\frac{\omega_T}{T} = \left(\frac{0.2}{295.54}\right)*100\%$$

$$= 0.068\ \%$$

Substituting the above values into Equation (B.7) gives the uncertainty in the inlet gas mass flow rate as

$$\frac{\omega_{\dot{m}}}{\dot{m}} = 2.53\%$$

B.2.2 Outlet Gas Flow Rate

The outlet gas contains both pure air and water vapour. For simplicity, the density of the outlet gas is treated as if it were pure air. This simplification introduces negligible errors.

In addition to the uncertainties considered for the inlet gas mass flow rate, there is an uncertainty introduced because of fluctuations of the air-water interface level in the measuring tank. Let $\omega_{\dot{m}_1}$ be the uncertainty associated with the variables considered for the inlet gas flow rate and would be given by Equation (B.7); therefore

$$\frac{\omega_{\dot{m}_1}}{\dot{m}} = \left[\left(\frac{\omega_{\dot{V}}}{\dot{V}}\right)^2 + \left(\frac{\omega_P}{P}\right)^2 + \left(\frac{\omega_R}{R}\right)^2 + \left(\frac{\omega_T}{T}\right)^2\right]^{0.5} \tag{B.13}$$

Further, let $\omega_{\dot{m}_2}$ be the uncertainty associated with the fluctuation in the air-water interface level in the measuring tank. The location of the interface was recorded at the beginning of data-taking for one feeder and also at the end of data-taking for the same feeder. The volume of the fluctuation during the time of data-taking for the feeder under consideration was calculated from the internal dimensions of the measuring tank and the change in the location of the interface. This volume was then converted into the equivalent mass of air and water. Dividing the mass by an average time that was required to take the data gave the equivalent air and water mass flow rates. Taking $\omega_{\dot{m}_2}$ into consideration allows for a conservative measure of uncertainty due to fluctuation in the measuring tank.

The fractional uncertainty in outlet gas mass flow rate is considered to be

$$\frac{\omega_{\dot{m}}}{\dot{m}} = \left[\left(\frac{\omega_{\dot{m}_1}}{\dot{m}} \right)^2 + \left(\frac{\omega_{\dot{m}_2}}{\dot{m}} \right)^2 \right]^{0.5} \tag{B.14}$$

The following sample calculation is done for the outlet gas flow from feeder number (1,1) in test number R-2.

Rotameter (AS3) linear scale reading = 22.8,

$F_{\dot{V}}$ = (0.25/22.8)*100% = 1.096%,

$D_{\dot{V}}$ = (0.25/22.8)*100%= 1.096%,

$C_{\dot{V}}$ = 1.0%, and

$I_{\dot{V}}$ = 1.65%.

The definition of the above variables is the same as in the case of inlet gas. The uncertainty in the volumetric flow rate is then calculated from Equation (B.8) as

$$\frac{\omega_{\dot{V}}}{\dot{V}} = \left[(1.096)^2 + (1.096)^2 + (1.0)^2 + (1.65)^2 \right]^{0.5}$$

$$= 2.475\ \%$$

In calculating the uncertainty in the absolute pressure of outlet air, the uncertainty in the barometric pressure cannot be neglected. Equation (B.10) now becomes

$$\frac{\omega_P}{P} = \left[\left(\frac{\omega_{P_{bar}}}{P} \right)^2 + F_{P_g}{}^2 + D_{P_g}{}^2 \right]^{0.5} \tag{B.15}$$

The subscript P_g in Equation (B.15) refers to the water manometer that was used to measure the gauge pressure of the outlet air.

Absolute air pressure, P = 14.320 psi,

Discrimination in the water manometer = 0.05 inches H_2O = 0.001806 psi, and

Discrimination in the mercury barometer = 0.1 mm Hg = 0.00193 psi (the only source of uncertainty in P_{bar}); therefore

$$\frac{\omega_{P_{bar}}}{P} = \frac{0.00193}{14.320} * 100\%$$

$$= 0.013\ \%$$

$$F_{Pg} \cong 0$$

$$D_{Pg} = \frac{0.001806}{14.320} * 100\ \%$$

$$= 0.013\ \%$$

The uncertainty in the outlet absolute pressure is

$$\frac{\omega_P}{P} = \left[(0.013)^2 + (0.013)^2 + (0)^2\right]^{0.5}$$

$$= 0.0185\ \%$$

Again,

$$\frac{\omega_R}{R} \cong 0 \text{ (negligible)}$$

Temperature of outlet gas:

$\omega_T = 0.2$ K,

T = 296.12 K.

The uncertainty in the temperature is

$$\frac{\omega_T}{T} = \left(\frac{0.2}{295.54}\right) * 100\%$$

$$= 0.068\%$$

Substituting the above values into Equation (B.13), we obtain

$$\frac{\omega_{\dot{m}1}}{\dot{m}} = 2.476\,\%$$

The fractional uncertainty due to the fluctuations in the measuring tank was calculated as follows.

Volume displaced in the measuring tank = 10.1 cm^3

Average time taken to record data = 1.5 minutes

$\omega_{\dot{m}2}$ = 0.0000136 kg/min

$\dot{m}$ = 0.03386 kg/min

$$\frac{\omega_{\dot{m}2}}{\dot{m}} = \frac{0.0000136}{0.03386} * 100\,\%$$

$$= 0.040\ \%$$

Substituting the above into Equation (B.14) gives the uncertainty in the outlet gas mass flow rate in feeder (1,1) as

$$\frac{\omega_{\dot{m}}}{\dot{m}} = \left[(2.476)^2 + (0.040)^2\right]^{.5}$$

$$= 2.48\ \%$$

B.3 Liquid Flow Measurement

B.3.1 Inlet Liquid Flow Rate

As mentioned earlier, calibration of water rotameters was done using a weigh-and-time method, so giving mass flow rates directly. All tests were done with essentially the same water temperature (room temperature); therefore, a constant density of 1000 kg/m^3 was used in the calculations with no uncertainty associated with it. Under these circumstances, Equation (B.3) applies as

$$\frac{\omega_{\dot{m}}}{\dot{m}} = \frac{\omega_{\dot{V}}}{\dot{V}} = \left[F_{\dot{V}}{}^2 + D_{\dot{V}}{}^2 + C_{\dot{V}}{}^2 + I_{\dot{V}}{}^2\right]^{0.5} \qquad \text{(B.16)}$$

The following sample calculation is done for inlet liquid flow in test number R-2. The uncertainty estimates are:

Rotameter (WM1) linear scale reading = 24.5,

$F_{\dot{V}}$ = (0.25/24.5)*100% = 1.020%,

$D_{\dot{V}}$ = (0.2/24.5)*100%= 0.816%,

$C_{\dot{V}}$ = 1.0%, and

$I_{\dot{V}}$ = 0%.

Substituting the above values into Equation (B.16), we get

$$\frac{\omega_{\dot{m}}}{\dot{m}} = \left[(1.020)^2 + (0.816)^2 + (1.0)^2 + (0)^2\right]^{0.5}$$

$$= 1.65\ \%$$

B.3.2 Outlet Liquid Flow Rate

Besides the uncertainties described above for inlet liquid flow rate, there is an additional uncertainty introduced because of changes in the level of the air-water interface in the measuring separation tank during data-taking. The treatment of this uncertainty was discussed in Section B.2.2. Again, let $\omega_{\dot{m}1}$ be the uncertainty associated with the variables considered for the inlet liquid flow rate calculated using Equation (B.16). Further, let $\omega_{\dot{m}2}$ be the uncertainty in outlet liquid flow rate associated with the change in the air-water interface level in the measuring tank. Again, Equation (B.14) applies

$$\frac{\omega_{\dot{m}}}{\dot{m}} = \left[\left(\frac{\omega_{\dot{m}1}}{\dot{m}} \right)^2 + \left(\frac{\omega_{\dot{m}2}}{\dot{m}} \right)^2 \right]^{0.5} \tag{B.17}$$

The following sample calculation is done for the outlet liquid flow from feeder number (1,1) in test number R-2. The uncertainty estimates are:

Rotameter (WS3) linear scale reading = 58.5,

$F_{\dot{V}}$ = (0.5/58.5)*100% = 0.855%,

$D_{\dot{V}}$ = (0.2/58.5)*100% = 0.342%,

$C_{\dot{V}}$ = 1.0%, and

$I_{\dot{V}}$ = 0%.

Substituting the above values into Equation (B.16), we get

$$\frac{\omega_{\dot{m}1}}{\dot{m}} = \left[(0.855)^2 + (0.342)^2 + (1.0)^2 + (0)^2 \right]^{0.5}$$

$$= 1.359\ \%$$

The fractional uncertainty due to the changes in the measuring tank was calculated as follows:

Volume displaced in the measuring tank = 10.1 cm^3,

Average time taken to record data = 1.5 minutes,

Displacement volume flow rate = 6.73 cm^3/min, and

$\dot{V}$ = 689.11 cm^3/min.

Therefore,

$$\frac{\omega_{\dot{m}_2}}{\dot{m}} = \frac{6.73}{689.11} \times 100\,\%$$

$$= 0.977\ \%$$

Substituting the above two results into Equation (B.17) gives the uncertainty in the outlet liquid mass flow rate through feeder (1,1) as

$$\frac{\omega_{\dot{m}}}{\dot{m}} = \left[(1.359\ )^2 + (0.977\ )^2\right]^{0.5}$$

$$= 1.68\ \%$$

B.4 Tabulated Measurement Uncertainty

Table B.1 through B.18 show the individual percentage uncertainties in the gas and liquid flow rates according to test and feeder numbers. The uncertainties in the mass flow rate of inlet gas and inlet liquid into the header did not vary significantly; therefore, a typical value is given for each test. The columns labelled 'Outlet Gas' and 'Outlet Liquid' are the uncertainties in the mass flow rate of outlet gas and outlet liquid from the indicated feeder, respectively.

Table B.1 Uncertainty Values for Test No. R-2

Inlet Gas (%): 2.5		
Inlet Liquid (%): 1.7		
Feeder Number	Outlet Gas (%)	Outlet Liquid (%)
(1,1)	2.5	1.7
(1,2)	2.5	3.0
(1,3)	2.5	1.4
(1,4)	2.1	3.3
(1,5)	2.0	6.5
(1,6)	2.3	1.3
(2,1)	2.2	1.7
(2,2)	2.3	2.5
(2,3)	2.3	3.0
(2,4)	2.3	1.5
(2,5)	2.4	3.2
(2,6)	3.6	1.6
(3,1)	2.8	2.1
(3,2)	4.7	1.7
(3,3)	3.1	4.2
(3,4)	3.4	1.9
(3,5)	3.1	2.2
(3,6)	13.1	5.9

Table B.2 Uncertainty Values for Test No. R-3

Inlet Gas (%): 3.1		
Inlet Liquid (%): 1.7		
Feeder Number	Outlet Gas (%)	Outlet Liquid (%)
(1,1)	2.6	5.0
(1,2)	3.1	3.2
(1,3)	3.5	1.8
(1,4)	2.0	2.7
(1,5)	2.1	8.5
(1,6)	2.3	3.0
(2,1)	3.1	7.0
(2,2)	2.4	3.7
(2,3)	2.4	5.0
(2,4)	2.4	3.6
(2,5)	2.9	10.3
(2,6)	6.3	3.1
(3,1)	3.2	4.0
(3,2)	5.1	2.7
(3,3)	5.8	8.7
(3,4)	8.9	8.2
(3,5)	2.4	1.4
(3,6)	46.0	5.9

Table B.3 Uncertainty Values for Test No. R-4

Inlet Gas (%): 4.4		
Inlet Liquid (%): 1.7		
Feeder Number	Outlet Gas (%)	Outlet Liquid (%)
(1,1)	4.1	5.2
(1,2)	2.1	4.2
(1,3)	2.0	5.5
(1,4)	2.3	3.3
(1,5)	2.3	7.1
(1,6)	3.4	1.6
(2,1)	2.3	1.7
(2,2)	3.9	6.7
(2,3)	3.2	2.0
(2,4)	3.0	4.9
(2,5)	3.5	2.4
(2,6)	3.5	2.1
(3,1)	2.5	2.4
(3,2)	6.9	7.2
(3,3)	4.3	2.5
(3,4)	30.1	9.3
(3,5)	10.4	4.1
(3,6)	15.0	2.6

Table B.4 Uncertainty Values for Test No. R-5

Inlet Gas (%): 3.3		
Inlet Liquid (%): 1.7		
Feeder Number	Outlet Gas (%)	Outlet Liquid (%)
(1,1)	5.0	2.5
(1,2)	3.2	10.4
(1,3)	2.5	6.8
(1,4)	3.1	10.4
(1,5)	3.2	38.6
(1,6)	6.5	10.6
(2,1)	2.3	2.0
(2,2)	3.6	3.2
(2,3)	3.9	1.9
(2,4)	3.6	2.9
(2,5)	3.7	1.7
(2,6)	8.9	3.0
(3,1)	7.3	6.6
(3,2)	32.8	21.9
(3,3)	2.9	1.9
(3,4)	23.6	5.5
(3,5)	2.8	2.5
(3,6)	5.2	2.1

Table B.5 Uncertainty Values for Test No. R-7

Inlet Gas (%): 3.3		
Inlet Liquid (%): 1.2		
Feeder Number	Outlet Gas (%)	Outlet Liquid (%)
(1,1)	2.0	3.7
(1,2)	2.0	3.6
(1,3)	2.0	2.5
(1,4)	2.0	2.1
(1,5)	2.5	16.8
(1,6)	2.2	2.3
(2,1)	2.0	4.4
(2,2)	2.0	2.6
(2,3)	2.0	4.0
(2,4)	2.0	5.5
(2,5)	2.3	7.0
(2,6)	2.4	1.1
(3,1)	2.3	6.6
(3,2)	2.8	2.0
(3,3)	2.0	19.7
(3,4)	1.9	5.0
(3,5)	2.6	7.4
(3,6)	12.5	5.7

Table B.6 Uncertainty Values for Test No. R-8

Inlet Gas (%): 2.5		
Inlet Liquid (%): 1.2		
Feeder Number	Outlet Gas (%)	Outlet Liquid (%)
(1,1)	2.1	1.4
(1,2)	2.2	1.3
(1,3)	2.2	1.2
(1,4)	2.0	4.0
(1,5)	2.5	6.2
(1,6)	9.0	5.7
(2,1)	2.0	1.7
(2,2)	2.2	1.3
(2,3)	2.2	4.0
(2,4)	2.1	3.0
(2,5)	3.6	6.9
(2,6)	5.1	2.2
(3,1)	2.6	3.0
(3,2)	3.0	3.4
(3,3)	3.7	18.1
(3,4)	2.8	5.3
(3,5)	4.8	6.2
(3,6)	31.0	9.7

Table B.7 Uncertainty Values for Test No. R-9

Inlet Gas (%): 3.0		
Inlet Liquid (%): 1.2		
Feeder Number	Outlet Gas (%)	Outlet Liquid (%)
(1,1)	2.1	2.6
(1,2)	2.2	1.8
(1,3)	2.2	2.1
(1,4)	2.2	1.8
(1,5)	2.1	4.1
(1,6)	2.8	1.3
(2,1)	2.2	4.5
(2,2)	2.2	3.0
(2,3)	2.1	2.6
(2,4)	2.2	4.5
(2,5)	2.4	2.4
(2,6)	8.4	2.8
(3,1)	2.5	1.9
(3,2)	3.1	8.9
(3,3)	3.2	3.1
(3,4)	3.2	4.2
(3,5)	4.3	3.7
(3,6)	19.4	4.2

Table B.8 Uncertainty Values for Test No. R-10

Inlet Gas (%): 4.4		
Inlet Liquid (%): 1.2		
Feeder Number	Outlet Gas (%)	Outlet Liquid (%)
(1,1)	2.6	3.1
(1,2)	2.2	3.6
(1,3)	2.3	4.5
(1,4)	2.5	2.9
(1,5)	3.8	11.7
(1,6)	2.8	1.5
(2,1)	2.9	3.6
(2,2)	2.6	2.9
(2,3)	2.3	1.4
(2,4)	2.2	1.4
(2,5)	5.2	3.4
(2,6)	3.5	2.1
(3,1)	4.0	4.4
(3,2)	5.1	8.6
(3,3)	4.5	6.1
(3,4)	3.5	2.5
(3,5)	2.6	1.5
(3,6)	14.8	2.4

Table B.9 Uncertainty Values for Test No. R-11

Inlet Gas (%): 4.3		
Inlet Liquid (%): 3.0		
Feeder Number	Outlet Gas (%)	Outlet Liquid (%)
(1,1)	1.9	9.6
(1,2)	1.9	5.0
(1,3)	2.9	23.9
(1,4)	2.4	10.3
(1,5)	2.0	7.0
(1,6)	1.9	9.4
(2,1)	2.3	5.8
(2,2)	2.3	5.1
(2,3)	3.7	8.8
(2,4)	2.2	4.6
(2,5)	2.7	2.2
(2,6)	2.1	4.1
(3,1)	3.4	3.8
(3,2)	3.4	2.8
(3,3)	7.8	5.5
(3,4)	3.1	3.3
(3,5)	4.1	1.8
(3,6)	17.7	10.8

Table B.10 Uncertainty Values for Test No. R-12

Inlet Gas (%): 6.3		
Inlet Liquid (%): 3.0		
Feeder Number	Outlet Gas (%)	Outlet Liquid (%)
(1,1)	2.0	6.1
(1,2)	2.2	20.7
(1,3)	2.0	6.0
(1,4)	3.0	5.4
(1,5)	2.2	16.6
(1,6)	2.3	17.8
(2,1)	3.6	11.3
(2,2)	2.4	3.5
(2,3)	5.0	4.0
(2,4)	8.5	15.7
(2,5)	3.1	12.1
(2,6)	2.3	1.9
(3,1)	5.3	8.1
(3,2)	6.0	5.5
(3,3)	9.2	3.0
(3,4)	5.1	5.6
(3,5)	5.3	8.2
(3,6)	21.5	5.9

Table B.11 Uncertainty Values for Test No. R-13

Inlet Gas (%): 4.6		
Inlet Liquid (%): 3.0		
Feeder Number	Outlet Gas (%)	Outlet Liquid (%)
(1,1)	2.4	26.9
(1,2)	2.5	22.7
(1,3)	2.1	12.2
(1,4)	2.1	2.6
(1,5)	2.3	11.1
(1,6)	3.1	59.9
(2,1)	3.9	6.1
(2,2)	3.4	1.4
(2,3)	5.0	3.8
(2,4)	5.4	5.5
(2,5)	4.1	13.2
(2,6)	2.7	2.6
(3,1)	3.9	4.6
(3,2)	15.6	7.8
(3,3)	34.2	14.9
(3,4)	9.8	10.0
(3,5)	9.2	11.1
(3,6)	16.9	3.6

Table B.12 Uncertainty Values for Test No. R-14

Inlet Gas (%): 6.1		
Inlet Liquid (%): 3.0		
Feeder Number	Outlet Gas (%)	Outlet Liquid (%)
(1,1)	2.5	7.1
(1,2)	2.5	88.4
(1,3)	3.4	15.2
(1,4)	2.6	7.5
(1,5)	3.2	2.4
(1,6)	2.2	6.4
(2,1)	2.9	3.1
(2,2)	3.5	2.3
(2,3)	6.3	4.2
(2,4)	2.2	1.9
(2,5)	4.0	1.8
(2,6)	5.4	6.6
(3,1)	3.4	3.6
(3,2)	11.9	3.7
(3,3)	76.0	12.2
(3,4)	12.2	11.8
(3,5)	4.3	4.6
(3,6)	112.9	10.1

Table B.13 Uncertainty Values for Test No. R-15

Inlet Gas (%): 3.5		
Inlet Liquid (%): 2.0		
Feeder Number	Outlet Gas (%)	Outlet Liquid (%)
(1,1)	2.0	1.8
(1,2)	2.0	1.6
(1,3)	2.6	1.3
(1,4)	1.9	3.1
(1,5)	2.0	3.8
(1,6)	2.0	3.5
(2,1)	2.0	5.5
(2,2)	2.0	2.2
(2,3)	2.4	1.9
(2,4)	2.0	3.2
(2,5)	2.0	1.9
(2,6)	2.3	2.0
(3,1)	2.2	3.1
(3,2)	2.5	8.5
(3,3)	2.3	2.3
(3,4)	2.2	3.2
(3,5)	2.1	3.4
(3,6)	4.0	1.2

Table B.14 Uncertainty Values for Test No. R-16

Inlet Gas (%): 4.2		
Inlet Liquid (%): 2.0		
Feeder Number	Outlet Gas (%)	Outlet Liquid (%)
(1,1)	2.0	2.8
(1,2)	2.0	2.7
(1,3)	3.5	5.6
(1,4)	2.2	8.3
(1,5)	2.0	6.1
(1,6)	2.4	6.2
(2,1)	2.0	1.5
(2,2)	2.1	3.4
(2,3)	3.1	1.5
(2,4)	2.0	1.8
(2,5)	2.0	3.2
(2,6)	2.7	1.2
(3,1)	2.4	1.5
(3,2)	2.4	5.8
(3,3)	3.5	3.0
(3,4)	2.4	1.2
(3,5)	2.7	3.9
(3,6)	2.9	2.7

Table B.15 Uncertainty Values for Test No. R-17

Inlet Gas (%): 6.3		
Inlet Liquid (%): 2.0		
Feeder Number	Outlet Gas (%)	Outlet Liquid (%)
(1,1)	2.4	2.5
(1,2)	2.5	4.2
(1,3)	5.0	4.5
(1,4)	2.5	9.3
(1,5)	2.7	2.0
(1,6)	2.1	3.3
(2,1)	2.1	3.6
(2,2)	2.2	5.4
(2,3)	6.4	2.4
(2,4)	2.1	1.3
(2,5)	2.3	1.4
(2,6)	6.2	2.4
(3,1)	3.0	3.6
(3,2)	3.7	7.2
(3,3)	27.8	8.3
(3,4)	2.5	1.9
(3,5)	4.0	3.4
(3,6)	9.9	2.1

Table B.16 Uncertainty Values for Test No. R-18

Inlet Gas (%): 4.6		
Inlet Liquid (%): 1.2		
Feeder Number	Outlet Gas (%)	Outlet Liquid (%)
(1,1)	2.6	4.7
(1,2)	2.8	2.1
(1,3)	6.3	3.8
(1,4)	2.9	5.0
(1,5)	3.1	2.1
(1,6)	2.6	3.4
(2,1)	2.2	1.7
(2,2)	2.5	2.2
(2,3)	17.4	2.0
(2,4)	2.4	2.1
(2,5)	2.5	3.9
(2,6)	4.3	2.0
(3,1)	2.8	2.8
(3,2)	4.8	4.3
(3,3)	24.5	3.7
(3,4)	3.5	3.8
(3,5)	4.5	3.0
(3,6)	6.0	2.1

Table B.17 Uncertainty Values for Test No. RPT-8

Inlet Gas (%): 2.4		
Inlet Liquid (%): 1.2		
Feeder Number	Outlet Gas (%)	Outlet Liquid (%)
(1,1)	2.1	1.4
(1,2)	2.2	3.8
(1,3)	2.2	4.5
(1,4)	2.0	4.1
(1,5)	3.4	12.7
(1,6)	7.1	3.8
(2,1)	2.1	2.6
(2,2)	2.2	4.6
(2,3)	2.0	5.3
(2,4)	2.0	3.7
(2,5)	2.0	3.1
(2,6)	2.4	1.4
(3,1)	2.5	1.3
(3,2)	3.0	4.4
(3,3)	2.0	4.8
(3,4)	2.8	3.4
(3,5)	2.6	2.6
(3,6)	14.2	4.7

Table B.18 Uncertainty Values for Test No. RPT-16

Inlet Gas (%): 4.2		
Inlet Liquid (%): 2.0		
Feeder Number	Outlet Gas (%)	Outlet Liquid (%)
(1,1)	2.0	5.2
(1,2)	2.0	2.7
(1,3)	2.5	4.7
(1,4)	2.1	2.7
(1,5)	2.1	6.8
(1,6)	2.3	5.3
(2,1)	2.1	4.5
(2,2)	2.1	1.4
(2,3)	3.3	1.9
(2,4)	2.1	4.7
(2,5)	2.0	3.2
(2,6)	2.9	1.4
(3,1)	2.4	1.7
(3,2)	2.5	6.0
(3,3)	8.2	5.8
(3,4)	2.5	2.5
(3,5)	2.7	6.1
(3,6)	2.6	2.5

APPENDIX C

EXPERIMENTAL DATA

This appendix contains tabulated values for all the experimental data obtained in this investigation. The data for tests RPT-8 and RPT-16 are given in Tables D.1 and D.2, respectively.

Table C.1 Experimental Results for Test No. R-2

Type of Injection: One turret
Inlet Gas Flow Rate (kg/min): 0.460
Inlet Liquid Flow Rate (kg/min): 15.19
Inlet Quality (%): 2.9
Header-to-Separator Pressure Difference (cm of water): 6.76
Mass Balance Error for Gas (%): -2.93
Mass Balance Error for Liquid (%): 0.03

Feeder Number	Gas Flow Rate (kg/min)	Liquid Flow Rate (kg/min)	Quality (%)
(1,1)	0.01693	0.3446	4.684
(1,2)	0.01706	0.3312	4.899
(1,3)	0.01924	0.3271	5.556
(1,4)	0.02461	0.2647	8.507
(1,5)	0.03973	0.1268	23.85
(1,6)	0.01814	0.4035	4.303
(2,1)	0.01294	0.4982	2.532
(2,2)	0.01319	0.4276	2.992
(2,3)	0.01392	0.4142	3.251
(2,4)	0.01519	0.4209	3.484
(2,5)	0.02330	0.3874	5.672
(2,6)	0.00308	1.236	0.2485
(3,1)	0.00705	0.8338	0.8388
(3,2)	0.00864	0.4289	1.976
(3,3)	0.01051	0.4818	2.135
(3,4)	0.00604	0.6141	0.9745
(3,5)	0.00495	0.6998	0.7028
(3,6)	0.00159	1.759	0.0903
Total	0.473	15.18	

Table C.2 Experimental Results for Test No. R-3

Type of Injection: One turret
Inlet Gas Flow Rate (kg/min): 0.237
Inlet Liquid Flow Rate (kg/min): 15.19
Inlet Quality (%): 1.5
Header-to-Separator Pressure Difference (cm of water): 3.33
Mass Balance Error for Gas (%): -0.12
Mass Balance Error for Liquid (%): 0.52

Feeder Number	Gas Flow Rate (kg/min)	Liquid Flow Rate (kg/min)	Quality (%)
(1,1)	0.00793	0.3071	2.519
(1,2)	0.00852	0.2409	3.416
(1,3)	0.01132	0.2039	5.259
(1,4)	0.01805	0.1378	11.59
(1,5)	0.02702	0.0418	39.24
(1,6)	0.00605	0.3995	1.491
(2,1)	0.00388	0.5173	0.745
(2,2)	0.00573	0.3633	1.554
(2,3)	0.00516	0.3821	1.333
(2,4)	0.00638	0.362	1.733
(2,5)	0.01133	0.2674	4.066
(2,6)	0.00148	1.500	0.098
(3,1)	0.00353	0.9634	0.365
(3,2)	0.00249	0.3971	0.624
(3,3)	0.00221	0.6221	0.354
(3,4)	0.00164	0.8525	0.192
(3,5)	0.00119	1.098	0.109
(3,6)	0.00043	1.730	0.025
Total	0.237	15.11	

Table C.3 Experimental Results for Test No. R-4

Type of Injection: One turret
Inlet Gas Flow Rate (kg/min): 0.115
Inlet Liquid Flow Rate (kg/min): 15.21
Inlet Quality (%): 0.75
Header-to-Separator Pressure Difference (cm of water): 2.29
Mass Balance Error for Gas (%): -6.71
Mass Balance Error for Liquid (%): -0.60

Feeder Number	Gas Flow Rate (kg/min)	Liquid Flow Rate (kg/min)	Quality (%)
(1,1)	0.00352	0.2541	1.366
(1,2)	0.00288	0.1701	1.665
(1,3)	0.00644	0.1232	4.968
(1,4)	0.01076	0.0659	14.04
(1,5)	0.01535	0.0098	61.01
(1,6)	0.00269	0.3044	0.8774
(2,1)	0.00203	0.6040	0.3342
(2,2)	0.00213	0.3137	0.6746
(2,3)	0.00326	0.3312	0.9756
(2,4)	0.00417	0.2462	1.665
(2,5)	0.00398	0.2965	1.326
(2,6)	0.00085	1.661	0.0513
(3,1)	0.00252	1.035	0.2431
(3,2)	0.00082	0.4125	0.1996
(3,3)	0.00112	0.9329	0.1200
(3,4)	0.00072	1.151	0.0621
(3,5)	0.00079	1.113	0.0711
(3,6)	0.00053	1.893	0.0278
Total	0.123	15.30	

Table C.4 Experimental Results for Test No. R-5

Type of Injection: One turret
Inlet Gas Flow Rate (kg/min): 0.0583
Inlet Liquid Flow Rate (kg/min): 15.17
Inlet Quality (%): 0.38
Header-to-Separator Pressure Difference (cm of water): 1.04
Mass Balance Error for Gas (%): -15.26
Mass Balance Error for Liquid (%): -0.63

Feeder Number	Gas Flow Rate (kg/min)	Liquid Flow Rate (kg/min)	Quality (%)
(1,1)	0.00118	0.2025	0.580
(1,2)	0.00104	0.1341	0.767
(1,3)	0.00348	0.0833	4.014
(1,4)	0.00632	0.0304	17.21
(1,5)	0.00831	0.0040	67.72
(1,6)	0.00101	0.2118	0.472
(2,1)	0.00169	0.6283	0.268
(2,2)	0.00086	0.2885	0.295
(2,3)	0.00182	0.2607	0.692
(2,4)	0.00203	0.2899	0.696
(2,5)	0.00259	0.2740	0.935
(2,6)	0.00092	1.616	0.057
(3,1)	0.00183	1.035	0.177
(3,2)	0.00041	0.3058	0.134
(3,3)	0.00081	1.098	0.074
(3,4)	0.00053	1.251	0.042
(3,5)	0.00053	1.237	0.043
(3,6)	0.00069	2.297	0.030
Total	0.0673	15.27	

Table C.5 Experimental Results for Test No. R-7

Type of Injection: One turret
Inlet Gas Flow Rate (kg/min): 0.969
Inlet Liquid Flow Rate (kg/min): 29.27
Inlet Quality (%): 3.2
Header-to-Separator Pressure Difference (cm of water): 44.91
Mass Balance Error for Gas (%): -0.93
Mass Balance Error for Liquid (%): -0.92

Feeder Number	Gas Flow Rate (kg/min)	Liquid Flow Rate (kg/min)	Quality (%)
(1,1)	0.03409	0.6398	5.058
(1,2)	0.03550	0.6025	5.564
(1,3)	0.04292	0.5911	6.770
(1,4)	0.04719	0.5211	8.304
(1,5)	0.02186	1.011	2.117
(1,6)	0.00495	2.186	0.226
(2,1)	0.02448	0.8116	2.928
(2,2)	0.03976	0.5968	6.247
(2,3)	0.05554	0.4791	10.39
(2,4)	0.06380	0.4115	13.42
(2,5)	0.01721	1.167	1.454
(2,6)	0.00388	2.555	0.152
(3,1)	0.01525	1.142	1.317
(3,2)	0.03373	0.5612	5.670
(3,3)	0.06598	0.2966	18.20
(3,4)	0.06655	0.4125	13.89
(3,5)	0.01218	1.403	0.861
(3,6)	0.00234	2.586	0.090
Total	0.978	29.55	

Table C.6 Experimental Results for Test No. R-8

Type of Injection: One turret
Inlet Gas Flow Rate (kg/min): 0.453
Inlet Liquid Flow Rate (kg/min): 29.33
Inlet Quality (%): 1.5
Header-to-Separator Pressure Difference (cm of water): 24.87
Mass Balance Error for Gas (%): -2.90
Mass Balance Error for Liquid (%): 0.47

Feeder Number	Gas Flow Rate (kg/min)	Liquid Flow Rate (kg/min)	Quality (%)
(1,1)	0.01629	0.6040	2.626
(1,2)	0.02111	0.5351	3.796
(1,3)	0.02294	0.5402	4.074
(1,4)	0.02646	0.5275	4.777
(1,5)	0.00757	0.9442	0.796
(1,6)	0.00274	2.0979	0.130
(2,1)	0.01196	0.7741	1.522
(2,2)	0.02242	0.5173	4.155
(2,3)	0.02541	0.4728	5.100
(2,4)	0.02518	0.5554	4.337
(2,5)	0.00519	1.275	0.405
(2,6)	0.00196	2.468	0.079
(3,1)	0.00749	1.042	0.714
(3,2)	0.01879	0.4950	3.657
(3,3)	0.03333	0.3813	8.040
(3,4)	0.02197	0.5665	3.733
(3,5)	0.00419	1.498	0.279
(3,6)	0.00160	2.586	0.062
Total	0.466	29.19	

Table C.7 Experimental Results for Test No. R-9

Type of Injection: One turret
Inlet Gas Flow Rate (kg/min): 0.241
Inlet Liquid Flow Rate (kg/min): 29.33
Inlet Quality (%): 0.81
Header-to-Separator Pressure Difference (cm of water): 15.34
Mass Balance Error for Gas (%): 1.77
Mass Balance Error for Liquid (%): -0.17

Feeder Number	Gas Flow Rate (kg/min)	Liquid Flow Rate (kg/min)	Quality (%)
(1,1)	0.00789	0.6154	1.266
(1,2)	0.01184	0.5020	2.303
(1,3)	0.01413	0.4944	2.778
(1,4)	0.01878	0.4537	3.974
(1,5)	0.00855	0.7390	1.144
(1,6)	0.00218	1.981	0.110
(2,1)	0.00610	0.7778	0.779
(2,2)	0.01154	0.5364	2.107
(2,3)	0.00928	0.5968	1.532
(2,4)	0.00733	0.6971	1.041
(2,5)	0.00406	1.212	0.334
(2,6)	0.00143	2.433	0.059
(3,1)	0.00424	1.098	0.385
(3,2)	0.01024	0.4818	2.081
(3,3)	0.00822	0.6623	1.225
(3,4)	0.00371	0.9278	0.399
(3,5)	0.00262	1.673	0.157
(3,6)	0.00103	2.460	0.042
Total	0.236	29.38	

Table C.8 Experimental Results for Test No. R-10

Type of Injection: One turret
Inlet Gas Flow Rate (kg/min): 0.1138
Inlet Liquid Flow Rate (kg/min): 29.28
Inlet Quality (%): 0.39
Header-to-Separator Pressure Difference (cm of water): 8.66
Mass Balance Error for Gas (%): 1.01
Mass Balance Error for Liquid (%): -0.34

Feeder Number	Gas Flow Rate (kg/min)	Liquid Flow Rate (kg/min)	Quality (%)
(1,1)	0.00328	0.5767	0.565
(1,2)	0.00513	0.4601	1.102
(1,3)	0.00688	0.4303	1.573
(1,4)	0.01223	0.3499	3.377
(1,5)	0.00461	0.5939	0.771
(1,6)	0.00154	1.823	0.084
(2,1)	0.00270	0.8116	0.332
(2,2)	0.00423	0.5084	0.824
(2,3)	0.00299	0.6398	0.465
(2,4)	0.00355	0.7227	0.489
(2,5)	0.00207	1.280	0.162
(2,6)	0.00085	2.527	0.034
(3,1)	0.00285	1.222	0.233
(3,2)	0.00302	0.4553	0.659
(3,3)	0.00262	0.8311	0.314
(3,4)	0.00195	1.151	0.170
(3,5)	0.00143	1.573	0.091
(3,6)	0.00071	2.702	0.026
Total	0.1127	29.38	

Table C.9 Experimental Results for Test No. R-11

Type of Injection: Two turret
Inlet Gas Flow Rate (kg/min): 0.471
Inlet Liquid Flow Rate (kg/min): 15.71
Inlet Quality (%): 2.9
Header-to-Separator Pressure Difference (cm of water): 6.30
Mass Balance Error for Gas (%): -2.10
Mass Balance Error for Liquid (%): 5.17

Feeder Number	Gas Flow Rate (kg/min)	Liquid Flow Rate (kg/min)	Quality (%)
(1,1)	0.02988	0.2047	12.74
(1,2)	0.03136	0.1813	14.75
(1,3)	0.02175	0.2607	7.698
(1,4)	0.01110	0.4142	2.611
(1,5)	0.03513	0.1065	24.81
(1,6)	0.03325	0.1622	17.01
(2,1)	0.01245	0.4499	2.692
(2,2)	0.01382	0.4182	3.198
(2,3)	0.00410	0.8520	0.479
(2,4)	0.00635	0.6111	1.029
(2,5)	0.02374	0.2978	7.385
(2,6)	0.00491	0.8204	0.595
(3,1)	0.00396	0.6784	0.580
(3,2)	0.00391	0.6355	0.612
(3,3)	0.00157	1.351	0.116
(3,4)	0.00460	0.7534	0.606
(3,5)	0.00905	0.4897	1.815
(3,6)	0.00169	1.435	0.118
Total	0.480	14.90	

Table C.10 Experimental Results for Test No. R-12

Type of Injection: Two turret
Inlet Gas Flow Rate (kg/min): 0.231
Inlet Liquid Flow Rate (kg/min): 15.72
Inlet Quality (%): 1.4
Header-to-Separator Pressure Difference (cm of water): 2.95
Mass Balance Error for Gas (%): -3.51
Mass Balance Error for Liquid (%): 1.85

Feeder Number	Gas Flow Rate (kg/min)	Liquid Flow Rate (kg/min)	Quality (%)
(1,1)	0.01392	0.1564	8.171
(1,2)	0.01770	0.0853	17.19
(1,3)	0.01353	0.1622	7.702
(1,4)	0.00638	0.2541	2.451
(1,5)	0.01767	0.0863	17.00
(1,6)	0.02022	0.0686	22.78
(2,1)	0.00411	0.4155	0.979
(2,2)	0.00509	0.3633	1.382
(2,3)	0.00163	1.069	0.153
(2,4)	0.00280	0.7365	0.378
(2,5)	0.00907	0.2488	3.516
(2,6)	0.00226	0.7528	0.300
(3,1)	0.00250	0.6811	0.365
(3,2)	0.00132	0.8820	0.150
(3,3)	0.00106	1.796	0.059
(3,4)	0.00216	0.9507	0.227
(3,5)	0.00227	0.5215	0.434
(3,6)	0.00095	1.796	0.053
Total	0.239	15.43	

Table C.11 Experimental Results for Test No. R-13

Type of Injection: Two turret
Inlet Gas Flow Rate (kg/min): 0.1177
Inlet Liquid Flow Rate (kg/min): 15.74
Inlet Quality (%): 0.74
Header-to-Separator Pressure Difference (cm of water): 1.24
Mass Balance Error for Gas (%): -6.89
Mass Balance Error for Liquid (%): 1.98

Feeder Number	Gas Flow Rate (kg/min)	Liquid Flow Rate (kg/min)	Quality (%)
(1,1)	0.00502	0.1195	4.028
(1,2)	0.00862	0.0513	14.38
(1,3)	0.00771	0.0948	7.519
(1,4)	0.00369	0.1860	1.945
(1,5)	0.00771	0.0732	9.527
(1,6)	0.01179	0.0304	27.95
(2,1)	0.00198	0.4728	0.418
(2,2)	0.00282	0.3097	0.901
(2,3)	0.00133	1.003	0.132
(2,4)	0.00164	0.7690	0.212
(2,5)	0.00387	0.2832	1.347
(2,6)	0.00193	0.7377	0.261
(3,1)	0.00231	0.7079	0.325
(3,2)	0.00104	1.0092	0.103
(3,3)	0.00175	1.9963	0.087
(3,4)	0.00231	1.116	0.206
(3,5)	0.00165	0.6650	0.248
(3,6)	0.00053	1.668	0.032
Total	0.126	15.42	

Table C.12 Experimental Results for Test No. R-14

Type of Injection: Two turret
Inlet Gas Flow Rate (kg/min): 0.0578
Inlet Liquid Flow Rate (kg/min): 15.72
Inlet Quality (%): 0.37
Header-to-Separator Pressure Difference (cm of water): 0.66
Mass Balance Error for Gas (%): -13.01
Mass Balance Error for Liquid (%): 1.89

Feeder Number	Gas Flow Rate (kg/min)	Liquid Flow Rate (kg/min)	Quality (%)
(1,1)	0.00111	0.1147	0.960
(1,2)	0.00448	0.0352	11.31
(1,3)	0.00395	0.0447	8.119
(1,4)	0.00102	0.1220	0.833
(1,5)	0.00324	0.0487	6.235
(1,6)	0.00527	0.0120	30.49
(2,1)	0.00159	0.5275	0.300
(2,2)	0.00156	0.3031	0.513
(2,3)	0.00125	1.093	0.114
(2,4)	0.00172	0.7490	0.229
(2,5)	0.00227	0.2541	0.884
(2,6)	0.00182	0.6971	0.260
(3,1)	0.00187	0.7748	0.241
(3,2)	0.00064	1.208	0.053
(3,3)	0.00066	2.085	0.032
(3,4)	0.00205	1.073	0.190
(3,5)	0.00133	0.6945	0.191
(3,6)	0.00025	1.591	0.016
Total	0.0654	15.43	

Table C.13 Experimental Results for Test No. R-15

Type of Injection: Two turret
Inlet Gas Flow Rate (kg/min): 0.920
Inlet Liquid Flow Rate (kg/min): 30.16
Inlet Quality (%): 3.0
Header-to-Separator Pressure Difference (cm of water): 42.04
Mass Balance Error for Gas (%): -4.02
Mass Balance Error for Liquid (%): 2.10

Feeder Number	Gas Flow Rate (kg/min)	Liquid Flow Rate (kg/min)	Quality (%)
(1,1)	0.05139	0.5696	8.276
(1,2)	0.05677	0.5427	9.470
(1,3)	0.01121	1.377	0.808
(1,4)	0.02759	0.9027	2.966
(1,5)	0.06390	0.3807	14.37
(1,6)	0.01515	1.259	1.189
(2,1)	0.03624	0.7615	4.543
(2,2)	0.04299	0.6828	5.923
(2,3)	0.00809	1.584	0.508
(2,4)	0.02997	0.7966	3.626
(2,5)	0.05685	0.4791	10.61
(2,6)	0.00705	1.894	0.371
(3,1)	0.01993	1.116	1.755
(3,2)	0.03848	0.6945	5.250
(3,3)	0.00778	1.704	0.455
(3,4)	0.02099	0.9532	2.155
(3,5)	0.04978	0.5321	8.555
(3,6)	0.00574	2.070	0.277
Total	0.957	29.53	

Table C.14 Experimental Results for Test No. R-16

Type of Injection: Two turret
Inlet Gas Flow Rate (kg/min): 0.470
Inlet Liquid Flow Rate (kg/min): 30.20
Inlet Quality (%): 1.5
Header-to-Separator Pressure Difference (cm of water): 20.12
Mass Balance Error for Gas (%): -4.79
Mass Balance Error for Liquid (%): 1.74

Feeder Number	Gas Flow Rate (kg/min)	Liquid Flow Rate (kg/min)	Quality (%)
(1,1)	0.02894	0.4906	5.571
(1,2)	0.03341	0.4626	6.736
(1,3)	0.00548	1.230	0.444
(1,4)	0.01416	0.7478	1.858
(1,5)	0.04182	0.3392	10.98
(1,6)	0.00892	1.101	0.804
(2,1)	0.01428	0.7878	1.780
(2,2)	0.02118	0.6427	3.190
(2,3)	0.00308	1.668	0.184
(2,4)	0.01058	0.8981	1.165
(2,5)	0.03226	0.4702	6.420
(2,6)	0.00327	2.004	0.163
(3,1)	0.00773	1.217	0.632
(3,2)	0.01372	0.7909	1.705
(3,3)	0.00268	1.981	0.135
(3,4)	0.00878	1.068	0.816
(3,5)	0.02199	0.5876	3.607
(3,6)	0.00234	2.348	0.100
Total	0.492	29.67	

Table C.15 Experimental Results for Test No. R-17

Type of Injection: Two turret
Inlet Gas Flow Rate (kg/min): 0.2293
Inlet Liquid Flow Rate (kg/min): 30.20
Inlet Quality (%): 0.75
Header-to-Separator Pressure Difference (cm of water): 9.63
Mass Balance Error for Gas (%): -4.95
Mass Balance Error for Liquid (%): 1.17

Feeder Number	Gas Flow Rate (kg/min)	Liquid Flow Rate (kg/min)	Quality (%)
(1,1)	0.01614	0.3566	4.331
(1,2)	0.01993	0.3405	5.529
(1,3)	0.00240	1.3182	0.181
(1,4)	0.00742	0.5868	1.249
(1,5)	0.02209	0.2951	6.962
(1,6)	0.00562	0.7140	0.781
(2,1)	0.00498	0.7966	0.621
(2,2)	0.00800	0.6470	1.222
(2,3)	0.00127	2.1097	0.060
(2,4)	0.00427	0.9442	0.450
(2,5)	0.01521	0.4370	3.363
(2,6)	0.00130	2.1156	0.062
(3,1)	0.00382	1.1994	0.317
(3,2)	0.00454	0.7695	0.586
(3,3)	0.00138	2.3592	0.058
(3,4)	0.00403	1.1032	0.364
(3,5)	0.00870	0.5083	1.684
(3,6)	0.00094	2.5858	0.036
Total	0.241	29.85	

Table C.16 Experimental Results for Test No. R-18

Type of Injection: Two turret
Inlet Gas Flow Rate (kg/min): 0.1155
Inlet Liquid Flow Rate (kg/min): 30.20
Inlet Quality (%): 0.38
Header-to-Separator Pressure Difference (cm of water): 4.85
Mass Balance Error for Gas (%): -4.09
Mass Balance Error for Liquid (%): 4.71

Feeder Number	Gas Flow Rate (kg/min)	Liquid Flow Rate (kg/min)	Quality (%)
(1,1)	0.00914	0.3218	2.763
(1,2)	0.00956	0.2779	3.326
(1,3)	0.00132	1.292	0.102
(1,4)	0.00337	0.5825	0.575
(1,5)	0.01107	0.2330	4.537
(1,6)	0.00322	0.5911	0.542
(2,1)	0.00261	0.7741	0.335
(2,2)	0.00324	0.5710	0.564
(2,3)	0.00038	2.157	0.017
(2,4)	0.00221	0.9135	0.242
(2,5)	0.00720	0.3593	1.965
(2,6)	0.00096	2.057	0.047
(3,1)	0.00269	1.222	0.220
(3,2)	0.00156	0.7186	0.216
(3,3)	0.00054	2.354	0.023
(3,4)	0.00264	1.108	0.237
(3,5)	0.00355	0.4500	0.782
(3,6)	0.00070	2.663	0.026
Total	0.120	28.78	

APPENDIX D

REPEATABILITY STUDIES

The results of the repeatability studies that were carried out to ensure the accuracy of the present data are discussed in this appendix. One repeatability test was done for each of the one-turret-injection and two-turret-injection tests.

The actual inlet conditions that were used for the one-turret-injection repeatability test RPT-8 closely matched those used for test R-8, namely, gas flow rate = 0.465 kg/min and liquid flow rate = 30 kg/min. The actual inlet conditions that were used for the two-turret-injection repeatability test RPT-16 also closely matched those used for test R-16 (gas flow rate = 0.465 kg/min and liquid flow rate = 30 kg/min). The actual inlet conditions, and all the outlet-flow measurements for tests RPT-8 and RPT-16 are given in the Tables D.1 and D.2, respectively. The actual inlet conditions, and all outlet flow measurements for the original tests (R-8 and R-16) are given in Tables C.6 and C.14, respectively. Figures D.1 and D.2 show comparisons of the original data and the repeat data for gas flow rate, liquid flow rate and quality in the individual feeders in the one-turret and two-turret repeatability tests. The figures show that there is good agreement in the data. In most feeders, to the scale shown in the figures, one cannot distinguish between the original data (solid symbols) and the repeat data (open symbols).

Table D.1 Experimental Results for Test No. RPT-8

Type of Injection: One turret
Inlet Gas Flow Rate (kg/min): 0.453
Inlet Liquid Flow Rate (kg/min): 29.36
Inlet Quality (%): 1.5
Header-to-Separator Pressure Difference (cm of water): 22.96
Mass Balance Error for Gas (%): -3.13
Mass Balance Error for Liquid (%): 1.23

Feeder Number	Gas Flow Rate (kg/min)	Liquid Flow Rate (kg/min)	Quality (%)
(1,1)	0.01654	0.6083	2.648
(1,2)	0.02027	0.5262	3.709
(1,3)	0.02210	0.5198	4.078
(1,4)	0.02501	0.5020	4.745
(1,5)	0.00786	0.8966	0.870
(1,6)	0.00239	2.251	0.106
(2,1)	0.01121	0.7615	1.451
(2,2)	0.02285	0.5046	4.333
(2,3)	0.02582	0.4664	5.246
(2,4)	0.02546	0.5300	4.584
(2,5)	0.00577	1.307	0.439
(2,6)	0.00160	2.456	0.065
(3,1)	0.00745	0.9964	0.742
(3,2)	0.02133	0.5030	4.068
(3,3)	0.03566	0.4310	7.642
(3,4)	0.02350	0.5532	4.075
(3,5)	0.00392	1.423	0.274
(3,6)	0.00141	2.435	0.058
Total	0.467	29.00	

Table D.2 Experimental Results for Test No. RPT-16

Test Number: RPT-16
Type of Injection: Two turret
Inlet Gas Flow Rate (kg/min): 0.468
Inlet Liquid Flow Rate (kg/min): 30.24
Inlet Quality (%): 1.5
Header-to-Separator Pressure Difference (cm of water): 19.15
Mass Balance Error for Gas (%): -1.72
Mass Balance Error for Liquid (%): 2.86

Feeder Number	Gas Flow Rate (kg/min)	Liquid Flow Rate (kg/min)	Quality (%)
(1,1)	0.02922	0.4575	6.002
(1,2)	0.03206	0.4410	6.778
(1,3)	0.00588	1.240	0.472
(1,4)	0.01359	0.7678	1.739
(1,5)	0.04111	0.3204	11.37
(1,6)	0.00858	1.069	0.796
(2,1)	0.01332	0.7503	1.745
(2,2)	0.02033	0.6398	3.079
(2,3)	0.00311	1.733	0.179
(2,4)	0.00986	0.8966	1.088
(2,5)	0.03064	0.4512	6.360
(2,6)	0.00305	1.981	0.154
(3,1)	0.00817	1.222	0.664
(3,2)	0.01236	0.7025	1.729
(3,3)	0.00270	2.006	0.135
(3,4)	0.00840	1.050	0.794
(3,5)	0.02083	0.5823	3.453
(3,6)	0.00248	2.322	0.107
Total	0.476	29.38	

The range, arithmetic mean and root mean square of the deviations between the original and repeat tests, as calculated from Equations (D.1) to (D.3), are summarized in Table D.3. The following are definitions of the terms used in Table D.3:

For any individual feeder,

$$Deviation,\ dev = \frac{(Original\ Value) - (Repeat\ Value)}{(Original\ Value)} \times 100, \quad \% \tag{D.1}$$

For measurements in the 18 feeders listed in Tables D.1 and D.2,

$$Arithmetic\ Mean = \frac{\sum (dev)}{N}, \quad \% \tag{D.2}$$

and

$$Root\ Mean\ Square = \left\{ \frac{\sum (dev)^2}{N} \right\}^{0.5}, \quad \% \tag{D.3}$$

where N is the number of measurements (18).

It is noted that the deviations in the two-turret-injection tests were better than those in the one-turret-injection tests. The maximum arithmetic mean of the deviations was 2.3% and the maximum root mean square of the deviations was 8.2%. Given the complexity of the flow tests, these deviations are deemed acceptable.

Table D.3 Deviation Between the Original and Repeatability Data in the Individual Feeders

	Deviation Between Tests R-8 and RPT-8 (%)			Deviation Between Tests R-16 and RPT-16 (%)		
	Gas Flow Rate	Liquid Flow Rate	Quality	Gas Flow Rate	Liquid Flow Rate	Quality
Arithmetic Mean	1.2	1.0	0.1	2.3	2.0	0.2
Root Mean Square	8.2	4.8	8.1	5.3	4.1	4.4
Range	-13.5 to 18.4	-13.0 to 5.8	-11.2 to 18.5	-7.3 to 9.9	-3.9 to 11.2	-7.7 to 6.6

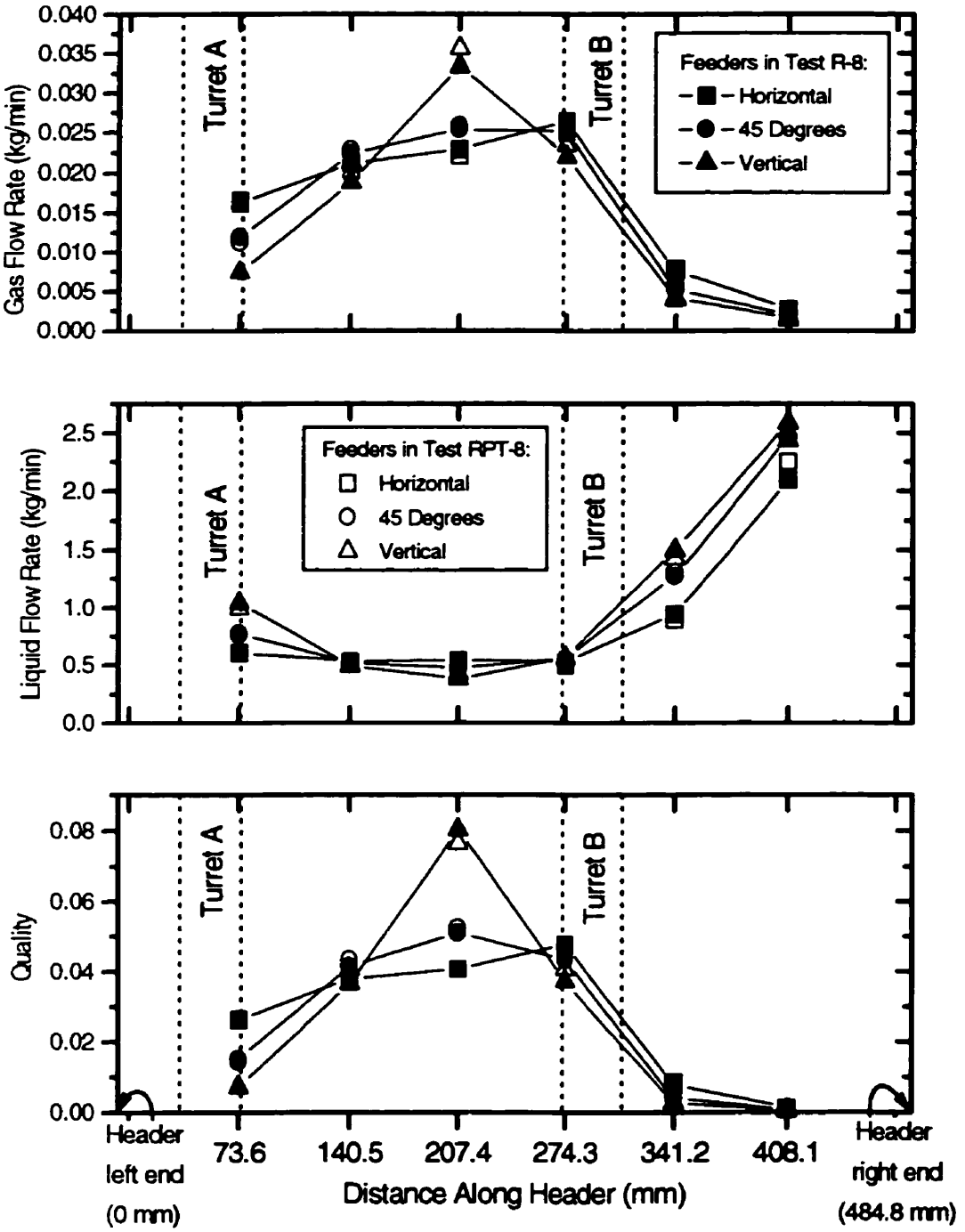

Figure D.1 Comparison of Individual Feeder Conditions in Test Nos. R-8 and RPT-8

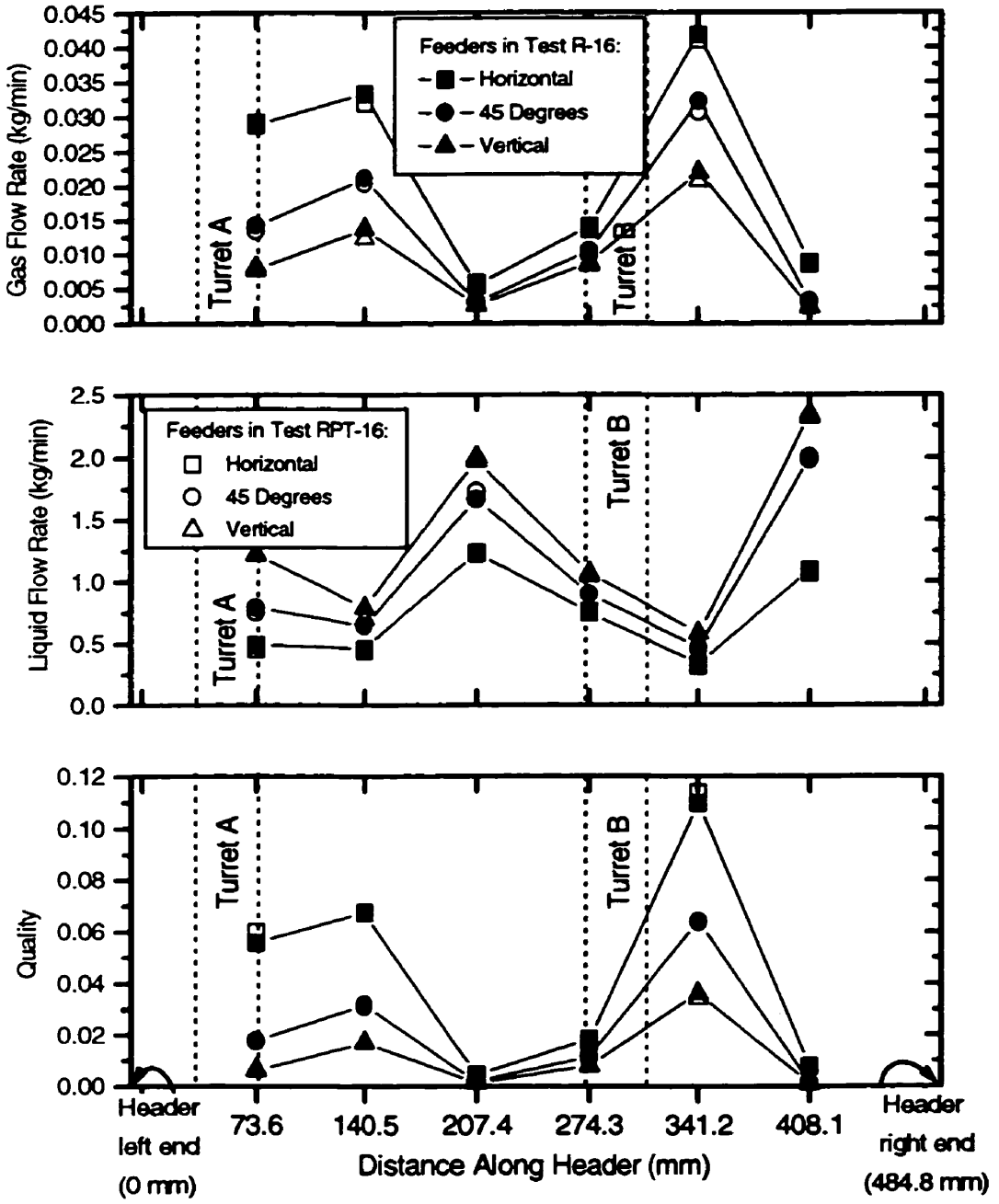

Figure D.2 Comparison of Individual Feeder Conditions in Test Nos. R-16 and RPT-16